Universidad de Valladolid

ESCUELA DE INGENIERÍAS INDUSTRIALES

DEPARTAMENTO DE INGENIERÍA QUÍMICA Y TECNOLOGÍA DEL MEDIO AMBIENTE

TESIS DOCTORAL:

GREEN PROCESSES APPLIED TO NANOPARTICLE TECHNOLOGY: SYNTHESIS AND FORMULATION

Presentada por Víctor Martín Velasco para optar al grado de doctor por la Universidad de Valladolid

Dirigida por:

Dra. Ing. Soraya Rodríguez Rojo
Prof. María José Cocero Alonso

Memoria para optar al grado de Doctor,

Con Mención Doctor Internacional,

Presentada por el Ingeniero Químico:

Víctor Martín Velasco

Valladolid, Junio de 2016

UNIVERSIDAD DE VALLADOLID

ESCUELA DE INGENIERÍAS INDUSTRIALES

Secretaría

La presente tesis doctoral queda registrada en el folio

número _____ del correspondiente libro de registro

número _____

Valladolid, a _____ de _____ de 2016

Fdo. El encargado del registro

Soraya Rodríguez Rojo

Investigadora Juan de la Cierva

Departamento de Ingeniería Química y Tecnología del Medio Ambiente

Universidad de Valladolid

y

María José Cocero Alonso

Catedrática

Departamento de Ingeniería Química y Tecnología del Medio Ambiente

Universidad de Valladolid

Certifican que:

Víctor Martín Velasco ha realizado bajo su dirección el trabajo "*Green Processes Applied to Nanoparticle Technology: Synthesis and Formulation*", en el Departamento de Ingeniería Química y Tecnología del Medio Ambiente de la Escuela de Ingenierías Industriales de la Universidad de Valladolid. Considerando que dicho trabajo reúne los requisitos para ser presentado como Tesis Doctoral expresan su conformidad con dicha presentación.

Valladolid, a _____ de _____ de 2016

Fdo. Soraya Rodríguez Rojo Fdo. María José Cocero Alonso

Reunido el tribunal que ha juzgado la Tesis Doctoral titulada "*Green Processes Applied to Nanoparticle Technology: Synthesis and Formulation*" presentada por el Ingeniero Químico Víctor Martín Velasco y en cumplimiento con lo establecido por el Real Decreto 99/2011 de 28 de enero de 2011 acuerda conceder por _____ la calificación de _____.

Valladolid, a _____ de _____ de 2016

PRESIDENTE SECRETARIO

1er Vocal 2º Vocal 3er Vocal

AGRADECIMIENTOS

En primer lugar, quisiera agradecer a la Universidad de Valladolid por concederme la beca FPI, gracias a la cual he podido realizar este trabajo. También quiero dar las gracias a María José Cocero, jefa del grupo de investigación Procesos a Alta Presión y cotutora de esta tesis junto con Soraya Rodríguez Rojo, a la que agradezco especialmente por todo el tiempo que ha dedicado a este proyecto y por su guía, sin la que hubiera sido imposible todo esto.

Me gustaría hacer una mención especial a Rut Romero Díez por ayudarme en los momentos más difíciles de la tesis y por su gran trabajo y apoyo durante el desarrollo del capítulo cuatro.

Quero agradecer à doutora Catarina Duarte pela proveitosa estada no seu laboratorio e pelo apoio recebido. Também agradeço aos meus colegas do ITQB: Agostinho, Liliana, Ana, Inês, Joana, Catia e especialmente a Vanessa pela valiosa ajuda.

También quiero agradecer a mis compañeros del Departamento de Ingeniería Química, en especial a Marta, Alberto, Ana, Álvaro C. y Marta Fraile por todos los momentos que hemos vivido juntos, fuera y dentro de la universidad.

Un agradecimiento especial va dedicado a mis amigos Laura R., Jose, Laura B., Álvaro S., Carmen, Andrés, Fernando, Julio y Ruben por todo su apoyo y hacer que la vida merezca la pena.

Por último, les doy las gracias a mis padres y al resto de la familia por su apoyo diario.

INDEX

INDEX

ABSTRACT

Abstract

Nowadays, nanoparticle technology is investigated for being applied in a lot of fields, for example, in catalysis, materials, electronics and biomedicine, one of the most promising. This versatility is because of their properties associated to their size and morphology, such as surface absorption plasmon effect, specific area, reduction of melting point, reduction of superconductivity transition temperature, and increment of metal magnetic force. In order to achieve the desired properties, several synthesis methods have been developed, top down methods that involves a chemical or mechanical size reduction, and bottom up methods in which the particle grows from smaller entities. The main disadvantage of these methods is the use of organic toxic solvents and extreme operation conditions.

Novel processes must be environmental sustainable for their application in the real world, because of the growing concern about the planet damage. Green chemistry and engineering provides all the necessary tools to achieve the design of new processes or the modification of existing processes to accomplish this important target. Novel processes must decrease or eliminate wastes production, generate nontoxic product wherever possible and eliminate or replace solvents by benign solvents as supercritical fluids, ionic liquids, water or ethanol. Moreover the processes must be energetically efficient, avoid separation steps, use catalysts when it is possible to increase the efficiency and use renewable feedstocks.

The aim of this thesis is the study of some processes related to nanoparticle technology with green chemistry tools. In chapter 1, metal nanoparticles have been synthetized by bioreduction with grape pomace extract. This process uses water as solvent, natural nontoxic reagents, near ambient conditions and renewable feedstocks instead of toxic compounds, high pressure/temperature conditions and high costs, that the traditional process imply. Chapter 2 deals with nanoparticle formulation, a lipid is loaded with metal nanoparticles by PGSS®, and this process uses supercritical carbon dioxide, being a green option. Also, the process is fast and the solvent is eliminated by decompression, avoiding separation steps. Traditional method uses organic toxic compounds and needs solvent separation. Finally in chapter 3 and 4, a nanoparticle coating process has been developed by supercritical anti-solvent process in a fluidized bed. The solvents used are supercritical

carbon dioxide and ethanol, both safe substances, reducing operation times and eliminating separation steps.

In **chapter 1**, metal copper nanoparticles have been produced by bioreduction method. This method consists on reducing metal ions in solution with compounds, produced by plant cells in their metabolism.

Usually plant extracts, which have all necessary compounds to achieve the reduction and stabilize the particle size, are used in instead of whole cells. It has been demonstrated that extract phenolic acids act as reducing agents while flavonols are capping agents, their concentration determines the particle size. In this work, grape pomace extract, a waste of wine industry, has been used, and their effect at different temperatures (30-55-80ºC), operation time (1-2-3 hours) and ratio (0.01- 0.05 - 0.1 g GAE/g Cu ion) studied, being temperature and time are the most influential variables. High temperatures increases the process yield but produce a fast consumption and/or degradation of capping agents, increasing the particle size to micrometric range. It is necessary a good selection of conditions to obtain particles in the nanometric range with the maximum possible yield.

Also, the growth process has been studied with and without capping agents in order to observe the effect, and changing temperature and ratio conditions. In this case, two phases can be observed, in the first the size is constant over time, and in the second the capping effect finishes and the size increases rapidly due to a drop in capping agent concentration.

Finally, metal copper nanoparticle composition and morphology have been determined by XRD, TEM and EDS. The results show that copper particles have been obtained with a spherical morphology.

Some authors have demonstrated that copper nanoparticles have anti-cancer properties, owing to their toxicity and the looked-for application, it is necessary to formulate them. Therefore, in **chapter 2**, copper nanoparticles have been formulated with a lipid by PGSS®, a technic that uses supercritical carbon dioxide as solute, which is a clean substance recognized by green chemistry science, avoiding the use of organic solvent and several separation steps. The objective of this chapter is to study the PGSS process main operational variables (pre-expansion temperature (60-80ºC) and pressure (100-150 bar), water content (0-40% w/w) and copper load (0.5-5% w/w), in order to encapsulate copper nanoparticles in lipid microparticles.

The main important operating variable was the relationship between the amount of carbon dioxide and lipid, the process is badly affected at higher ratios. On the other hand, temperature and pressure in the studied range have not any critical effect in the process yield and in the final product particle size. Process yield presents a minimum when copper amount is increased due to stirring in pre-expansion chamber, but the particle size is barely affected.

This process allows incorporating copper in aqueous solution instead of copper in solid form. The effect of water depends on copper concentration. At higher concentration (5% w/w) the process yield do not change while particle size decreases, on the contrary, at low concentration (0.2% w/w) process yield remains constant until reach a concentration of water (20% w/w) where process yield decreases and particle size is increased.

Regarding the dispersion of copper metal in the lipid microparticles, the lower content of copper, the better dispersion is achieved due to the absence of copper agglomerates which is presented at high copper nanoparticle concentrations (5%w/w). Water have a positive effect on dispersion even though agglomeration is not avoided.

In chapter 3 and 4, a green coating process of inorganic nanoparticle agglomerates have been developed and their parameters studied. This process combines nanoparticle fluidization with supercritical carbon dioxide and anti-solvent process (SAS). This study has been carried out in two steps:

In **chapter 3**, fluidization of nanoparticles with supercritical carbon dioxide, as alternative to enhance fluidization quality, has been investigated by means of the determination of minimum fluidization velocity and its variation with supercritical fluid density and particle nature (primary size, bulk density…).

Nanoparticles belong to group C in Geldart classification, these particles are characterized by a high cohesion tendency, which causes problems in the fluidized bed, such as preferential paths, in addition, particles forms agglomerates and their size augments. Agglomeration takes place owing to cohesive forces, as London Van der Waals attractive forces, which depends on particle size. In order to solve this problem some technics such as vibrations, ultrasounds or electromagnetic fields, have been proposed. As an alternative, in this work, SFC has been used as fluidizing media due to the good results that it provided for microparticles fluidization.

Abstract

In this work, titanium oxide, magnetite and aluminum oxide nanoparticles have been considered. Minimum fluidization velocity varies with fluid density, at high densities (above 500 kg/m^3) the velocity is between 0.020 and 0.060 cm/s while at densities below 500 kg/m^3 reach values up to 0.180 cm/s. Also, at high densities the same behavior have been observed for all nanoparticles but at low densities each particle has a different tendency related with primary particle size. Particles with lower primary particle size form bigger agglomerates and then, it is necessary a bigger velocity to fluidize them.

Titanium dioxide has been chosen as nanoparticle model and it has been coated with a polymer (Pluronic F-127) in **chapter 4**. An ethanolic solution of this polymer is pumped to fluidization chamber, supercritical carbon dioxide dissolves ethanol and polymer crystalizes on nanoparticle agglomerates. The main factors, that affect the process, have been studied: the ratio between the velocity of carbon dioxide through the bed and the minimum fluidization velocity (u_{mf}), with values from 1.5 to 2.5 times the u_{mf}; the density of carbon dioxide, varying from 640 kg/m^3 to 735 kg/m^3 approximately; the flow rate of solution, within an interval between 0.5-2 mL/min; the concentration of the solution, from 0.030 mg/mL to 0.090 mg/mL and the mass ratio polymer-particle, 0.45-1.8 g/g.

The most critical variables are solution flow rate and solution concentrations. These parameter can change process yield from 30% to 95% being the best option to work at low flows and concentrations. Polymer-particle mass ratio affects drastically the final coated particle size varying from 0.6 to 3.0 µm.

Final product has been analyzed by fluorescence microscopy and Fourier Transform Infrared Spectroscopy (FT-IR). These tests show that the polymer is present over the whole agglomerate. Coated particle bulk density has been measured in order to check the process, which increases linearly with the polymer-particle ratio, enhancing the manipulation of particles.

INTRODUCTION AND OBJECTIVES

Introduction and Objectives

This work forms part of SHYMAN project: Sustainable Hydrothermal Manufacturing of Nanomaterials (FP7-NMP-2011-LARGE-280983). This European project is funded by the 7th Framework Program for Research and Technological Development. It is a large scale collaborative project coordinated by Nottingham University in United Kingdom as lead of a consortium of European universities and companies: University of Valladolid, Institute of High Pressure Physics, Czech Technical University, Applied Physics Research Group from Trinity College of Dublin, GTVT s.r.o., Promethean Particles, Centro Ricerche FIAT, PPG Industries, Repsol, Solvay, Endor, TopGaN, Itaprochim, Ceramisys, Van Loon Chemical Innovations and Pielaszek Research.

The SHYMAN Project will stablish continuous hydrothermal synthesis as one of the most flexible and sustainable means of manufacturing nanomaterials on a large scale, serving industries of strategic importance to Europe. Nanomaterials are the building blocks for any successful application of nanotechnology. In 2009 the largest nanotechnology segment was in nanomaterials with $9 billion is sales, and the predictions to 2020 indicate that it will rise to $75.8 billion [1].

Continuous hydrothermal synthesis is an enabling technology that is ready to be proven at industrial scale as a result of recent breakthroughs in reactor design which suggest that it could now be scaled over 100 tons per annum. A main objective of SHYMAN project is to develop the know-how to scale up the current scale system based on reactor modelling (figure 1), kinetics and metrology knowledge of the different partners involved in the project.

Selected project partners with expertise in sustainability modelling and life cycle assessment will quantify the environmental impact and benefits of a process that uses water as a recyclable solvent, whilst producing the highest quality, dispersed and formulated products. In addition to scale up production, the process will be improved through case studies with industrial end users in four key areas, namely printed electronics, surface coating, healthcare and medical application and hybrid polymers and materials

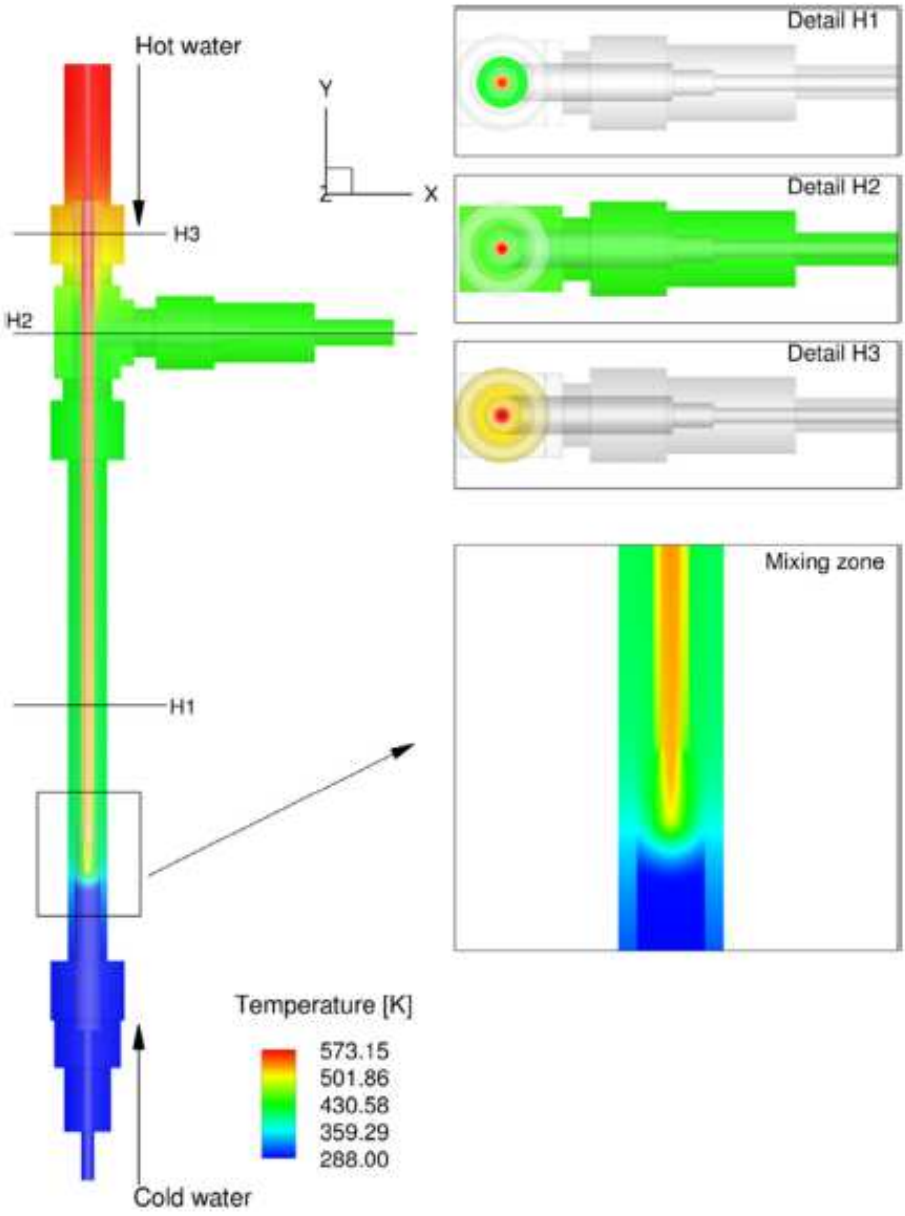

Figure 1: SHYMAN project reactor modelling example developed by UVa group [2].

Further value will be added to the Project by working on new materials that have been identified as key future targets, such as novel functional catalyst based on titanium dioxide and composed materials such as magnetic ceramics, which currently cannot be produced with the adequate quality and/or in the required amount. The consortium is founded on the principle that the whole value chain (from nanoparticle production to final product) must be involved in the development of the technology.

SHYMAN Project objectives

This project has as main objective, the construction of a plant with a production capacity of 100 Tm/year of nanoparticles and their formulations. This plant will permit to study the different applications that will be developed by the industrial partners.

This objective is divided in 9 technical work packages with different targets, and two administrative work packages: dissemination and exploitation, and management. Technical packages are:

1. Pilot Scale Manufacture: This package has two objectives, to produce nanomaterials at kilo scale in a pilot reactor for their use in other work packages, and to obtain the materials with a high degree of control in terms of specification and formulation.
2. Metrology and Online Characterization: it is focused on metrology approaches which must be developed to quantify the improvements made through formulation, and process optimization through rapid analysis method in real time or as close to real time as possible.
3. Formulation and Surface Modification: The objective is to integrate formulation systems into the production method where the nanomaterials are non-agglomerated, surface activated and prepared for use in a single stage.
4. Case Study Development: This work package is specifically for testing the materials made during work package 1 in the different companies of the consortium.
5. Process Dynamics and Modelling: The objective is the generation of an integrated kinetics model that can predict particle size and particle size distribution of a range of different nanomaterials with the continuous system at production scales of 1, 10 and 100 tons per annum.
6. Life Cycle Assessment, Health and Safety: The aim is to evaluate the hydrothermal process in terms of a techno-economic assessment by quantifying the benefits and drawbacks compared with other existing technologies
7. New Materials Development: The goal of work package 7 is to ensure that the project does not only focus on the immediate needs but also allows the project to maintain a progressive view of the nanomaterials market ensuring the development of new products

8. Plant Design and Assembly: This work package uses the information from 1, 4 and 5 to re-design the full scale reactor as well as carrying out focused on energy integration.
9. Full Scale Manufacture: The objective is the production of up to half a ton of each material for each of the end-users of nanoparticles to demonstrate capabilities within each industrial segment.

Thesis framework

Actually, few applications incorporate pristine nanoparticles. Most requires some kind of formulation before application into a vapor or liquid phase owing to be dispersed in a material matrix, or placed on a surface. Achieving the dispersion requires the addiction of surfactants or capping agents to stabilize it. Furthermore, several applications require high weight loadings. End-users of nanomaterials require from technologies: enhanced product functionality and dispersed nanoparticles. In order to accomplish all requirements nanoparticles must be formulated. Figure 2 shows the process followed from nanoparticles to finished product. To use nanoparticles in commercial applications, it can be formulated in two stages: dry synthesis methods and formulation or in one step by wet synthesis where hydrothermal process is included.

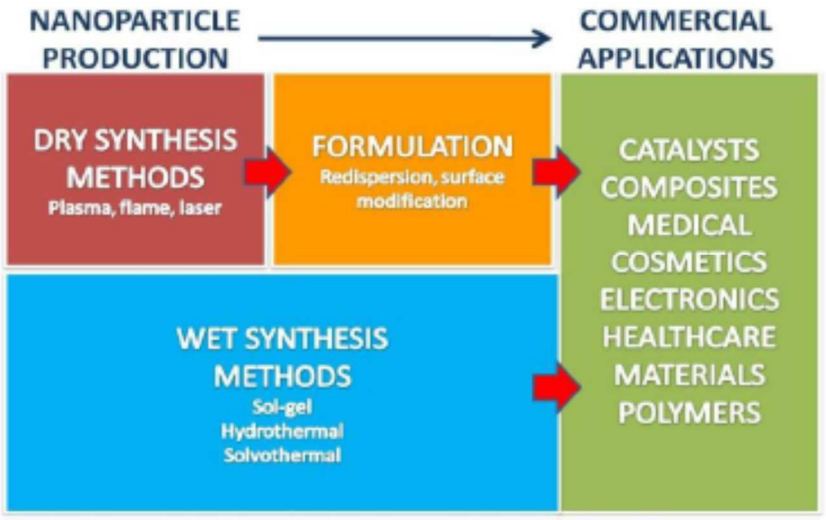

Figure 2: The link between nanoparticles and products with nanomaterials.

Continuous hydrothermal synthesis produces aqueous suspensions of nanomaterials at low concentrations (< 1%w/w), which is a critical problem in wet synthesis methods, that will be try to solve in the project, because in industry, at least, 5-

30% w/w are required, and the cost of water elimination is high. Also water can produce problems in certain application for example in catalysis or in polymerization processes where completely dry particles are required. The main objective of SHYMAN formulation package is to create a flexible system that can produce nanomaterials with a specific coating in an aqueous or non-aqueous fluid, at a specific weight loading. This system must avoid most of the downstream processing stages, which all conventional methods have.

In this thesis, some aspects related with SHYMAN project work package 3 have been presented. An alternative process for the synthesis of nanoparticles in aqueous medium, a bioreduction process performed at near ambient conditions have been proposed. Furthermore, dry particle formulations have been explored as alternative to one step wet process.

Other green synthesis of nanoparticles in aqueous media different from continuous hydrothermal has been studied trying to revalorize a wine industry byproduct. This process is bioreduction with plant extracts [3, 4]. Plants produce in their metabolism all necessary compounds to carry out their physiological activity which includes metal reduction. For this reason, these organism extracts have reducing and capping agents, such as, polyphenols. When a plant extract is put in contact with a metallic salt solution, metallic ions are reduce to metal state. Depending on reaction parameters (time, temperature, extract-metal ion ratio, pH...), it is possible to obtain nanoparticles with the desired properties. This study is presented in chapter 1.

Formulation has the main objective of protecting and modifying original physical and chemical material properties: shape, color, bulk density, surface characteristics, chemical reactivity, mechanical properties, hygroscopicity or particle size. Inorganic particles, such as silica, gold, silver, copper, iron oxide, titanium oxide, exhibit interesting properties (quantum dots, magnetism or cytotoxicity), for this reason they have applications in biomedicine (controlled release, chemotherapy, imaging…), new material production (hybrid materials), catalysis and other knowledge fields [5]. In order to apply them, nanoparticle properties must be improved by coating or other kinds of formulation.

Polymer encapsulation of iron oxides, cobalt, silver and other inorganic substances has been achieved by several traditional technics: polymer adsorption, layer-by-layer assembly, emulsion polymerization [6], monomer adsorption followed by polymerization

or double emulsion process [7]. Regarding lipid based loaded particles, traditional processes are fusion processes, cold or hot high-pressure homogenization and multi-step solvent processes, such as emulsification and ultrasonication [8].

In this thesis work, green techniques based on supercritical fluid micronization processes have been applied, alone or in combination with conventional coating processes such as fluidized bed technology.

The first method is Particles from Gas Saturated Solutions (PGSS®) (figure 3), in this process carbon dioxide is the solute. Copper nanoparticles have been included into a lipid matrix in order to protect them for biomedical applications, such as, chemotherapy or imaging. This method can be used with dry and wet nanoparticles (particle concentration in aqueous suspension from 0.6 to 50 % w/w are allowed) due to its versatility. Copper nanoparticles are mixed with melting lipid in presence of supercritical carbon dioxide and expanded through a nozzle obtaining particles in micrometric range. In chapter 2, this study is developed.

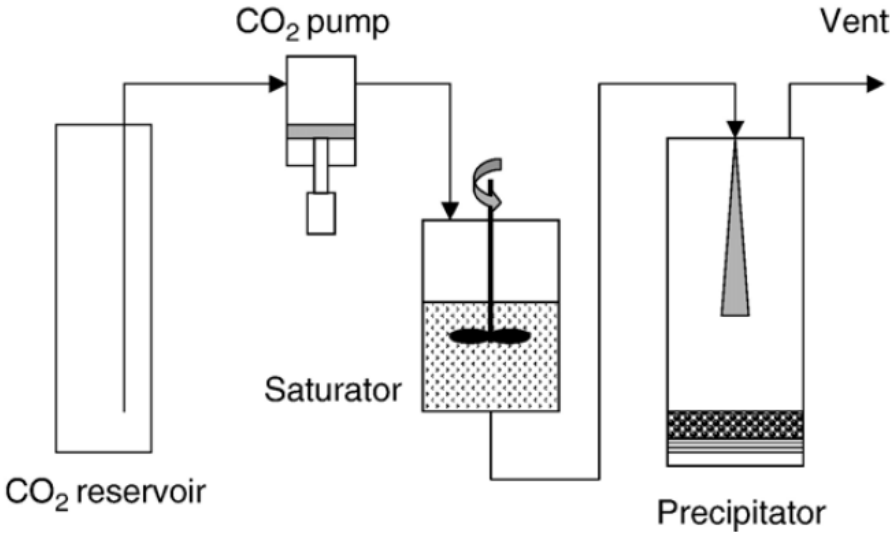

Figure 3: PGSS® process [9].

The second formulation method studied is supercritical antisolvent process (SAS) (figure 4), in a fluidized bed that involves the use of dry nanoparticles. In this case, carbon dioxide acts as antisolvent as well as fluidization agent. The product must be solved in an organic solvent, when the solution is putted in contact with supercritical fluid, the solvent, which has more affinity with SC-CO_2 is eliminated and the solute precipitates over the particle surface. Titanium oxide nanoparticles (particles objective in

SHYMAN project) have been coated with a polymer to protect them and improve properties, such as bulk density (handling enhancement). Pristine dry nanoparticles, due to their small size show high cohesion tendency, due to cohesive forces: Van der Waals attractive forces, electrostatic attractive or repulsive forces and liquid bridges, form nanoparticle agglomerates [10] and will be therefore, processed in this manner. In order to perform this study, it is divided in two parts: Firstly, in chapter 3, it is demonstrated that fluidization of nanoparticle agglomerates with supercritical carbon dioxide is enhanced, and next, in chapter 4, the coating process with a ethanolic polymer solution is evaluated taking into account all process parameters (carbon dioxide and polymer solution flow rates, temperature, pressure and polymer concentration). Chapter 3 shows fluidization while coating process is developed in chapter 4.

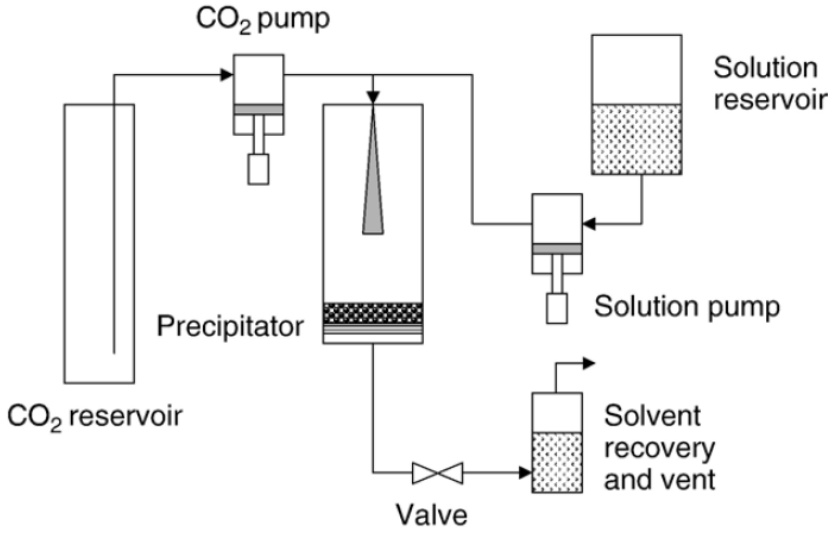

Figure 4: SAS process [9].

With this thesis, the knowledge in formulation of nanoparticles will be augmented, extending SHYMAN project frontiers with dry formulations and other aqueous nanoparticle synthesis method.

This thesis main objectives are:

1) Synthesis of metallic copper nanoparticles with grape pomace extract, a wine production waste, as reducing agent, as well as capping agent:

- Study of principal process variables (temperature, operation time and reagents amount) effect in final product particle size and process yield.
- Study of particle growth during the synthesis and the influence of the concentration of main phenolic compounds along the reaction
- Study of nanoparticle morphology and chemical composition.

2) Formulation of copper nanoparticles with a lipid compound for potential biomedical applications with PGSS® process:

- Stablish the PGSS® process optimal conditions according to process yield and product particle size: Temperature, pressure, nanoparticle load and water content.
- Study of nanoparticle dispersion into the lipid matrix.

3) Coating of titanium dioxide nanoparticles with a polymer by means of process that combines SC-CO_2 fluidized bed and SC-CO_2 antisolvent precipitation technologies:

- Study of nanoparticle fluidization with supercritical carbon dioxide: minimum fluidization velocity variation with carbon dioxide density and powder properties (primary particle size, agglomerate size and bulk density).
- Study of the effect of main variables of the combined process (carbon dioxide ratio respect minimum fluidization velocity, carbon dioxide density, polymer solution concentration and flowrate, polymer-particle ratio) on coating process quality verified by process yield, final particle size and coating uniformity.

REFRENCES

1. Limited, R.E.-S.P., *Global Nanotechnology Market Outlook 2022*. 2015.

2. J. Sierra-Pallares, T. Huddle, E. Alonso, F.A. Mato, J. García-Serna, M.J. Cocero, and E. Lester, *Prediction of residence time distributions in supercritical hydrothermal reactors working at low Reynolds numbers.* Chemical Engineering Journal, 2016. **299**: p. 373-385.

3. A.K. Mittal, Y. Chisti, and U.C. Banerjee, *Synthesis of metallic nanoparticles using plant extracts.* Biotechnology Advances, 2013. **31**: p. 346-356.

4. O.V. Kharissova, H.V. R. Dias, B.I. Kharisov, B.O. Pérez, and V.M.J. Pérez, *The greener synthesis of nanoparticles.* Trends in Biotechnology, 2013. **31**(4): p. 240-248.

5. S. Horikoshi and N. Serpone, *Introduction to Nanoparticles*, in *Microwaves in Nanoparticle Synthesis*, Wiley-VCH Verlag GmbH & Co. KGaA, Editor. 2013.

6. G.T. Vladisavljevíc, *Structured microparticles with tailored properties produced by membrana emulsification.* Advances in Colloid and Interface Science, 2015. **225**: p. 53-87.

7. R. Ladj, A. Bitar, M.M. Eissa, H. Fessi, Y. Mugnier, R.L. Dantec, and A. Elaissari, *Polymer encapsulation of inorganic nanoparticles for biomedical applications.* International Journal of Pharmaceutics, 2013. **458**: p. 230-241.

8. C.A. García-González, A.R. Sampaio da Sousa, A. Argemí, A. López Periago, J. Saurina, C.M.M. Duarte, and C. Domingo, *Production of hybrid lipid-based particles loaded with inorganic nanoparticles and active compounds for prolonged topical release.* International Journal of Pharmaceutics, 2009. **382**: p. 296-304.

9. A. Martín and M.J. Cocero, *Micronization processes with supercritical fluids: Fundamentals and mechanisms.* Advanced Drug Delivery Reviews, 2008. **60**: p. 339-350.

10. J.R van Ommen, J.M. Valverde, and R. Pfeffer, *Fluidization of nanopowder: a review*. Journal of Nanoparticle Research, 2012. **14**.

CHAPTER 1

Green Synthesis of Copper Nanoparticles with Grape Pomace Extract

Abstract

The synthesis of metallic nanoparticles is a promising field where Green Chemistry approach is specially focused in to propose novel processes to reduce the dangerous organic compounds used in conventional techniques. In this study bioreduction is proposed as green alternative process to synthesize copper nanoparticles from a copper salt using grape pomace extract as reducing agent.

This extract, a byproduct of red wine production, has both the reducing compounds, as phenolic acids, and capping agents, as flavonols, that control the size during the reaction. The influence of process variables in yield and copper particle size was studied using a Box-Behnken design of experiments varying temperature (30ºC - 80ºC), reaction time (60 - 180 minutes), and antioxidant – copper ion ratio (0.01 - 0.1 g GAE/g Cu ion). Nanoparticles growth was followed over reaction time finding a first controlled phase where particle size remains essentially constant and a second phase where size increases rapidly due to the insufficient concentration of capping agents in the medium.

Metallic copper state of nanoparticles was verified by EDS and XRD. Particle morphology was shown by TEM.

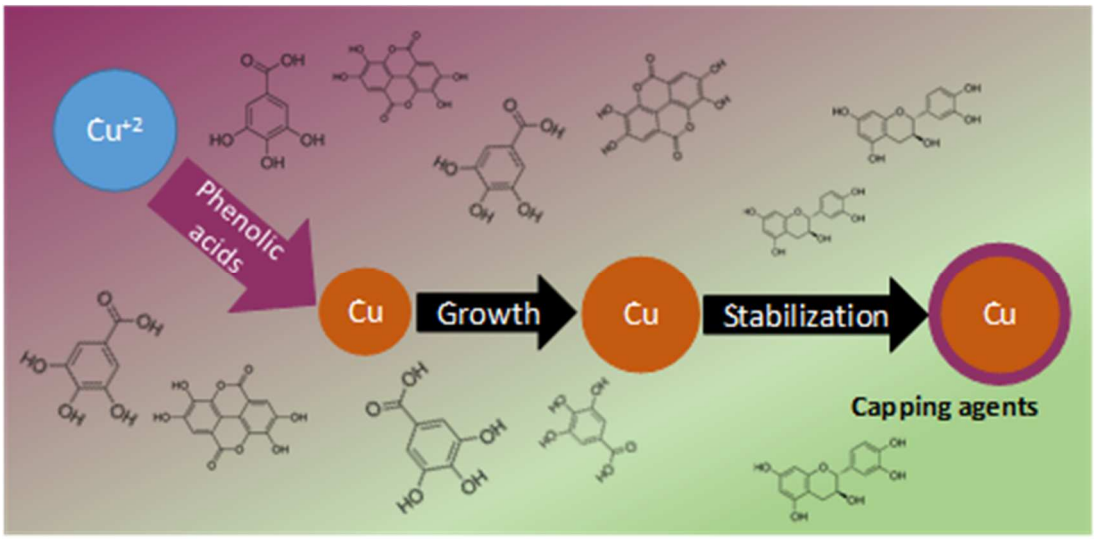

1. Introduction

Copper nanoparticles have a lot of interest due to their high stability, catalytic properties, electrical and thermal conductivity and low cost comparing to other metallic particles. All these properties give this material a high range of applications as heat transference systems, antimicrobial systems owing to its cytotoxic activity, sensors and catalyst [1]. Also it has been found anti-cancer and anti-fungal activity in these particles [2]. In the synthesis of nanoparticles, it is critical to control factors, which affect the nanoparticle properties such as size, shape and monodispersity [1, 3]. Traditionally, the methods used to achieve the required specifications are chemical methods such as chemical reduction, micro-emulsions, thermal decomposition and electrochemical synthesis. The mentioned bottom up processes use toxic chemicals such as hydrazine, sodium borohydride or cetyl-trimethylammonium bromide; or they involve the use of high pressure and temperature as in thermal decomposition or high amounts of electrical energy as in electrochemical processes [1].

In general, the methods for obtaining nanoparticles can be classify as “top down” or “bottom up” techniques. In bottom up processes, as the ones referred previously, nanoparticles grow from smaller entities. Other conventional bottom up methods, are vapor deposition, atomic/ molecular condensation, sol-gel, spray or laser pyrolysis or aerosol. In contrast, top down methods are based on reducing bulk material size by physical and chemical methods like mechanical milling, chemical etching, thermal or laser ablation, explosion processes or sputtering [4]. In both approaches, the consumption of great amounts of energy and/ or the use of hazardous reagents is involved.

Green chemistry has the main objectives of design new synthesis pathways to a) reduce or eliminate the use and generation of toxic substances for human health and environment, b) use the energy efficiently. Besides, it is important to use renewable raw materials rather than depleting when it is possible [5]. In order to transform the synthesis of Cu-nanoparticles in a process within the framework of green chemistry bioreduction of cupper ion has been applied.

Bioreduction is the reduction process carried out by cells in their metabolism. Microbial synthesis is scalable, environmental benign and compatible with medical applications, though the production of microorganism is expensive in comparison with other methods and several steps of purification processes are necessary to obtain the

particles. Alternatively, cell-free aqueous extract (i.e. plants, fungi or algae extracts) have both the reducing and the capping agents to carry out the metal reaction [4, 6], therefore they can be used directly and the cost associated to this raw material is not high. These characteristics make bioreduction with aqueous extracts compatible with green chemistry principles since it uses renewable raw materials, non-hazardous compounds, non-toxic solvents, the pressure and temperature conditions are near to ambient and the number of steps in the synthesis is reduced [3].

Green synthesis of nanoparticles by means of plant extracts (bioreduction) is simple. The extract is put in contact with a metal salt solution, in a short time comparing to conventional process, the reaction is complete. Similarly to conventional process, synthesis of metallic particles by bioreduction is carried out in three steps: reduction to metal state, particle growth and stabilization, where capping agents bonds to metal surface avoiding the particle growth, with the advantage that in this green method the extract has already the reducing and capping agents. The reduction is carried out by phenolic, terpenoid, and flavonoids. Some of these molecules such as terpenoids and flavonoids act, as well, like capping agents, stabilizing the particles [2, 6-8].

This process has been widely studied with gold and silver nanoparticles synthetized with extracts of *Ocumum Sanctum* [9], *Cinnamomum Camphora* [10], *Coriandrum Sativum* [8], red and white wine and grape pomace extract [11], *Hibiscus Sabdariffa* [12], *Trichoderma viride* and *Hypocrea lixi* (Fungi) [13], Bacillus amyloliquefaciens [14], orange peel [15] or *Rhizopus oryzae* protein extract [16] among others, obtaining particles in the nanometric scale. However, the green synthesis of copper nanoparticles is not enough studied. It has been achieved by means of L-ascorbic acid solutions [2, 7], and extract from *Ginkgo biloba* [17] or *Euphorbia esula* [18]. These works are not systematic, extracts are not well characterized and they are focused on studying particle morphology, size and reactivity instead of the reaction performance. Also copper (II) oxides have been synthetized [19-22] by bioreduction due to the fact that the most stable form of copper is its oxide form [1].

In this work grape pomace extract is used. Red wine is one of the most important products with a world's production of 29 millions of tons, this production cause the formation of 240 millions of tons of grape pomace, this waste consists of skins, seeds, and pieces of stem, and constitutes about 16% of the original fruit [23]. Grape pomace contains

a variety of polyphenols such as phenolic acids, phenolic alcohols, flavan-3-ols and flavonoids [24]. These compounds are extracted from pomace with a mixture of acidified water and ethanol [25].

The aim of this work is to study the reaction between copper ions and grape pomace extract analyzing the main reaction parameters (temperature, time and extract-copper ions ratio) that influence particle size and process yield. Copper nanoparticle growth variation overtime with temperature and extract ratio has been measured. Further, electrochemical active reducing compounds in extract have been identified and their effect in growth tested. Finally, the obtained nanoparticles have been characterized attending to their composition and morphology.

2. Experimental

2.1 Materials

Copper (II) nitrate trihydrate has been used as copper nanoparticle precursor, it has been obtained from Sigma-Aldrich with a purity of 99%. Grape pomace extract, the reducing agent, was supplied by Matarromera (Spain). The extraction has been carried out with water and ethanol 50% mixture at 60°C [25]. The total concentration of polyphenols in the extract was 3.9 equivalent grams of Gallic acid (GAE) per liter. In order to study the reaction some pure compounds were used: Gallic acid with a purity of 99% and kaempferol with a purity bigger than 90%, both supplied by Sigma Aldrich.

2.2 Experimental procedure

An aqueous solution of copper (II) nitrate 0.124 M was prepared and 100 ml were taken and heated up to the desired temperature. Then, the chosen amount of grape pomace extract was added to the solution and the mixture was stirred during the predefined reaction time. After that process the reaction was stopped rapidly by cooling the vessel in an ice bath. The pH was monitored over the reaction procedure and a constant value about 2.6 was observed.

2.3 Design of experiments (DOE)

In order to study the process main variable effect and reduce the number of experiments carried out, a statistic design of experiment was done. Box-Behnken with three continuous factors response surface was used, each factor took three different levels, and the central point was repeated three times. Temperature (35, 55, 80°C), time (60, 120, 180 minutes) and the amount of extract (0.01, 0.05, 0.1 g GAE per gram of copper (II) ion, that is a volume of extract of 2, 11, 20 mL, respectively, were the continuous factors chosen, being the central point 55°C, 120 minutes and 11 ml of extract, and the output variables were reaction yield and metallic particle size. The order of the experiments was fully random (Table 1). An analysis of variance (ANOVA) with 95% confidence level was done for each response variable in order to test the polynomial model proposed (Eq.1), where Y is the response variable to be optimized, Xj,and Xi are the continuous factors and β0, βj, βjj and βij are the regression coefficients to be determined. B0 is the constant while Xj represents the independent factor, Xj2 the quadratic term and XjXi the interaction between

variables. The significance of each factor was determined using the F-value test, at a 95% confidence level and reported as p-value. Experimental results were analyzed by means of a commercial software (Minitab 17).

$$Y = \beta_0 + \sum_{j=1}^{K} \beta_j X_j + \sum_{j=1}^{K} \beta_{jj} X_j^2 + \sum_{j=1}^{K} \sum_{i=1}^{K} \beta_{ij} X_i X_j \qquad \text{(Eq.1)}$$

Table 1: Design of experiments: summary of results

Std. Order	Run Order	time (min)	Temperature (ºC)	Ratio gGAE/gCu^{+2}	dp (nm)	% Yield
6	1	180	55	0.01	1003	30.7
9	2	120	30	0.01	18	6.2
12	3	120	80	0.1	1140	58.9
8	4	180	55	0.1	2160	52.2
2	5	180	30	0.05	18	11.5
10	6	120	80	0.01	688	30.6
7	7	60	55	0.1	82	9.7
3	8	60	80	0.05	54	15.4
1	9	60	30	0.05	23	5.6
14	10	120	55	0.05	91	11.9
13	11	120	55	0.05	50	12.2
5	12	60	55	0.01	34	6.8
4	13	180	80	0.05	1550	47.6
15	14	120	55	0.05	43	12.4
11	15	120	30	0.10	32	8.3

2.4. Analytical techniques

2.4.1 Measure of reaction yield

Reaction yield was determined by measuring the concentration of unreacted copper (II) ions by Inductive coupling plasma with optic emission spectrometry technic (ICP-OES). It was performed with an atomic emission spectrophotometer ICP-OES Varian 725-ES using argon as carrier gas. Samples of the reaction media were taken after rapid cooling, filtered (0.22 µm, nylon) and storage at -20ºC until analysis. Reaction yield percentage was calculated according to equation 2, where C_0 is the initial copper ion concentration and C_f is the final copper ion concentration in the reaction medium, previously analyzed.

$$\%\, Yield = \frac{C_0 - C_f}{C_0} \times 100 \qquad \text{(Eq. 2)}$$

2.4.2 Analysis of phenolic compounds

The total concentration of phenolic compounds present in grape pomace extract was determined according to the modified Folin Ciocalteau colorimetric method [26-28].

The concentration of discrete phenolic compounds in grape pomace extract have been obtained by high performance liquid chromatography (HPLC) using the method described in literature [29] with a UV-DAD detector Waters 2998 PDA and a column Mediterranea Sea C18 5 µm 250x4.6mm.

The electrochemical characterization of extract and reaction media was performed using a HPLC system Thermo Finnigan (Surveyor model) equipped with an autosampler, pump and photodiode-array detector (PDA) accopled to an ED 40 electrochemical detector, Dionex. Chromatographic separation of compounds was carried out on a Lichrocart RP-18 column (250 x 4 mm, particle size 5 µm, Merck) and a Manu-cart® RP-18 pre-column in a thermostated oven at 35ºC. The detection was monitored using three individual channels, 280, 320 and 360 nm, at a speed of 10 Hz with a bandwidth of 11 nm. In order to prepare the samples of reaction media, copper salt was eliminated by means of a C18 cartridge.

2.4.3 Solid characterization

Particle size was directly measured after rapid cooling the reaction medium by dynamic light scattering (DLS) in a Zetasizer Nano ZS90 (Malvern) with a He-Ne laser of 633nm.

Elemental analysis of final particles was performed by energy dispersive X-ray spectroscopy (EDS) with a Hitachi S2400 equipment with Bruker light elements EDS detector 15 kV. Previously, the sample was dried overnight at 80°C in a conventional oven.

X-ray diffraction has been performed with a Bruker Discover D8 in order to identify the sample composition and its crystallinity. The sample was frozen to -85°C and freeze-dried during 48 hours afterwards, it was measure in the equipment.

Morphology has been characterized by transmission electron microscopy (TEM) using a JEOL JEM-1230 microscope operating at an accelerating voltage of 40 to 120 kV.

3 .Results and discussion

3.1 Effect of main reaction parameters

In order to carry out this study, the design of experiments described in section 2.3 was performed. Copper particle size and copper formation yield were chosen as output variables.

Table 2: ANOVA analysis of the particle size model

Model		p-value
Linear		0.004
	time (min)	0.002
	Temperature (°C)	0.008
	Ratio (gGAE/gCu^{+2})	0.085
Square		0.072
	time (min) x time (min)	0.058
	Temperature (°C) x Temperature (°C)	1.000
	Ratio (gGAE/gCu^{+2}) x Ratio (gGAE/gCu^{+2})	0.036
2-Way Interaction		0.083
	time (min) x Temperature (°C)	0.041
	time (min) x Ratio (gGAE/gCu^{+2})	0.100
	Temperature (°C) x Ratio (gGAE/gCu^{+2})	0.462

In figure 1a, it can be seen the effect of variables in particle size. This variable is linearly affected by temperature and time (p-value < 0.01, Table 2), and to a minor degree by the ratio (p-value<0.05, Table 2). When temperature increases, the size increases due to two effects, the increment of reaction rate and the degradation of capping agents. The effect of time is similar because of the rise in contact time between reagents.

Regarding process yield, all the variables are significant since all the parameters have a p-value lower than 0.05 as can be seen in Table 3, being also the linear coefficients the most significant (p-value<0.05, Table 3). The maximum yield in the studied range is

achieved at high temperature, long times and high extract ratio as figure 1b shown. This behavior is contrary to the production of particles in the nanometric range. Nevertheless, the final particle size of copper nanoparticles can be controlled by the appropriate selection of temperature and reaction time and ca. 100 nanometers particles can be obtained with process yields up to 30%, as it is shown in the contour plot diagram (Figure 2).

Table 3: ANOVA analysis of the % yield model

Model		p-value
Linear		0.001
	time (min)	0.002
	Temperature (°C)	0.001
	Extract Volume (ml)	0.030
Square		0.124
	time (min) x time (min)	0.364
	Temperature (°C) x Temperature (°C)	0.235
	Extract Volume (ml) x Extract Volume (ml)	0.039
2-Way Interaction		0.109
	time (min) x Temperature (°C)	0.098
	time (min) x Extract Volume (ml)	0.211
	Temperature (°C) x Extract volume (ml)	0.098

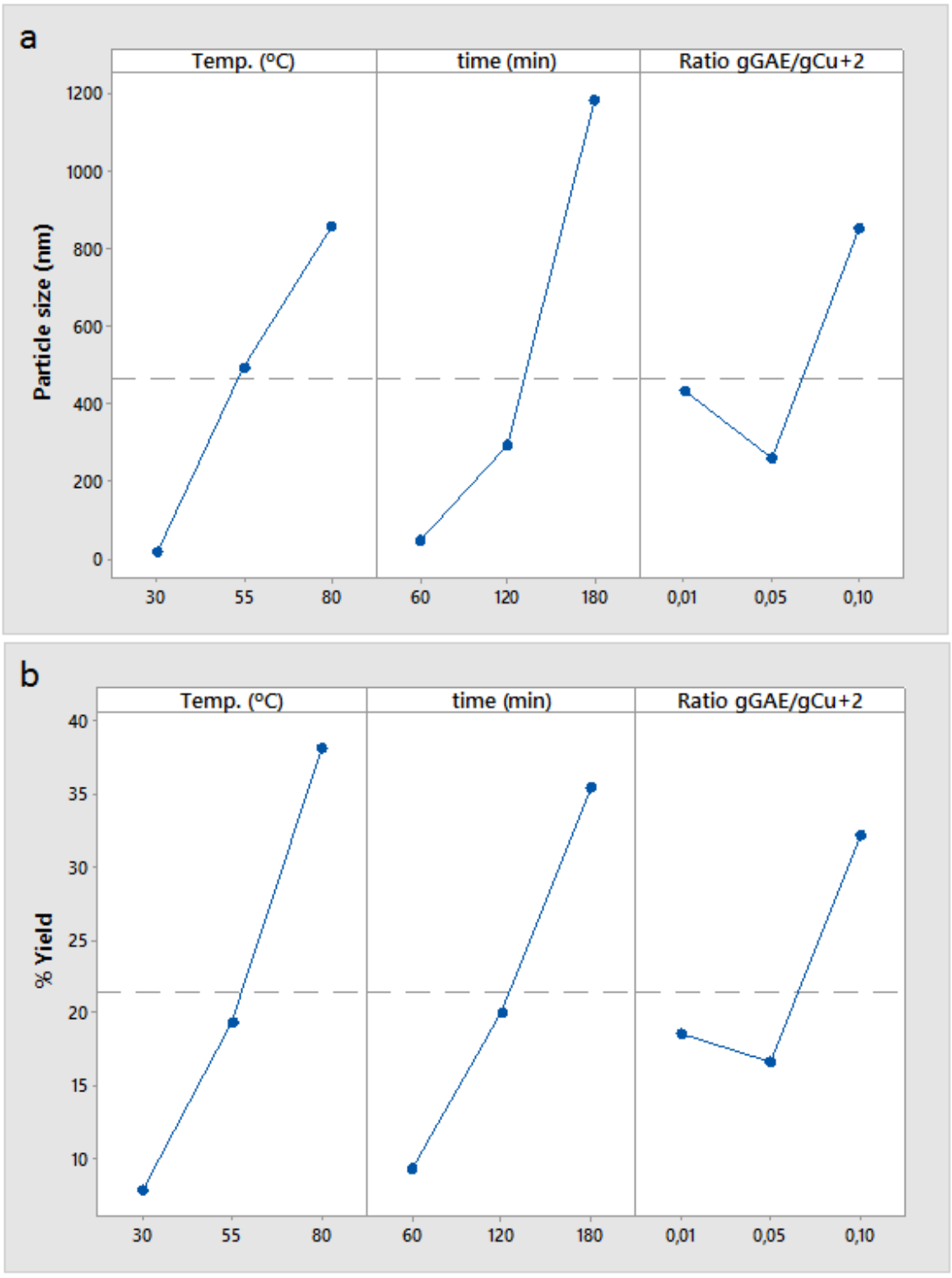

Figure 1: DOE main effects plot for particle size (a) and process yield (b).

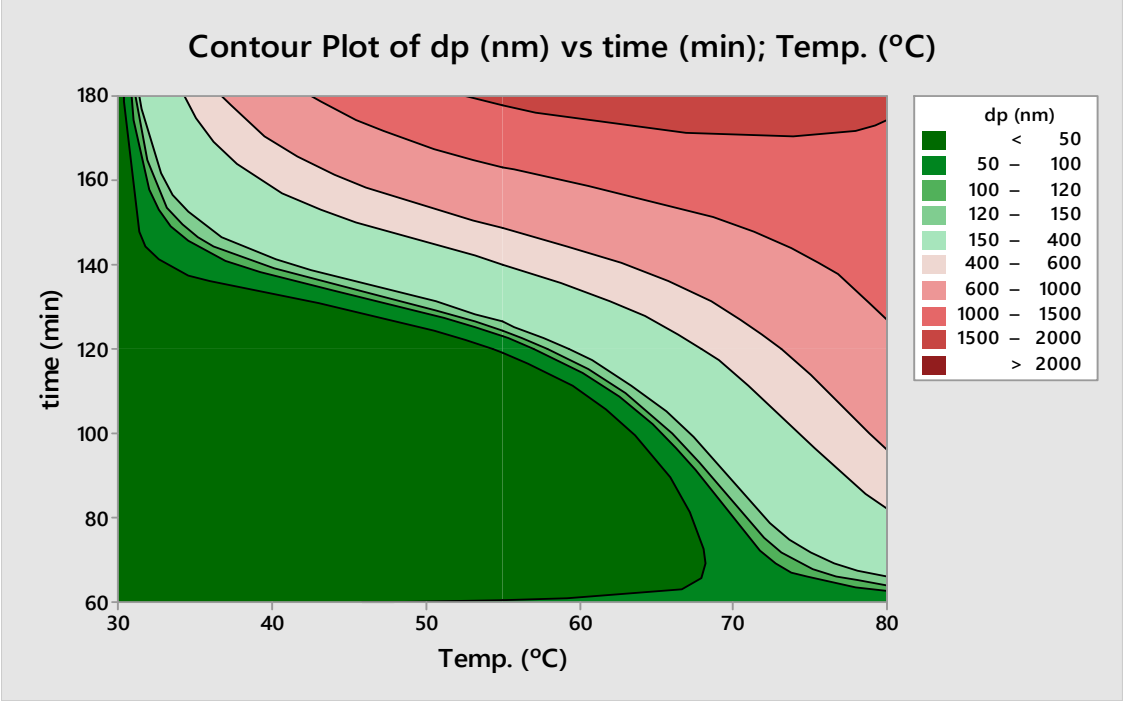

Figure 2: Contour plot diagram of particle size versus time and temperature at 0.05 g GAE/ g Cu^{+2}.

3.2 Growth during the reaction

In order to achieve better control of final particle size, its evolution over time has been recorded. A series of experiments has been performed by measuring particle size distribution during the reaction at 55°C and 80°C with the same extract-copper ion mass ratio. As it can be observed in figure 3a, results show that the particle size is constant in the course of the reaction at 55°C with a value of ca. 60 nm; while in the reaction at 80°C, two behaviors can be observed. From the beginning of the reaction to 90 minutes the particle size is stable around 60 nm, from this point, the particle size increases rapidly, producing an uncontrolled growth. This fact can be due to the reduction of capping agent concentration produced by temperature increment (reaction rate is increased and phenolic compounds are degraded [26]). Hence, metallic particle surface is exposed (no longer protected by capping agents) and nanoparticle coalescence takes place producing the uncontrolled growth of particles.

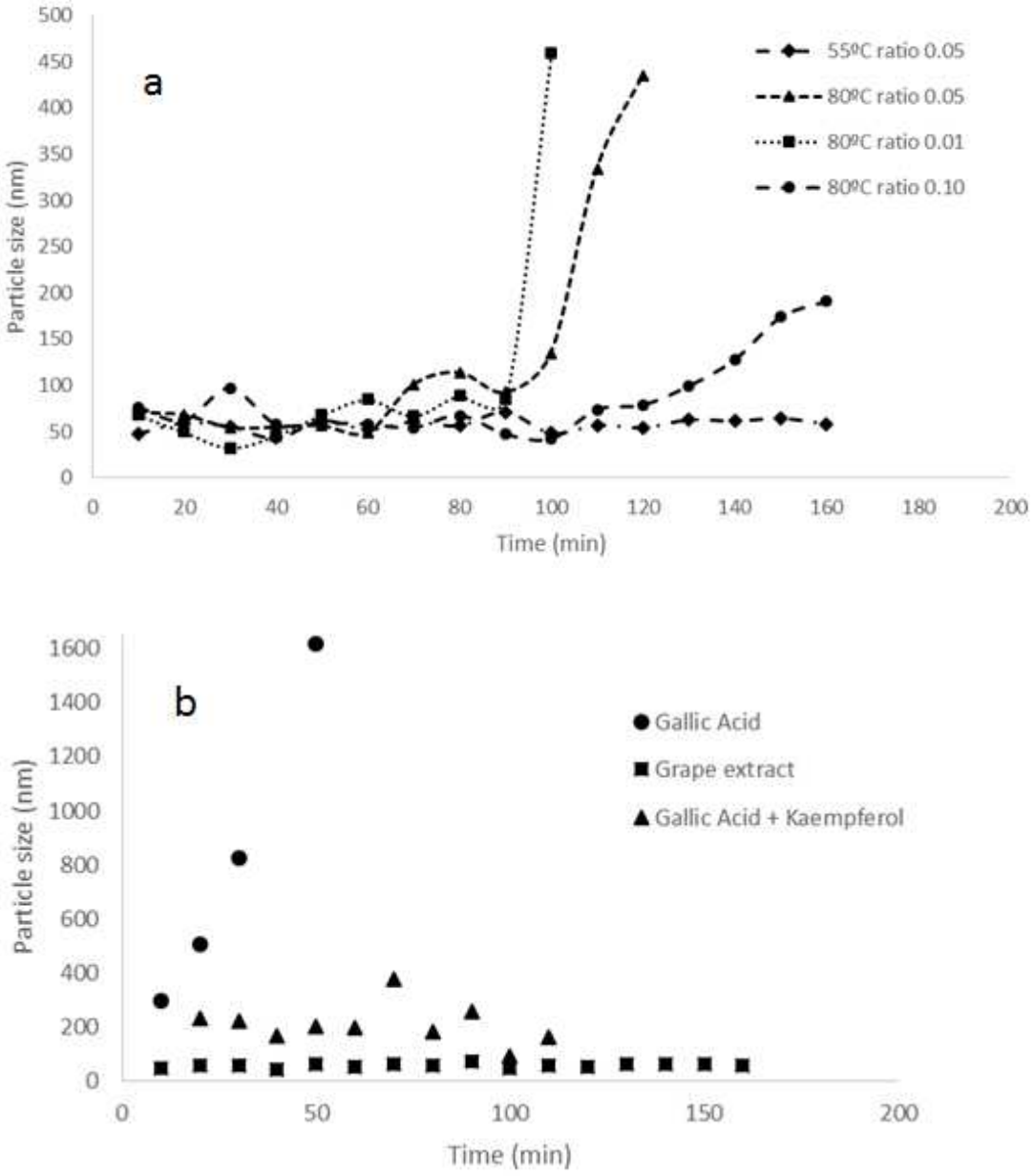

Figure 3: Particle size evolution over time: a) at different operating conditions using grape pomace extract as reducing agent. b) at 55°C with a ratio of 0.05 g GAE/gCu^{+2} using selected reducing agents.

In order to check this hypothesis, a deep study of 80°C reaction has been performed varying extract-copper ion ratio, the extract amount used. When the ratio is 0.01 g GAE/ g copper ion, the uncontrolled growth takes place before and in a faster way than in 0.05 ratio case. That means that the rate of growth in uncontrolled process is higher when the

extract-copper ions ratio is smaller. The same conclusions can be obtained analyzing the reaction results with a ratio of 0.10. These evidences support the previous hypothesis, faster degradation and/ or consumption of capping agents takes place at 80°C because there is a dependence between extract amount used and the length of the duration of the controlled growth period.

3.3 Identification of main active compounds in process

In order to gain an insight in the reaction mechanism, identification of the main compounds in the extract with electrochemical activity has been performed owing to the fact that copper formation is a redox process. Figure 4 shows the profiles of extract and various reaction media at the end of the experiment. It can be observed in extract line that the compounds identified are gallic acid, catechin, 10-cyanidin-3-glucoside and ellagic acid. Gallic and ellagic acids are phenolic acids while catechin belongs to flavonol family, and 10-cyanidin-3-glucoside is an anthocyanin. The following compounds have been identified and quantified, gallic acid (61 mg/L), catechin (60 mg/L) and ellagic acid (5 mg/L), furthermore this extract contains feluric (2.3 mg/L) and cumaric (1.8 mg/L) acids, resveratrol (0.5 mg/L) and quercetin (1.3 mg/L) in a minor concentration, which do not have electrochemical activity but they can act as capping compounds [4].

Experiments in lines B and C are similar (Figure 4). In both cases, anthocyanin and phenolic alcohols disappear totally while catechin (flavonol) continue present in the reaction medium. It is not possible a quantification of disappeared catechin because of the chromatogram is only qualitative. Experiment D shows that the main compounds at 30°C are not totally consumed and phenolic acids are still present, meaning that this temperature is not enough to carry out the reaction at high rate. The same peaks can be observed in experiment E at 80°C, in this case the reaction takes place quickly but there is a high

concentration of polyphenols after 120 minutes, since initial ratio of polyphenols to copper ion was high, which explain the controlled growth seen in the previous section.

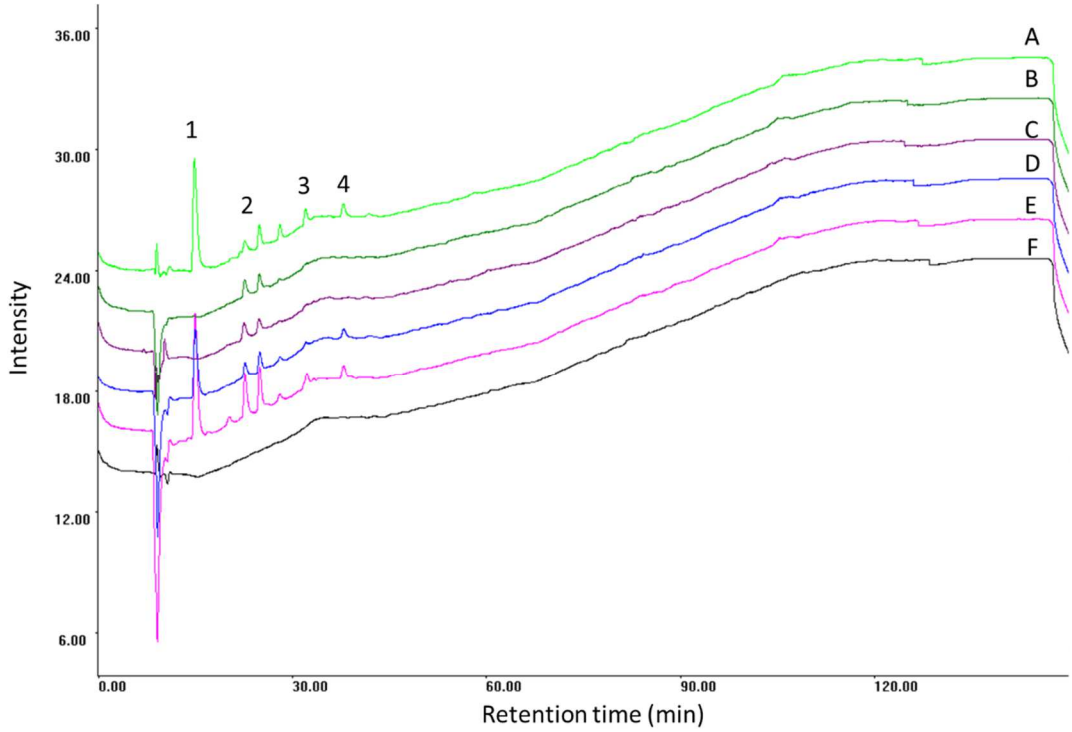

Figure 4: High performance liquid chromatography (HPLC) electrochemical qualitative profile: A: Grape Pomace Extract, B: Experiment (55°C/0.05/120 min), C: Experiment (80°C/0.05/60 min), D: Experiment (30°C/0.05/180 min), E: Experiment (80°C/0.10/120 min) and F: Solvent (Water). The identified compounds are gallic acid (1), catechin (2), 10-cyanidin-3-glucoside (3) and rutin + ellagic acid (4).

In order to check the effect of flavonols as capping agents, the reaction has been performed only with gallic acid as reducing agent (0.05 gGA/gCu^{+2}), as it can observed in figure 3b, in 50 minutes the particle growth from atomic size to more than 1 micrometer. Adding kaenpferol (<0.02 mg/mL), a flavonoid compound, in the gallic acid solution, the behavior is totally different. In this case, the particle size overtime is constant. This result confirms the capping effect of flavonols in the reaction [4, 7].

3.4 Chemical and morphological nanoparticle characterization

Copper obtained nanoparticles have been analyzed by mean of two technics owing to know their chemical composition, these technics are energy dispersive X-ray spectroscopy (EDS) and X-ray diffraction (XRD). Figure 5a shows EDS nanoparticle spectrum, it can be observed the three metallic copper characteristic peaks (CuLα, CuKα and CuKβ) with a high intensity signal, which confirm copper presence in the product. The cupper atomic composition in the sample was 28.4%. In the spectrum, traces of gold are detected (0.5%) owing to SEM coating. The remainder of the total composition is carbon (29.8%) and oxygen (40.2%). The presence of carbon is due to organic material residues from the extract stuck on particle surface; the oxygen can be from the organic rest of the extract, bond with carbon, or it can come from metal oxides formed during nanoparticle drying process, a necessary step to perform these two characterization techniques.

Thanks to EDS technic the main elements in the particles have been identified, but this information is not enough, XRD complete the chemical characterization, it shows how the compounds are bond through material crystallinity. The XRD pattern can be observed in figure 5b. The main peaks of three related compounds are identified CuO, Cu_2O and metallic Cu. It can be concluded that the nanoparticles are a mixture of metallic copper and its oxides owing to drying step. The reaction product is metallic copper; besides, the acid pH of the reaction media prevents the production of copper oxide.

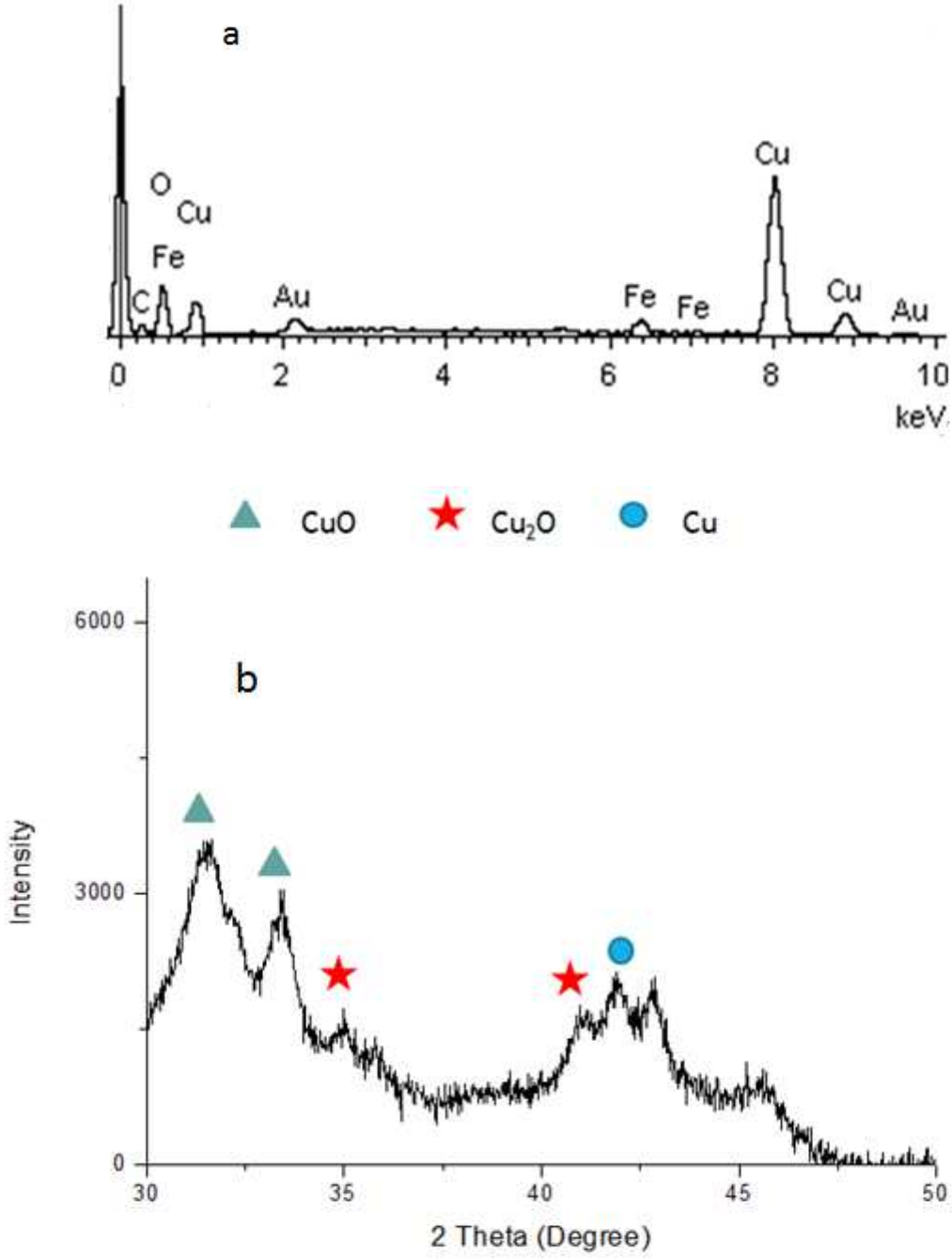

Figure 5: Chemical characterization of copper synthetized nanoparticles a) EDS spectrum. b) XRD spectrum

As it can be seen in figure 6, TEM microscopy shows particles of copper in aqueous suspension. Dispersed nanoparticles with narrow particle size distribution and spherical shape can be observed.

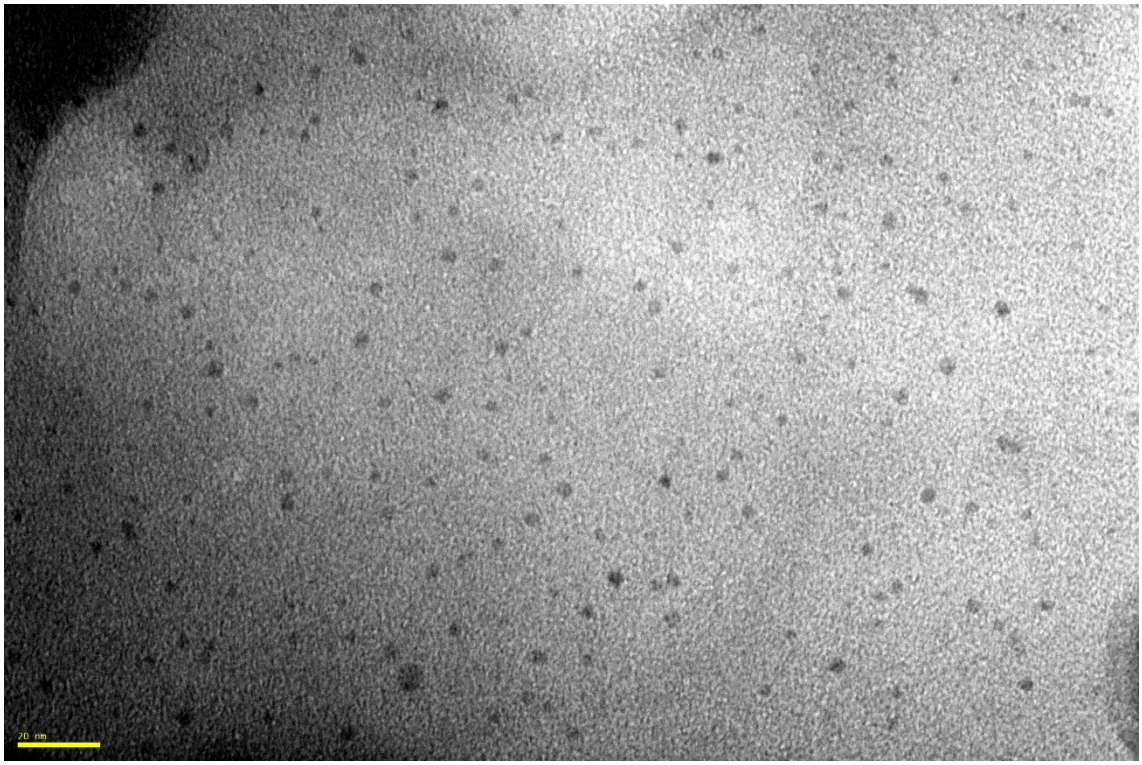

Figure 6: TEM image of copper nanoparticles obtained at 80°C, 100 minutes and an antioxidant ratio of 0.05 (scale bar 20 nm).

4. Conclusions

In summary, it has been demonstrated that copper nanoparticles can be produced by means of a simple method that reduce the process environmental impact by following the principles of green chemistry, i.e. replacing toxic reagents and using near ambient conditions. Bioreduction synthesis method allows to obtain particles (30 % yield:) with a size around 65 nanometers at 80°C with a reactant ratio of 0.1 g GAE/g Cu^{+2} and a reaction time of 100 minutes. The active compounds in red grape extract have been identified by HPLC coupled with electrochemical detector being phenolic acids and anthocyanins responsible for the reduction of copper ions to metallic state, and flavonols those working as capping agents, as expected according to literature. Capping agents control the particle size during the reaction, although their effect is reduced at high temperatures due to the increase in the reaction rate and to their thermal degradation. The obtained nanoparticles are composed by metallic copper and their morphology is spherical.

REFERENCES

1. F. Parveen, B. Sannakki, M.V. Mandke and H.M. Pathan. Copper nanoparticle: Synthesis methods and its light harvesting performance. *Solar Energy Materials & Solar Cells*, 2016, 144, 371-382.

2. M. Valodkar, R.N. Jadeja, M.C. Thounaojam, R.V. Devkar, and S. Thakore. Biocompatible synthesis of peptide capped copper nanoparticles and their biological effect on tumor cells. *Materials Chemistry and Physics*, 2011, 128, 83-89.

3. M. Cinelli, S. R. Coles, M. N. Nadagouda, J. Btaszczynski, R. Stowinski, R.S. Varma and K. Kirwan. A green chemistry-based classification model for the synthesis of silver nanoparticles. *Green Chemistry*, 2015, 17, 2825-2839.

4. A.K. Mittal, Y. Chisti, and U.C. Banerjee. Synthesis of metallic nanoparticles using plant extracts. *Biotechnology Advances*, 2013, 31(2), 346-356.

5. P.T. Anastas and J.C: Warner, Green Chemistry: Theory and Practice, Oxford university Press, New York, 1998.

6. O.V. Kharissova, H.V. Dias, B.I. Kharisov, B.O. Perez, and V.M. Perez. The greener synthesis of nanoparticles. *Trends in Biotechnology*, 2013, 31(4), 240-248.

7. J. Xiong, Y. Wang, Q. Xue, and X. Wu. Synthesis of highly stable dispersions of nanosized copper particles using L-ascorbic acid. *Green Chemistry*, 2011, 13, 900-904.

8. G.M. Nazeruddin, N.R. Prasad, S.R. Prasad, Y.I. Shaikh, S.R. Waghmare, and P. Adhyapak. *Coriandrum sativum* seed extract assisted in situ green synthesis of silver nanoparticle and its anti-microbial activity. *Industrial Crops and Products*, 2014, 60, 212-216.

9. D. Philip and C. Unni. Extracellular biosynthesis of gold and silver nanoparticles using Krishna tulsi (*Ocimum sanctum*) leaf. *Physica E*, 2011, 43, 1318-1322.

10. J. Huang, L. Lin, Q. Li, D. Sun, Y. Wang, Y. Lu, N. He, K. Yang, X. Yang, H. Wang, W. Wang, and W. Lin. Continuous flow biosynthesis of silver nanoparticles by lixivium of sundried *Cinnamomum camphora* leaf in tubular microreactors. *Industrial and Engineering Chemistry Research*, 2008, 47, 6081-6090.

11. B. Baruwati and R.S. Varma. High value products from waste: Grape pomace extract a three in one package for the synthesis of metal nanoparticles. *ChemSusChem*, 2009, 2, 1041-1044.

12. P. Mishraa, S. Raya, S. Sinhaa, B. Das, Md. I. Khana, S. K. Beherac, S. Yund, S. K. Tripathya and A. Mishra. Facile bio-synthesis of gold nanoparticles by using extract of *Hibiscus sabdariffa* and evaluation of its cytotoxicity against U87 glioblastoma cells under hyperglycemic condition. *Biochemical Engineering Journal*, 2016, 105, 264-272.

13. A. Mishra, M. Kumari, S. Pandey, V. Chaudhry, K.C. Gupta and C.S. Nautiyal. Biocatalytic and antimicrobial activities of gold nanoparticles synthesized by *Trichoderma sp*. *Bioresource Technology*, 2014, 166, 235-242.

14. X. Wei, M. Luo, W. Li, L.Yang, X. Liang, L. Xu, P. Kong and H. Liu. Synthesis of silver nanoparticles by solar irradiation of cell-free *Bacillus amyloliquefaciens* extracts and $AgNO_3$. *Bioresource Technology*, 2012, 103, 273-278.

15. G. A. Kahrilas, L. M. Wally, S. J. Fredrick, M. Hiskey, A. L. Prieto and J. E. Owens. Microwave-assisted green synthesis of silver nanoparticles using orange peel extract. *ACS Sustainable Chem. Eng.*, *2*014, 2 (3), 367–376.

16. S.K. Das, C. Dickinson, F. Lafir, D.F. Brougham and E. Marsili. Synthesis, characterization and catalytic activity of gold nanoparticles biosynthesized with *Rhizopus oryzae* protein extract. *Green Chemistry*, 2012, 14, 1322-1334.

17. M. Nasrollahzadeh and S.M. Sajadi. Green synthesis of copper nanoparticles using *Ginkgo biloba L*. leaf extract and their catalytic activity for the Huisgen [3+2] cycloaddition of azides and alkynes at room temperature. *Journal of Colloid and Interface Science*, 2015, 457, 141-147.

18. M. Nasrollahzadeh, S.M. Sajadi, A. Rostami-Vartooni, M. Bagherzadeh and R. Safari. Immobilization of copper nanoparticles on perlite: Green synthesis, characterization and catalytic activity on aqueous reduction of 4-nitrophenol. *Journal of Molecular Catalysis A: Chemical*, 2015, 400, 22–30.

19. R. Sivaraj, P.K. Rahman, P. Rajiv, H.A. Salam, and R. Venckatesh. Biogenic copper oxide nanoparticles synthesis using *Tabernaemontana divaricate* leaf extract and its antibacterial activity against urinary tract pathogen. *Spectrochimica Acta A: Molecular and Biomolecular Spectroscopy*, 2014, 133, 178-181.

20. Jayalakshmi and A. Yogamoorthi. Green synthesis of copper oxide nanoparticles using aqueous extract of flowers of *Cassia alata* and particles characterization. *International Journal of Nanomaterials and Biostructures*, 2014, 4(4), 66-71.

21. S. Gunalan, R. Sivaraj and R. Venckatesh. *Aloe barbadensis Miller* mediated Green synthesis of mono-disperse copper oxide nanoparticles: Optical properties. *Spectrochimica Acta A: Molecular and Biomolecular Spectroscopy*, 2012, 97, 1140-1144.

22. R. Sankar, P. Manikandan, V. Malarvizhi, T. Fathima, K.S. Shivashangari and V. Ravikumar Green synthesis of colloidal copper oxide nanoparticles using

Carica papaya and its application in photocatalytic dye degradation. *Spectrochimica Acta A: Molecular and Biomolecular Spectroscopy*, 2014, 121, 746-750.

23. C. Botella, A. Diaz, I. de Ory, C. Webb and A. Blandino. Xylanase and pectinase production by Aspergillus awamori on grape pomace in solid state fermentation. *Process Biochem*istry, 2007, 42, 98–101.

24. Y. Lu and L. Yeap Foo. The polyphenol constituents of grape pomace. *Food Chemistry*, 1999, 65, 1–8.

25. C. Moro Gonzalez. Procedimiento de extracción de polifenoles a partir de orujo de uva procedente de destilación. ES 2 319 032 B1, 2010.

26. K. Sólyom, R. Solá, M.J. Cocero and R.B. Mato. Thermal degradation of grape marc polyphenols. *Food Chemistry*, 2014, 159, 361-366.

27. A.T. Serra, R. O. Duarte, M.R. Bronze and C.M.M. Duarte. Identification of bioactive response in traditional cherries from Portugal. *Food Chemistry*, 2011, 125, 318–325.

28. V.L. Singleton and J.A. Rossi. Colorimetry of total phenolics with phosphomolybdic-phosphotungstic acid reagents. *American Journal of Enology and Viticulture*, 1965, 16, 144–158.

29. S. Gómez-Alonso, E. García-Romero, and I. Hermosín-Gutiérrez. HPLC analysis of diverse grape and wine phenolics using direct injection and multidetection by DAD and fluorescence. *Journal of Food Composition and Analysis*, 2007, 20(7), 618-626.

CHAPTER 2

Production of Copper Loaded Lipid Microparticles by PGSS

Abstract

Production of lipid particles loaded with metal nanoparticles by supercritical fluids based process has been barely studied. In this work, glyceryl palmitostearate particles loaded with copper nanoparticles have been produced by PGSS® (Particles from Gas Saturated Solution), that is, through the fast expansion of the melted lipid carrier mixed with copper nanoparticles, saturated with carbon dioxide. The effect of typical PGSS variables, namely pre-expansion pressure (100-150 bar) and temperature (60-80ºC), solute –copper load (0.2-5%) and SCF-carrier ratio (4.5-9 w/w), in final lipid particle size and encapsulation efficiency has been studied. The dispersion of metal nanoparticles in the lipid has been determined by SEM-FIB EDS mapping. In all cases, mean particle size values lower than 70 μm have been obtained, and encapsulation efficiencies around 60% have been achieved. Besides, since nanoparticles are commonly synthetized in aqueous medium, it has been demonstrated that not only the process works with water addiction, but it also improves the dispersion of the metal nanoparticles.

1. Introduction

Nanoparticles, especially noble metal nanoparticles, have an emergent importance in biomedicine field. Their uses are diverse, for example, in molecular imaging, targeted drug delivery systems, targeted therapies (hyperthermia, gene silencing or radiotherapy), and biosensors. These are possible thanks to nanoparticle properties such as specific area, superior narrow range of emission, photo stability, broad excitation wavelength, quantum dots and the possibility of being functionalized [1, 2].

One of the most interesting metal is copper. These transition metal forms have biological activity as anti-inflammatory, anti-proliferative, and biocidal agent, and present some radioisotopes useful for nuclear imaging and radiotherapy [3]. On one hand, copper organometallic complexes can be used to deliver copper ions or radionuclides to diseased tissues or to modify pharmacokinetics. These copper compounds can be managed by organism since copper is an essential microelement in contrary to other transition metals. For example, since copper (II) complexes have anti-inflammatory and anti-proliferative properties, they could be used in chemotherapy. Moreover, copper in metallic form possess antimicrobial activity, already used in agriculture. It can degrade DNA by mean of the generation singlet oxygen [4], because of this, it is studied as anti-cancer and anti-proliferative agent [3, 5, 6].

In order to apply copper nanoparticles for biomedical applications it is necessary to encapsulate it in order to protect the metal until arrives to the desired zone, to avoid the damage owing to their cytotoxicity in heathy cells. Lipids are well tolerated by human body and have low toxicity, for these reasons they are good carriers for this application. Besides, they present advantages over other colloidal carriers in terms of active compound stability and protection. Moreover, lipid formulations can be administrated in inhalable, transdermal, intravenous or oral form [7].

Conventional methods for producing lipid microparticles are microemulsions or double emulsions followed by spray drying or spray chilling [8, 9]. However, these methods involve the use of organic solvents, severe operation conditions and purification steps. PGSS® (Particles from Gas Saturated Solutions) is a technique with the capacity of avoiding conventional technic mentioned drawbacks. In this process, the lipid is melted with the dissolved or suspended active compound, and the final mixture saturated with supercritical carbon dioxide. Then, this suspension is expanded through a nozzle into an

expansion chamber and fine copper lipid coated particles are formed [7, 10, 11]. One of the advantages of PGSS® in relation to other supercritical fluid technologies is that the substance does not need to be soluble in carbon dioxide. Metallic nanoparticles loaded into lipid particles are not enough studied. Bertucco et al. produced lipid microparticles magnetically active with excellent results by mean of this technic with triestearin, phosphatidylcholine and magnetite nanoparticles [12]. In contrast, there are studies about processes in which a polymeric matrix is used in spite of lipid. These processes are based on emulsion technology (microemulsions, miniemulsions, double emulsions) [13, 14]. For example, magnetite nanoparticle loaded in poly (lactic-co-glycolic) acid (PLGA) matrix have been formulated by mean of supercritical fluid extraction of emulsions [15].

In this work, a study of PGSS® process to obtain copper lipid loaded microparticles will be performed. The operation conditions will be chosen regarding the nature of the lipid used and the variation of its properties when supercritical carbon dioxide interacts with it, and the consequence in the final particle morphology and size. Also, the effect of metallic nanoparticle amount in the product and encapsulation efficiency will be studied attempting to establish an operational limit. Finally, because of nanoparticles are usually obtained in aqueous dispersion, the effect of water in the process, in the dispersion of metal in the lipid matrix and particle morphology will be observed.

2. Materials and methods

2.1 Materials

Precirol® ATO 5 (glyceryl palmitostearate) was kindly supplied by Gattefossé (France). Imwitor® 600 was supplied by Sasol (Germany). Carbon dioxide with 99.95 mol% purity was delivered by Air Liquide (Portugal). Copper nanoparticles were purchased from Alfa Aesar with a particle size of 20 to 30 nm. All the chemicals have been used without any purification step.

2.1.1. Biosynthesized copper nanoparticles

Three experiments have been performed using biosynthesized copper nanoparticles with a particle size ($d_{0.5}$) around 40 nm (similar to purchased particles), in order to use a real process. This synthesis has been performed by adding grape pomace

extract (4g of equivalent gallic acid each liter) to copper (II) nitrate solution (30 g/l) with a ratio of 0.1 grams of polyphenols per gram of copper ion at 80ºC during 120 minutes. Then, copper particles were washed with pure water and centrifuged twice. TGA of particles shows a copper content of 41.5%, corresponding to the residual mass of the sample after increasing temperature up to 600ºC, being the other percentage organic material. This technic is capable to synthesize nanoparticles at mild operating conditions and with relative short reaction times, while it contributes to the valorization of a byproduct [16-18].

2.2 Precipitation of copper loaded lipid particles by particles from gas saturated solutions (PGSS®)

In order to produce the loaded particles, Precirol 5 ATO is placed in a 50 cm^3 high pressure stirred vessel, electrically thermostated at the selected operation temperature. Then, the required amount of copper nanoparticles, water (if the experiment needs it), and 3 mg of Imwitor® 600 are added. Imwitor® is a water/oil emulsifier that is necessary to enhance the mixture between water and lipid, since Precirol has low hydrophilic lipophilic balance (HLB = 2). Thereafter, the vessel is closed and the mixture stirring (150 rpm) begins. Carbon dioxide is pumped by a high pressure pneumatic piston pump to the vessel until experimental pressure is achieved.

The mixture and the supercritical carbon dioxide are brought into contact during 15 minutes. Then the mixture is depressurized through a nozzle (250 µm) by means of an automated valve to expansion chamber. In this chamber access, the expanded suspension is mixed with compressed air for improving drying. The particles are collected in an 18 L container. The equipment flow diagram can be seen in figure 1 [10].

First of all, some experiments were performed to check the influence of pressure and temperature in pre-expansion chamber to set these operational variables. Then, copper -lipid ratio, added water and SC-CO_2 – lipid ratio were varied. Random experiments were repeated to check reproducibility of the process.

2.3 Particle characterization

Particles have been characterized regarding their size distribution, morphology and metal dispersion in the lipid matrix.

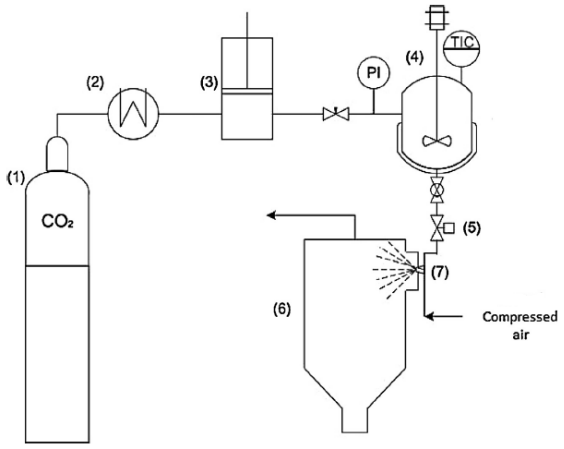

Figure 1: Experimental setup: (1) carbon dioxide cylinder, (2) cryostate, (3) pneumatic pump, (4) stirred vessel, (5) depressurization valve, (6) cyclone and (7) nozzle.

2.3.1 Particle size distribution

Particle size distribution was measured by laser diffraction using a Mastersizer 2000 (Malvern Instruments) with red light (max. 4 mW helium–neon, 632.8 nm). This equipment has an accuracy and a reproducibility better than 1%. The particles were dispersed in water with surfactant (Pluronic) to improve the dispersion due to the Precirol 5 ATO low HLB. The results are expressed as particle volume distribution average diameter ($d_{0.5}$) and spam. Average diameter and spam values are an average from three different measurements. Spam is defined as the ratio between the $d_{0.5}$ and the difference between $d_{0.9}$ and $d_{0.1}$. If the value is near to 1, the particle size distribution is narrow. Precirol refractive index selected was a generic lipid index (1.6).

2.3.2 Morphology and metal dispersion

Particle morphology and copper metallic nanoparticles dispersion in the lipid matrix were analyzed by scanning electron microscopy (SEM). Images were taken by JEOL JSM-820, 20 kV, 23-mm working distance at vacuum conditions equipment. Previous to the analysis, the samples were coated with gold in an argon atmosphere. Furthermore, particles were studied through focused ion beam (FIB) couple to SEM using a Carl Zeiss AURIGA CrossBeam (FIB-SEM) workstation instrument, equipped with an Oxford EDS spectrometer. The particles were dispersed in carbon tape and covered with

an Au/Pd conductive film. Ga^+ ions were accelerated to 30 kV at 50 pA. The etching depth is around 0.2 micron.

2.4 Chemical characterization

The metal load in the particle has been analyzed by inductive coupling plasma with optic emission spectrometry technic (ICP-OES). It was performed with an atomic emission spectrophotometer ICP-OES Varian 725-ES using argon as carrier gas. The samples were digest with nitric acid in a microwave oven in order to oxide copper to ionic state and eliminate the lipid. The results are expressed as mg of copper per gram of lipid. The method has an error in calibration lower than 2%. Some samples were random repeated in order to check the repeatability of process.

Encapsulation efficiency has been calculated from metal load data, as it can be seen in equation 1. C_0 is the theoretical concentration, the product introduced in the process, while C_i is the real concentration measured by ICP.

$$\%\ yield = \frac{C_i}{C_0} \times 100 \quad (1)$$

ICP chemical analysis was confirmed by thermogravimetry analysis (TGA) showing similar data in all the cases with a difference between both methods lower than 7%, additionally the amount of water in the final encapsulated product was obtained. The equipment utilized was TGA/SDTA RSI analyzer of Mettler Toledo. Samples of approximately 10 mg were heated from 50ºC to 600ºC at a rate of 20 ºC/min under N_2 atmosphere (60 N mL/min flow). Water loss was taken into account from 25ºC to 120ºC.

3. Results and discussion

All performed experiment conditions and main results are summarized in table 1.

3.1 Effect of temperature and pressure conditions

The selection of range of temperatures used in this work was made in accordance with the lipid melting point variation in the presence of carbon dioxide, studied by A.R.S. de Sousa et al. [19]. The authors verify that the melting point reduces from 63°C to 50°C, when pressure increases from ambient to 100 bar, then, the value remains almost constant up to 300 bar. For this reason, the range of temperature proved has been between 60 and 80°C, increasing this value to reduce the mixture viscosity [20]. The range of pressure

has been chosen above the critical point and the effect between 100 and 150 bar studied, since at high pressures carbon dioxide solubility enhances [21].

Table 1: PGSS experiment list.

Experiment	Precirol (g)	Copper load (w/w%)	Water content* (w/w%)	Pressure (bar)	Temperature (ºC)	Encapsulation efficience (w/w%)	Particle size $d_{0.5}$ (µm)	Particle size spam
1	2.985	0.5	0	100	60	35	49	1.9
2	2.850	5.0	0	100	60	60	47	1.9
3	2.850	5.0	0	100	80	49	45	1.7
4	2.850	5.0	20	100	60	57	61	2.0
5	2.850	5.0	10	100	60	55	55	1.5
6	2.925	2.5	0	100	60	42	33	2.0
7	2.850	5.0	30	100	60	58	34	1.9
8	2.850	5.0	40	100	60	59	32	1.8
9	2.993	0.2	0	100	60	63	41	1.6
10	2.993	0.2	20	100	60	64	43	1.7
11	2.993	0.2	40	100	60	43	74	1.7
A	2.256	0.083	27	125	70	29	14	1.9
B	2.243	0.083	29	150	80	27	14	1.7
C	2.267	0.083	36	100	60	31	13	1.8

* Water content respect lipid + copper mass.

Concerning particle morphology, it is important to observe that the temperature does not have any effect, as it can be seen in figure 2. The same flaked morphology remains when the temperature increased (Images A and B). The final particle size does not experiment changes when temperature or pressure is increased (previous experiments, not shown). Figure 3 shows two particle size distributions at different values of temperature, maintaining the other parameters constant. The two distributions are almost identical, meaning that particle formation is almost unaffected by neither the temperature nor the pressure in this experimental range.

In conclusion, in the studied range conditions, temperature has effect in the final product quality. In the experiment 2 at 60ºC, encapsulation efficiency is higher than in experiment 3 at 80ºC. For these reasons, the experiments were performed with the lower values of pressure and temperature (60º and 100 bar).

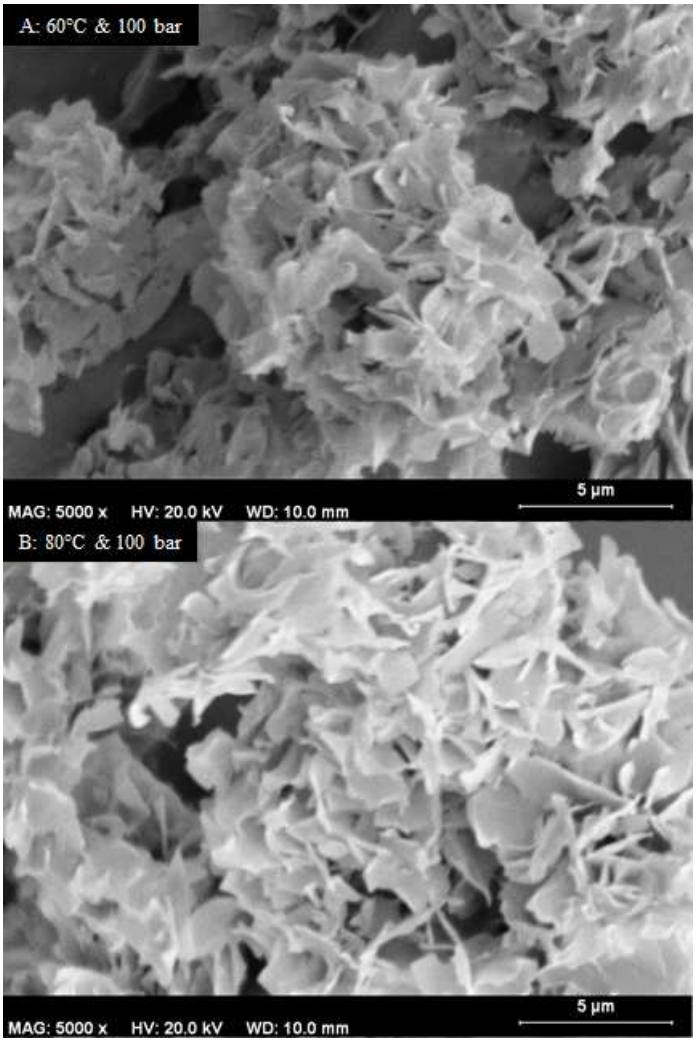

Figure 2: SEM micrographs of copper-lipid particles produced by PGSS®. Particles in A at 60°C and 100 bar (Exp. 2, table 1) and particles in picture B at 80°C and 100 bar (Exp. 3, table 1).

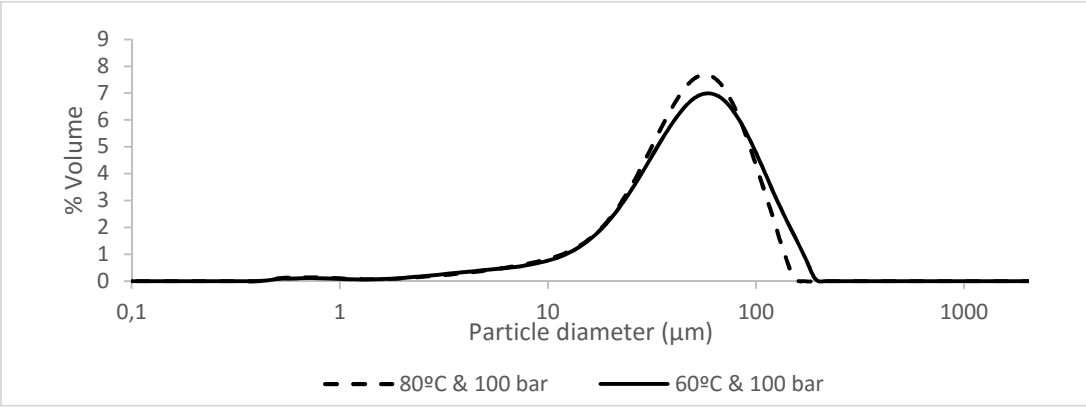

Figure 3: Particle size distributions in volume at various temperature conditions (copper load 0.2%, water amount near 30%) (Exp. 2 and 3, table 1).

3.2 Influence of metal dispersion and metal load

The dispersion of copper nanoparticles in the lipid matrix have been measured. The results can be observed in figure 4.

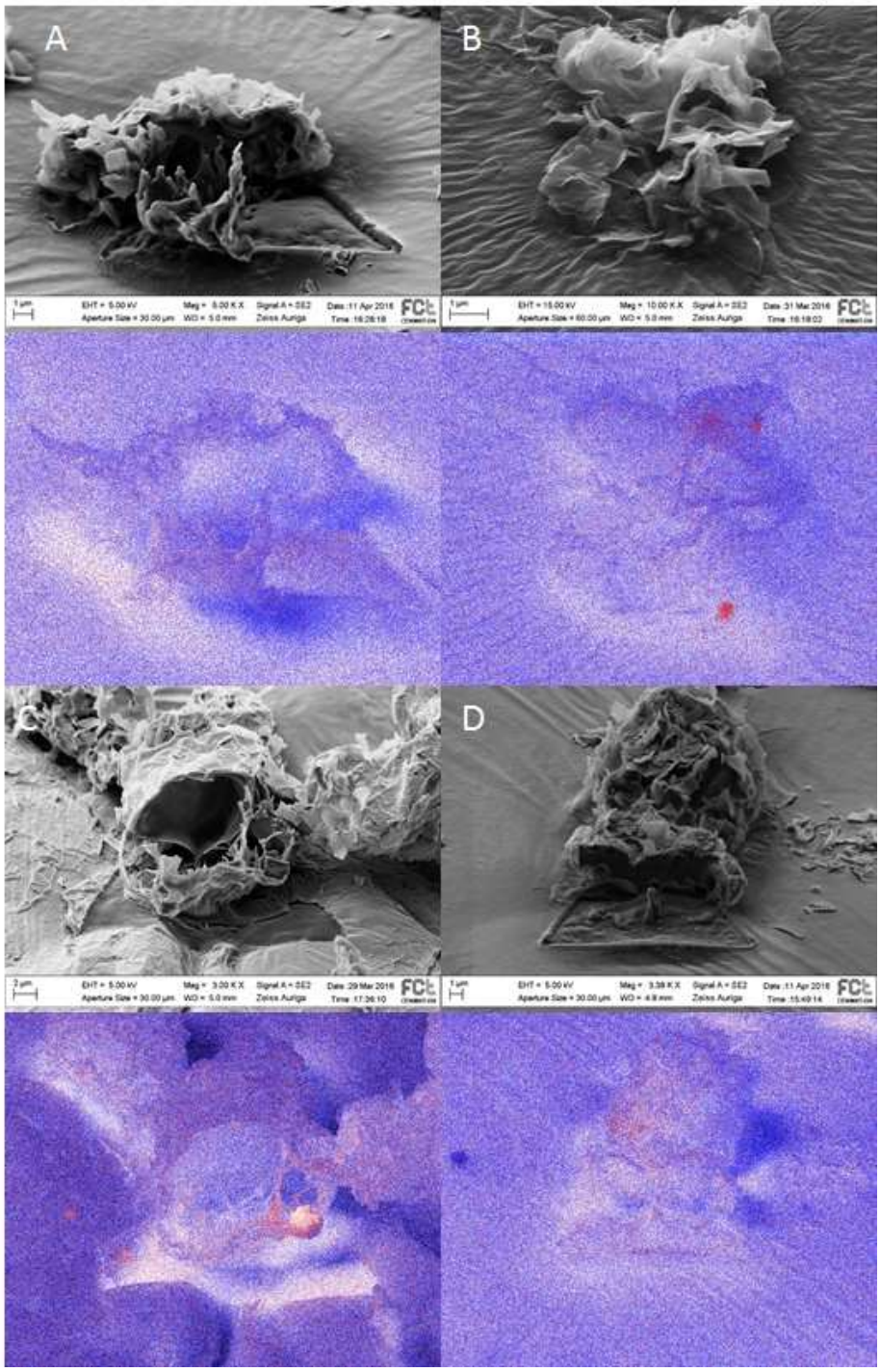

Figure 4: SEM-FIB analysis of copper loaded lipid particles with EDS mapping (blue-Carbon and red-Copper): A-0.2% Cu, T = 60°C , P = 100 bar, initial water content = 0%, B- 5% Cu, T=60°C, P= 100 bar, initial water content = 0%, C- 5% Cu, T=60ºC, P= 100 bar, initial water content = 40% and D- 5% Cu, T=80ºC, P= 100 bar, initial water content = 0%.

In the experiment with 0.2% of copper without water at 60ºC and 100 bar (figure 4.a), it can be seen over the particle a good dispersed copper because of the red color is in the particle contour uniformly, while in the other three images (4b, 4c and 4d), which have 5% of copper, it can be observed tiny particles agglomerations. We can conclude that the higher copper amount in the particle, the higher agglomeration and the worse dispersion. Regarding the influence of temperature, comparing figure 4b and 4d there is not substantial difference between them, agglomerates appear in the lipid structure. Finally, water has a positive effect in the dispersion, in spite of the appearance of big agglomerates, nanoparticles are better distributed because it is detected a homogenous red zone for all the particle, when figures 4b and 4c are compared.

All obtained particles, when it have been cut with FIB technic, have some big hollows spaces inside, and nanoparticles are present in the thin lipid membranes, which define these light structures.

Different values of copper mass were tested. This parameter was varied from 0.007 to 0.150 grams, maintaining the total amount in the chamber of 3.000 grams. These values correspond with a theoretical load from 0.2 to 5%. As it can be seen in figure 5 the efficiency is higher at low loads (0.2%), then the encapsulation efficiency decreases when the load is increased (0.5%), presenting a minimum. This tendency changes and the efficiency augments to achieve similar values to 0.2% when the load is 5%.

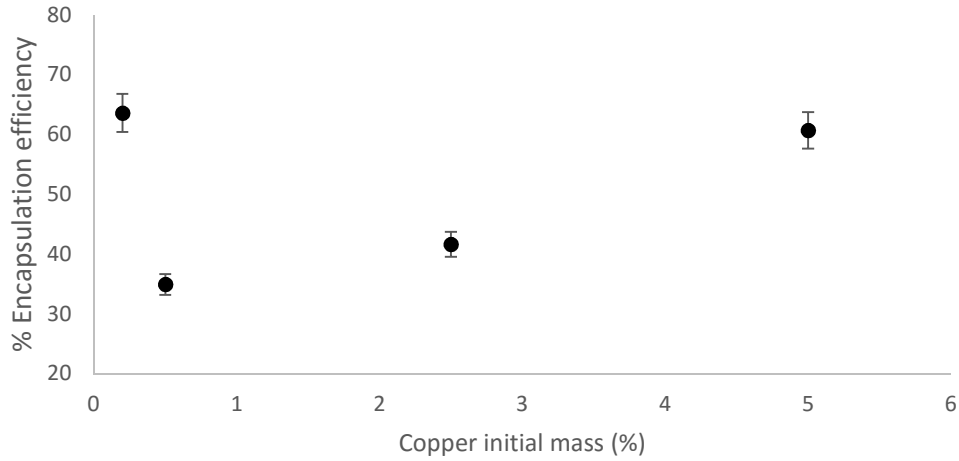

Figure 5: Copper mass influence in encapsulation efficiency.

That fact can be due to mixing chamber stirring system and morphology. At low amounts of copper the dispersion is more homogenous, for this reason the efficiency is high (around 65%). When copper concentration is increased, nanoparticles are agglomerated. This fact added to work in the maximum equipment stirring power, that begins to be insufficient to disperse the amount of nanoparticles introduces in the lipid, implies huge material loss because of sedimentation. On the other hand, the increment of copper mass enhances the encapsulation efficiency from 35% to 60%, thanks to particle agglomerate size increases and it augments the probability of find a bigger number of them suspended in the melted lipid.

Regarding particle size, there are not significantly differences associated to mass copper variation (Table 1. experiments 2, 3 and 9) obtaining values between 43 and 49 µm, unless the experiment with the minimum efficiency, which presents a minor size (33 µm).

3.3 Initial water influence

In numerous processes, it possible to obtain nanoparticles in aqueous suspension (for example bioreduction), trying to reduce separation steps necessaries to obtain solid nanoparticles, PGSS® process has been proved with amounts of water to study the effect in the dispersion and micronization processes.

Water amount was varied from 0 to 40% to determine its effect in process performance at two different copper loads maintaining the other parameter constant. In figure 4, it can be seen an improvement in dispersion but there is not a significant effect on encapsulation efficiency (figure 6), independently of copper load (0.2% and 5%) with the exception when there are low metal loads and high water content (40%). When copper mass is 0.15 g (5% w/w) there is not a significant difference when water is added. On the contrary, when a lower mass of copper is used (0.007 g, 0.2 % w/w), it can be observed the encapsulation efficiency remains constant until a value of water, where the efficiency is reduce from 60 (similar to 5% of copper) to 40%. That fact means, there are a critical water concentration related to copper concentration in the mixture, which gets worse the dispersion of nanoparticles in the pre-expansion chamber.

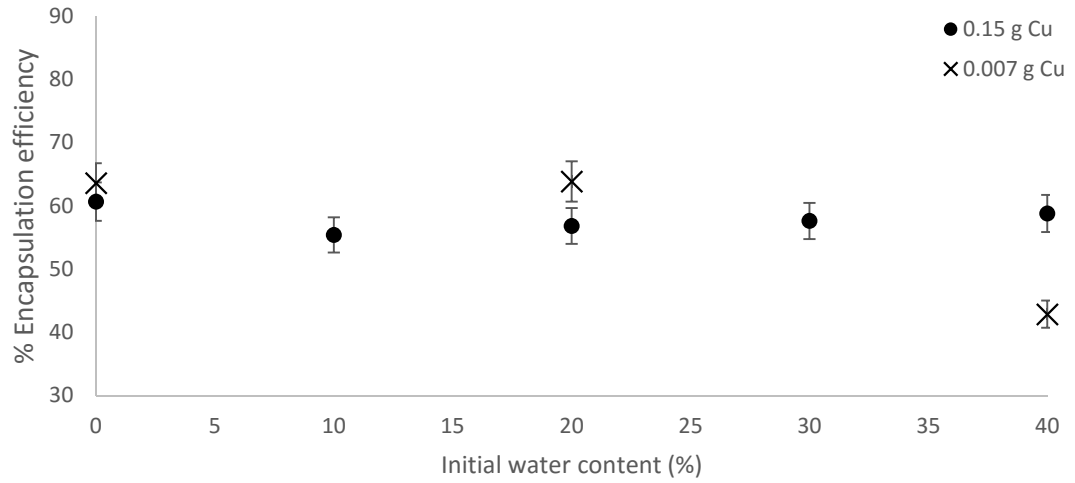

Figure 6: Variation of encapsulation efficiency with initial content of water for different particles loads (Pressure 100 bar, temperature 60 ºC)

On the other hand, particle size behavior presents differences regarding to encapsulation efficiency as can be seen in figure 7. In the highest copper amount proved, when water is increased the size increases too, and then, the tendency is reversed and water reduces final particle size. In contrast, the lowest amount of copper preserves at low water content the size and then, the size is increased.

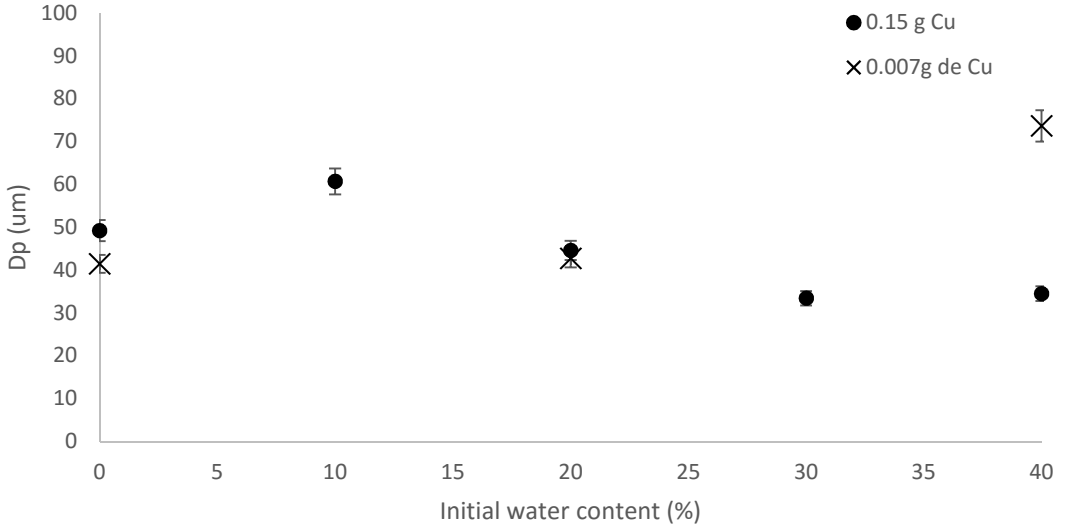

Figure 7: Variation of final product particle size with initial content of water for different particles loads (Pressure 100 bar, temperature 60 ºC)

Regarding particle morphology, water presence makes flaked particles to be more compact as it can be seen comparing figure 8 with figure 2.

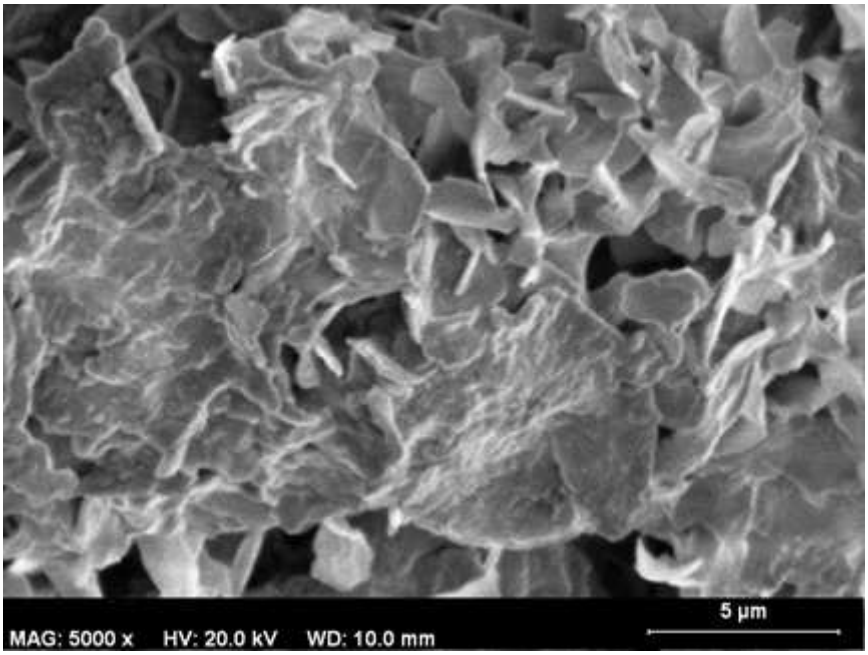

Figure 8: Effect of water in morphology. SEM image from experiment 4 (temperature 60ºC, pressure 100 bar, copper load 5% and water content 20%).

Finally, thermogravimetric analysis shows that the amount of water in the final encapsulate product is over 0.7% for the experiments with the higher amount of water, being a good result which indicates that all the water is eliminated in expansion process.

3.4. Encapsulation of biosynthesized copper nanoparticles

Three experiments have been performed with copper nanoparticles synthesized by bioreduction with grape pomace extract as it have been explain in materials section (2.1.1). In table 1, experiments A, B and C show the results, it can be seen that the results of encapsulation efficiency are lower than the expected, in spite of the low encapsulation load. This fact can be due to the influence of high content of organic impurities present in the particles (51.5% according to TGA results) that can also have an effect in the process and the high amount of particles necessaries to achieve a bigger load in the lipid formulation. A purification process would be necessary to improve the product quality. On the other hand, it is expected that water amount get worst the process as it has been demonstrated in the previous section.

Regarding particle size, particle are lower than 14 µm, but this can be owing to the low load used (0.083%).

4. Conclusions

Lipid microparticles loaded with copper metal nanoparticles have been successfully produced by PGSS process. This is a one-step green process that involves the use of carbon dioxide as unique external agent to generate the particles in the micrometric range from a molten mixture.

Effect of operating conditions has been studied, finding that main process parameters are copper content (%) and water amount (%). When copper mass is augmented the encapsulation efficiency increases, that hardly affect the particle size. About water content, at higher copper amounts the efficiency remains constant while particle size decreases, but at low copper mass the efficiency remains constant up to reach a concentration of water, where the efficiency decreases. The particle size increases with this point is reach.

The better dispersion of nanoparticles in the lipid structure is obtained in the particles with the lowest copper concentration (0.2%) because there are not agglomeration and nanoparticles are present in the whole particle. Temperature has not effect on dispersion, but water content improves it.

Biogenic copper nanoparticles have been successfully encapsulated in lipid. However, lower encapsulation efficiencies were obtained, probably due to the low load of these particles.

REFERENCES

1. M.S. Amjad, N. Sadiq, H. Qureshi, G. Fareed, and S. Sabir, *Nano particles: An emerging tool in biomedicine.* Asian Pacific Journal of Tropical Disease, 2015. **5**(10): p. 767-771.

2. J. Conde, G. Doria, and P. Baptista, *Noble metal nanoparticles applications in cancer.* J Drug Deliv, 2012. **2012**: p. 1-12.

3. P. Szymanski, T. Fraczek, M. Markowicz, and E. Mikiciuk-Olasik, *Development of copper based drugs, radiopharmaceuticals and medical materials.* Biometals, 2012. **25**(6): p. 1089-112.

4. G.P. Jose, S. Santra, S.K. Mandal, and T.K. Sengupta, *Singlet oxygen mediated DNA degradation by copper nanoparticles: potential towards cytotoxic effect on cancer cells.* J Nanobiotechnology, 2011. **9**: p. 9.

5. H. Palza, *Antimicrobial polymers with metal nanoparticles.* Int J Mol Sci, 2015. **16**: p. 2099-116.

6. M. Valodkar, R.N. Jadeja, M.C. Thounaojam, R.V. Devkar, and S. Thakore, *Biocompatible synthesis of peptide capped copper nanoparticles and their biological effect on tumor cells.* Materials Chemistry and Physics, 2011. **128**: p. 83-89.

7. A. R. Sampaio de Sousa, A.L. Simplício, H.C. de Sousa, and C.M.M. Duarte, *Preparation of glyceryl monostearate-based particles by PGSS®—Application to caffeine.* The Journal of Supercritical Fluids, 2007. **43**(1): p. 120-125.

8. A.Puri, K. Loomis, B. Smith, J.H. Lee, A. Yavlovich, E. Heldman, and R. Blumenthal, *Lipid-Based Nanoparticles as Pharmaceutical Drug Carriers: From Concepts to Clinic.* Crit. Rev. Ther. Drug Carrier Syst., 2009. **26**(6): p. 523-580.

9. J.H. Kang and Y.T. Ko, *Lipid-coated gold nanocomposites for enhanced cancer therapy.* International Journal of Nanomedicine, 2015. **10**: p. 33-45.

10. V.S. Goncalves, S. Rodriguez-Rojo, A.A. Matias, A.V. Nunes, I.D. Nogueira, D. Nunes, E. Fortunato, A.P. de Matos, M.J. Cocero, and C.M Duarte, *Development of multicore hybrid particles for drug delivery through the precipitation of CO2 saturated emulsions.* Int J Pharm, 2015. **478**(1): p. 9-18.

11. A. Pestieau, F. Krier, P. Lebrun, A. Brouwers, B. Streel, and B. Evrard, *Optimization of a PGSS (particles from gas saturated solutions) process for a fenofibrate lipid-based solid dispersion formulation.* Int J Pharm, 2015. **485**(1-2): p. 295-305.

12. K. Vezzù, C. Campolmi, and A. Bertucco, *Production of Lipid Microparticles Magnetically Active by a Supercritical Fluid-Based Process.* International Journal of Chemical Engineering, 2009. **2009**: p. 1-9.

13. G.T. Vladisavljevic, *Structured microparticles with tailored properties produced by membrane emulsification.* Adv Colloid Interface Sci, 2015. **225**: p. 53-87.

14. R. Ladj, A. Bitar, M.M. Eissa, H. Fessi, Y. Mugnier, R. Le Dantec, and A. Elaissari, *Polymer encapsulation of inorganic nanoparticles for biomedical applications.* Int J Pharm, 2013. **458**(1): p. 230-41.

15. M. Furlan, J. Kluge, M. Mazzotti, and M. Lattuada, *Preparation of biocompatible magnetite–PLGA composite nanoparticles using supercritical fluid extraction of emulsions.* The Journal of Supercritical Fluids, 2010. **54**(3): p. 348-356.

16. M. Valodkar, R.N. Jadeja, M.C. Thounaojam, R.V. Devkar, and S. Thakore, *Biocompatible synthesis of peptide capped copper nanoparticles and their biological effect on tumor cells.* Materiales Chemistry and Physics, 2011. **128**: p. 83-86.

17. O.V. Kharissova, H.V. Dias, B.I. Kharisov, B.O. Perez, and V.M. Perez, *The greener synthesis of nanoparticles.* Trends Biotechnol, 2013. **31**(4): p. 240-248.

18. A.K. Mittal, Y. Chisti, and U.C. Banerjee, *Synthesis of metallic nanoparticles using plant extracts.* Biotechnol Adv, 2013. **31**(2): p. 346-56.

19. A.R.S. de Sousa, M. Calderone, E. Rodier, J. Fages, and C.M.M. Duarte, *Solubility of carbon dioxide in three lipid-based biocarriers.* The Journal of Supercritical Fluids, 2006. **39**(1): p. 13-19.

20. P. S. Nalawade, F. Picchioni, and L.P.B.M. Janssen, *Supercritical carbon dioxide as a green solvent for processing polymer melts: Processing aspects and applications.* Progress in Polymer Science, 2006. **31**(1): p. 19-43.

21. Z. Mandžuka and Ž. Knez, *Influence of temperature and pressure during PGSS™ micronization and storage time on degree of crystallinity and crystal forms of monostearate and tristearate.* Journal of Supercritical Fluids, 2008. **45**(1): p. 102-111.

CHAPTER 3

Fluidization of Nanoparticles Agglomerates enhanced by Supercritical Carbon Dioxide

Abstract

The present work is focused on the study of fluidization of nanoparticle agglomerates with SC-CO_2 at different temperatures (300-320 K) and pressures (7.7-14.4 MPa). These conditions allow to work in a wide range of density, varying from 200 to 800 kg/m^3. Three materials with different bulk density have been tested: aluminum oxide (Al_2O_3, 40 kg/m^3), titanium oxide (TiO_2, 90 kg/m^3) and magnetite (Fe_3O_4, 840 kg/m^3). Regarding fluidization, two different behaviors have been detected, according to the variation of minimum fluidization velocity (u_{mf}) with carbon dioxide density. At high densities (> 500 kg/m^3) only hydrodynamic forces control the process, therefore, the same behavior of u_{mf} vs density was found for the three materials. Meanwhile at low densities (< 500 kg/m^3) both hydrodynamic and cohesive forces affect the fluidization process. Moreover, minimum fluidization velocity values have been compared with other fluidization enhancing techniques reported in literature for titanium dioxide and aluminum oxide particles: pulsed gas flow and acoustic fields. Regarding the first method, supercritical fluid method achieves minimum fluidization velocities between 10 and 100 times lower, depending on selected density. While comparing with acoustic fields, both methods accomplish similar values (0.02-0.180 cm/s).

1. Introduction

Fluidized bed technology is a proved technology to carry out a lot of different industrial processes (coating, separation, drying, granulation, crystallization, heating/cooling and reaction) due to it permit a good mass and heat transfer [1]. These advantages have been applied widely to particles from millimeters to micrometers, but regarding nanoparticles, this process presents some problems, such as channeling, due to nanoparticle characteristics, such as strong cohesive forces because of their size lower than 100 nm. They are not fluidized as individual entities, but as agglomerates [2].

Main parameter of fluidized bed is the minimum fluidization velocity that this point the pressure drop behavior of a fixed bed is described by Ergun's equation (Eq.1), derived from Navier-Stokes equation for Newtonian fluids that flows through a particle bed. This equation takes into account the viscous and inertial forces. When pressure drop is equal to effective bed weight (Eq.2), it represents fluidized state and can be used to determine minimum fluidization velocity.

$$-\frac{\Delta P}{H} = 150\frac{(1-\varepsilon)^2}{\varepsilon^3}\cdot\frac{\mu\cdot u}{\left(\phi_s\cdot d_{p,s}\right)^2} + 1.75\frac{(1-\varepsilon)}{\varepsilon^3}\cdot\frac{\rho_f\cdot u^2}{\phi_s\cdot d_{p,s}} \quad (1)$$

$$\Delta P = \frac{m_p\cdot g\cdot\left(\rho_p-\rho_s\right)}{\rho_s\cdot S} \quad (2)$$

Theoretical calculation of u_{mf} is difficult because of the high variation of some parameters when the bed changes to fluidized state such as porosity (ε) and agglomerate nature, since agglomerate diameter remains unknown and its density is different from that of the material itself and from that of the bulk powder, as it will be discussed in the next sections. Porosity remains constant until pressure drop is equal to bed weight, in this moment the bed expands and this parameter is increased. Minimum fluidization porosity is a high sensitive parameter, its value depends on temperature [3] and pressure [4]. For this reason, some correlations have been stablished for different solids, fluids and operation conditions, their general structure can be seen in equation 3.

$$Re_{mf} = (a^2 + b\cdot Ar)^{0.5} - a \quad (3)$$

Nanoparticles belong to Geldart group C, these particles are characterized by high cohesion tendency. In addition, particles form agglomerates and their particle size augments. The process of agglomeration is consequence of cohesive forces. The most important is London Van der Waals attractive forces, as a result of temporal fluctuations in

the dipolar character, this force is related with the radius, in the case of nanoparticles the radius is extremely small and the force huge [1, 5]. Other cohesive forces are electrostatic interactions due to particle surface electric charge, it can be attractive or repulsive, and liquid bridges when there is a liquid adsorb in particle surface, the absorbed liquid generates bridges between particles, which also cause agglomeration [1, 6]. Van der Waals force dominates in fluid-solid systems when a dry fluid is used [7].

Furthermore, in cohesive particle fluidized beds, there are two types of aggregation, dynamic and stationary. Dynamic aggregation takes place inside the bed when there is dynamic equilibrium between inertial and cohesive forces; aggregates are form and break continuously in collisions. By the other hand, stationary aggregation is due to cohesive forces because of packing conditions during handling, shipping and storage [1]. In order to know the agglomerate size, theoretical estimations based on the balance between buoyancy, gravitational, interparticle and dynamic collision forces, have been developed to ambient conditions [8, 9]. On the other hand, researchers have developed several experimental methods to near ambient conditions, which are used to check enhancing methods, such as laser-based planar imaging [10], particle droplet image analysis (PDIA) [1] or sample extraction systems followed by scattering electron microscopy (SEM) [11].

Many authors classify nanoparticle fluidization in two kinds or regimens, agglomerate particulate fluidization (APF) and agglomerate bubbling fluidization (ABF) [2, 12]. The first type takes place when nanoparticle bulk density is lower than 100 kg/m^3, it is characterized by the formation of porous light agglomerates in a multistage process. The fluidization takes place at very low minimum fluidization velocities, without bubbles formation. Bed expansion is homogeneous and bulk density decreases when fluid rate increases. On the other hand, agglomerate bubbling fluidization takes place when bulk density is higher than 100 kg/m^3, in this case, agglomerates are compact, weighty and they are formed in a single stage. Bulk density does not change when fluid velocity increases. Particulate fluidization is profitable for coating, and in reactions since improves conversion and selectivity, while bubbling fluidized bed, despite the fact that increase particle agglomeration, has excellent properties to maintain the temperature homogeneity in exothermic reactions through enhancing the solid mixing.[13]

Several assisted fluidization methods have been developed to avoid the typical Geldart group C particle problems: agglomeration and channeling. These methods include

the use of surfactants, mechanical vibration, stirring, acoustic fields, pulsed gas flow, centrifugal fields, and magnetic or electric fields, which work breaking particle agglomerates enhancing fluidization quality [2, 11, 14-18].

Other method, which has been evidenced, is supercritical bed fluidization. Supercritical fluids have densities and viscosities with values between those typical for gases and liquids, which can be tuned by means of slight changes in pressure and temperature [19]. Pressure stabilizes the bed and the homogeneous fluidization region is broader. Several researchers have addressed the importance of hydrodynamic forces against interparticle forces, as a factor that stabilizes the homogeneous expanded state of the bed [20]. Furthermore, it has been demonstrated that supercritical fluidized bed follows Ergun's equation and typical correlations of the form of equation 3 such as Wen and Yu [13, 21]. Unfortunately, despite this fact, it cannot be used in nanoparticle fluidization because the agglomerate particle size is unknown in supercritical fluidization conditions, and there are not any study about it.

Up to the author's knowledge, fluidization with supercritical fluids of nanoparticles is barely investigated. This method avoids the use of mechanical devices and supplies a green medium where reactions or coatings can be carry out. In this work, this process has been studied through the determination of minimum fluidization velocity. Pressure has been varied from 7.7 to 14.4 MPa and temperature from 308 to 320 K, to obtain a range of densities between 200 and 800 kg/m^3. Three different particles have been used, aluminum oxide (Al_2O_3), titanium oxide (TiO_2) and magnetite (Fe_3O_4), in order to find a relation between the particle nature (primary size, bulk density…) and the process behavior.

2. Experimental

2.1. Materials

Carbon dioxide was of 99.5% purity and was provided by Carburos Metálicos S.A. (Spain). Aluminum oxide, which trade name is AEROXIDE® Alu C, and titanium oxide, AEROXIDE® TiO_2 P25 were supplied by Evonik Industries (Germany), while Magnetite, Iron (II, III) oxide nanopowder was bought to Sigma Aldrich with a purity superior to 98%. Their properties can be seen in table 1.

Table 1: Nanoparticles physical properties.

Material	Particle Diameter (nm)	Skeletal Density (kg/m^3)	Bulk density (kg/m^3)	Specific surface area (BET) m^2/g
Fe_3O_4	< 50 nm	4800-5100	840	> 60
Al_2O_3	13 nm	3270	40	85-115
TiO_2	21 nm	3800	90	35-65

2.2. Experimental device

In Figure 1, the schematic flow diagram of the equipment is displayed: Carbon dioxide, stored in a gas cylinder (a) at 5.0-5.5 MPa, is pumped in liquid state (T<5ºC) by a membrane pump (b, EH-M-510V1, Lewa) until the operating pressure is reached. This pressure is controlled at the end of the line by a backpressure valve (h, BP-66, GO Inc) with an accuracy of 0.1 bar. After the pump, there is an equalizing reservoir (c) in order to avoid pressure and flow oscillations due to the pulsating flow of the pump. This vessel has a volume of 1.2L, the same as the vessel for the fluidization bed (e). A stainless steel basket (H = 0.323 mm; D= 41 mm), with stainless steel sintered plates at bottom and top, is used to introduce the particles inside the vessel and to make their handling easier. The bottom plate acts as fluid distributor. At the outlet of the fluidized bed vessel, there is a filter to avoid that any particle could be recirculated with the fluid. An amount of 8 grams of particles were charged into the basket.

The fluidized state was assured by means of pressure drop across the bed measurements that were carried out with a (j) differential pressure meter (f, 3051CD, Fisher-Rosemunt) by means of two concentric tubes of 1/8 and 1/4 in. inside the bed. The equipment was calibrated in the range of -1mbar to 3 mbar. In a previous work of microparticles fluidization with SC-CO_2, it was tested that this device has no influence on the fluidization performance.

The flow rate was controlled with a flow controller (d, Mini Cori-Flow M14- RGD-220S, Bronkhorst). It allows controlling the flow rate with a mean incertitude of 0.5% of the measured value for values above 500 g/h and a maximum of 3% incertitude for values between 100 and 500 g/h.

Additionally, the temperature in both vessels is controlled by water circulating through the jacket of each vessel from two external thermostatic baths with an accuracy of +/- 2ºC.

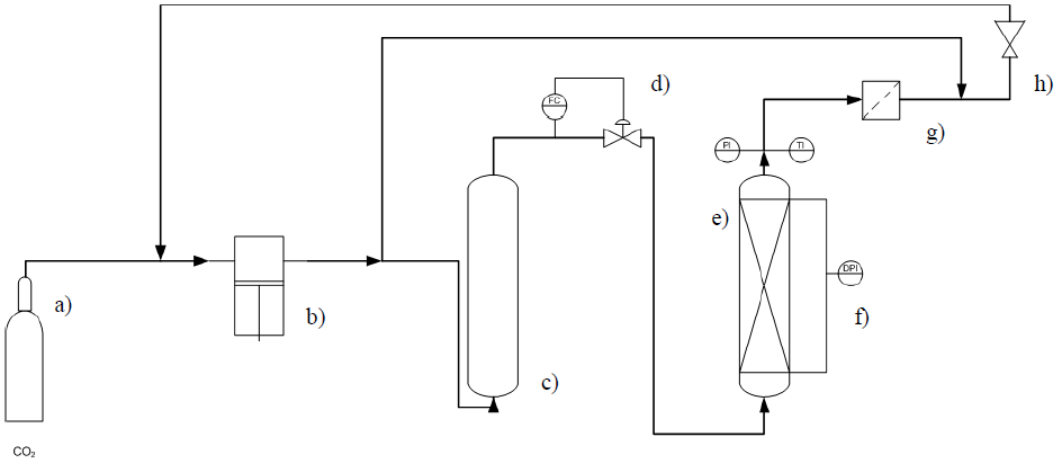

Figure 1: Schematic flow diagram of the experimental device: a) carbon dioxide cylinder, b) pump, c) preheater vessel, d) automatic valve, e) fluidization chamber, f) differential pressure measurement instrument, g) line filter and h) control pressure valve.

2.3. Methods

2.3.1. Particles characterization

With the purpose of determining the stationary agglomerate particle size distribution, a laser diffraction equipment Malvern Mastersize 2000, in wet via or dry via, with red light (max. 4 mW helium–neon, 632.8 nm) was used. The equipment has an accuracy and a reproducibility better than 1%. The measures have been in volume percentage and the value used was $d_{0.5}$.

Furthermore, the nanoparticle agglomerate morphology was study by Scanning Electron Microscopy (SEM). The equipment was a FEI - Quanta 200 FEG with a resolution of 1.5 nm at 30 kV which can work at high and low vacuum. The equipment has an acceleration voltage from 0.2 to 30 kV and a Schottky filament.

2.3.2. Minimum fluidization velocity determination

In order to determine this parameter, the pressure drop method has been applied. This procedure consists on measuring the pressure drop across the bed while fluid

superficial rate increases or decreases. First of all, particles have been fluidized at high rates owing to avoid segregation. Then, the velocity has been drastically reduced to zero and has been increased slowly measuring continuously the drop pressure; when the velocity increases, this parameter augments, as far as minimum fluidization velocity is reach. Finally, the pressure drop is maintained constant in spite of velocity increases until drag regime (figure 2).

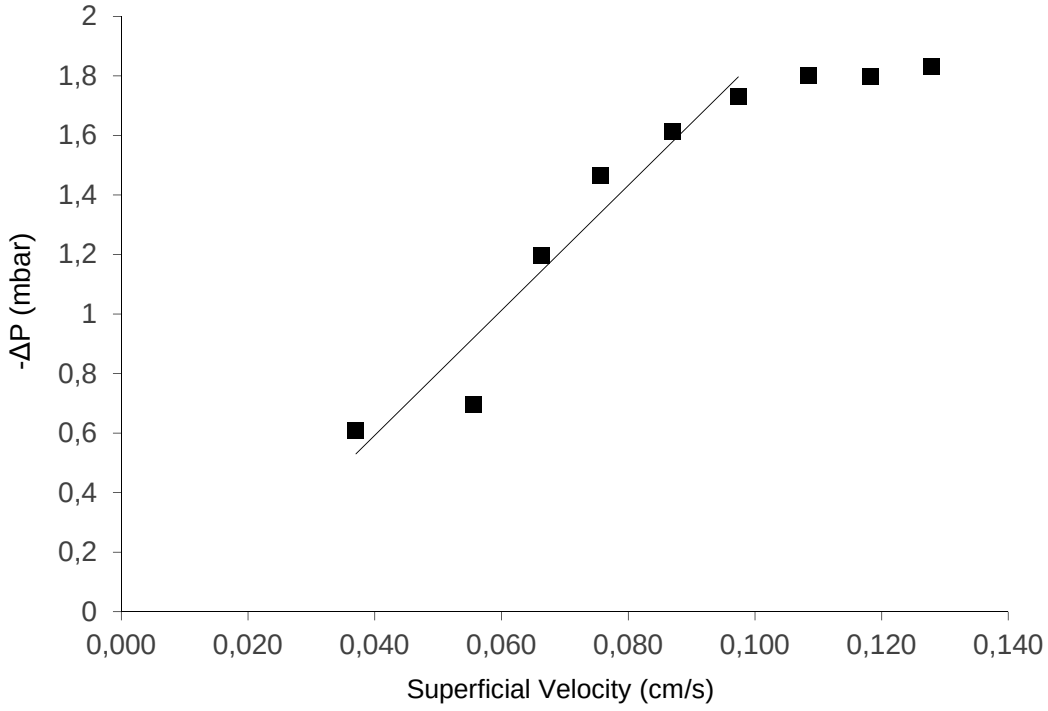

Figure 2: Minimum fluidization velocity determination (TiO_2, 310 K and 80 bar)

3. Results and discussion

3.1 Nanoparticle size and morphology

First of all, nanoparticle structure has been analyzed in order to determine in what way these properties affect fluidization process. Particles are agglomerated because of cohesive interparticle forces, the size and morphology of these agglomerates cannot be measured easily in processes carried out at high pressures and the methods mentioned in introduction section cannot be implemented in the experimental system: the extraction of a sample may change the conditions in the bed and in the agglomerate structure, while the installation of an internal electronic device required for the laser methods compromises the

closure system at high pressure. In this paper the study has been performed by extrapolation of results at ambient conditions.

Ambient condition agglomerate size was 8.6 μm for magnetite, 9.3 μm for Al_2O_3 and 3.4 μm for TiO_2, determined by laser diffraction with no significant differences for the determination using air or in water as dispersing media. Comparing the values with properties in table 1, the lower primary particle size, the higher agglomerate size is. This can be due to Van der Waals cohesive force, which is higher when the particle size is smaller (it is proportional to the inverse of diameter to the sixth power [5]). Furthermore, the higher specific surface area the higher agglomerate size, because of the contact surface between particles is bigger and this fact produce higher degree of agglomeration.

Concerning particle morphology, in figure 3 can be observed a SEM study of the three particles used. In the three cases, nanoparticles are agglomerated in big quasi-spherical structures. Titanium dioxide (3A) and aluminum oxide (3C) are more porous than magnetite (3E), which have a more compact appearance that explain its bulk density of 840 kg /m^3. In agreement with bulk density data, TiO_2 agglomerates are less porous than Al_2O_3 particles: in figure 3C, it is possible to distinguish smaller particle chains in agglomerate surface while in figure 3A more compact particle formations are presented. In figures 3B, 3D and 3F, it can be checked that agglomerates have similar sizes in spite of bigger and smaller particle conglomerates are observed. Regarding agglomerate size, in figures 3B, 3D and 3F, it is observed all titanium oxide particles form agglomerates smaller than 10 μm, while aluminum oxide form structures of 10 μm. Magnetite agglomerate medium size is also over 7 μm (count from SEM image). These results are similar to those obtained by laser diffraction, and follow the same trend.

3.2 Minimum fluidization velocity

In figure 4, it can be seen the minimum fluidization velocity variation of aluminum oxide when fluid density increases. At low densities, the velocity is around 0.180 cm/s, when density is increased, the velocity decreases up to 0.020 cm/s. A similar change can be seen with viscosity (not shown). This variation responds to changes in fluid properties (density and viscosity), these properties affect the process how Ergun's equation (Eq. 1) indicates.

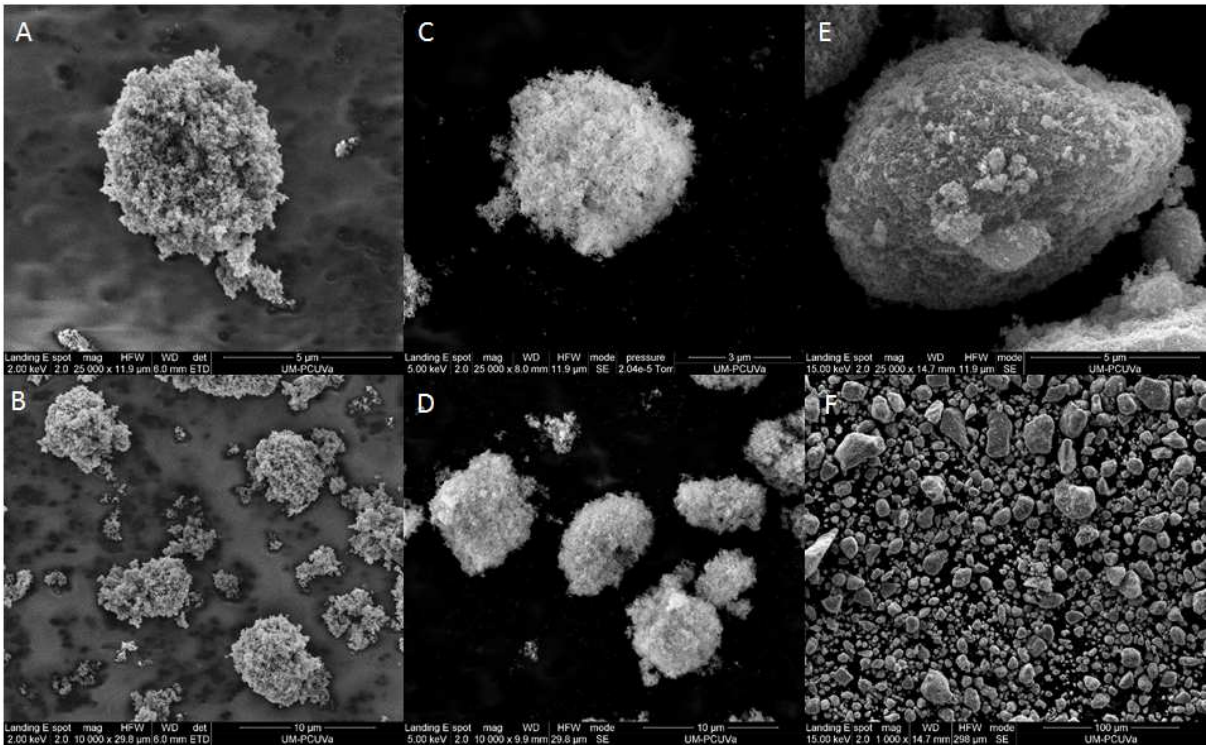

Figure 3: SEM images of titanium dioxide (A and B), aluminum oxide (C and D) and magnetite (E and F).

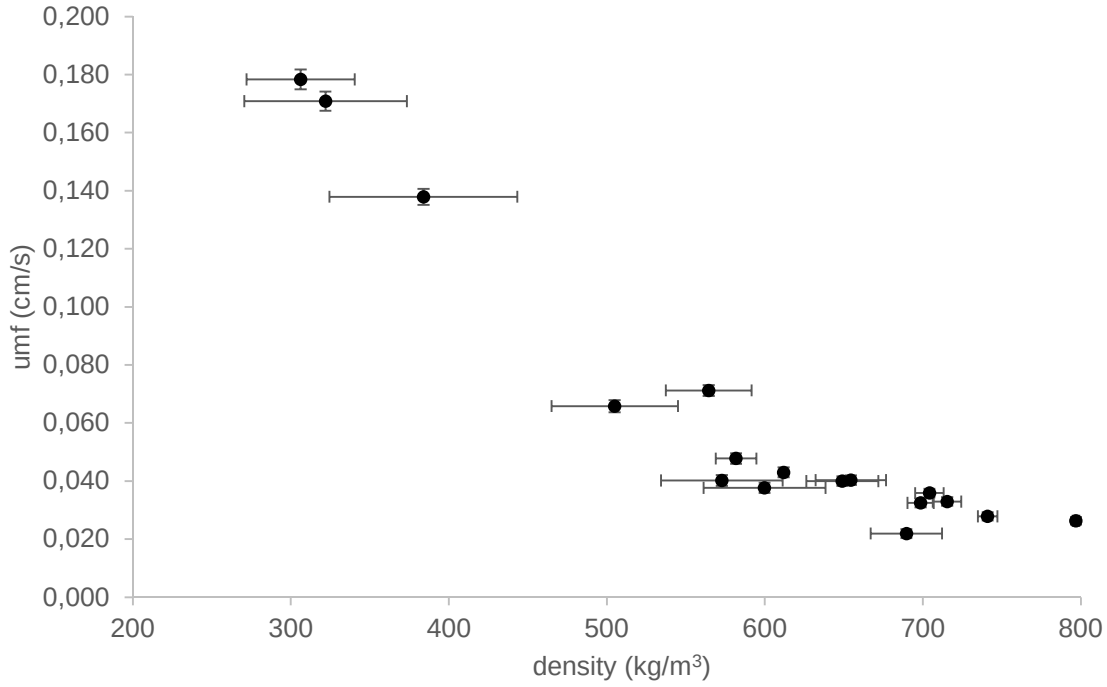

Figure 4: Minimum fluidization velocity variation of Al_2O_3 with density fluid.

The behavior previously described is equal for all tested particles, but depending on particle nature there are changes, as figure 5 shows. It can be seen two clearly differentiated behaviors:

At higher densities (500-800 kg/m^3), it cannot be appreciated any difference between the three types of particles, since all have a similar minimum fluidization rate, meaning that hydrodynamic forces dominate against cohesive forces, and the process (followed by this parameter) does not depends on particle nature, only on operation parameters temperature and pressure. On the other hand, at lower values of CO_2 density (200-500 kg/m^3) the two forces take part in the process, since minimum fluidization velocity, in this case, depends on primary particle size and fluid properties. It can be observed, for the same value of density, each particle reaches a different velocity. It is necessary higher fluid superficial velocity to fluidize aluminum oxide particles than the others. This is due to their agglomerate size is bigger, as it has been discussed in the previous section, more hydrodynamic force is necessary to suspend it in the fluid. The same conclusions can be obtained to titanium oxide and magnetite. Furthermore, magnetite belongs to agglomerate bubbling fluidization regime (bulk density higher than 100 kg/m^3) and this material shows the same behavior that aluminum oxide and titanium oxide, which belong to agglomerate particulate fluidization regime (APF). The difference between the two behaviors proves that cohesive forces can be drastically decreased using supercritical fluids, enhancing fluidization quality. This improvement can be observed in several works that use supercritical fluid fluidization to coat different particles, such as titanium dioxide or curcumin nanoparticles with a polymeric compound [22, 23] .

Finally, comparing the minimum fluidization velocity values with other published works, titanium dioxide (both AEROXIDE TiO_2 P25) fluidizes at ambient conditions with nitrogen when gas superficial velocity is 5.76 cm/s, applying gas pulsations this value is reduce until 1.62 cm/s [24], while with supercritical carbon dioxide, the value, changing the density (200-800 kg/m^3), varies from 0.1 to 0.02 cm/s, a drastically reduction. Regarding aluminum oxide (primary particle size <50 nm in both works), at ambient condition with nitrogen, the value of minimum fluidization velocity is about 3 cm/s, this value can be improved to 0.05 cm/s with an acoustic field at 140 dB and 120 Hz [11]. This results are similar to the obtained with supercritical carbon dioxide, which can be reduced to 0.03 cm/s.

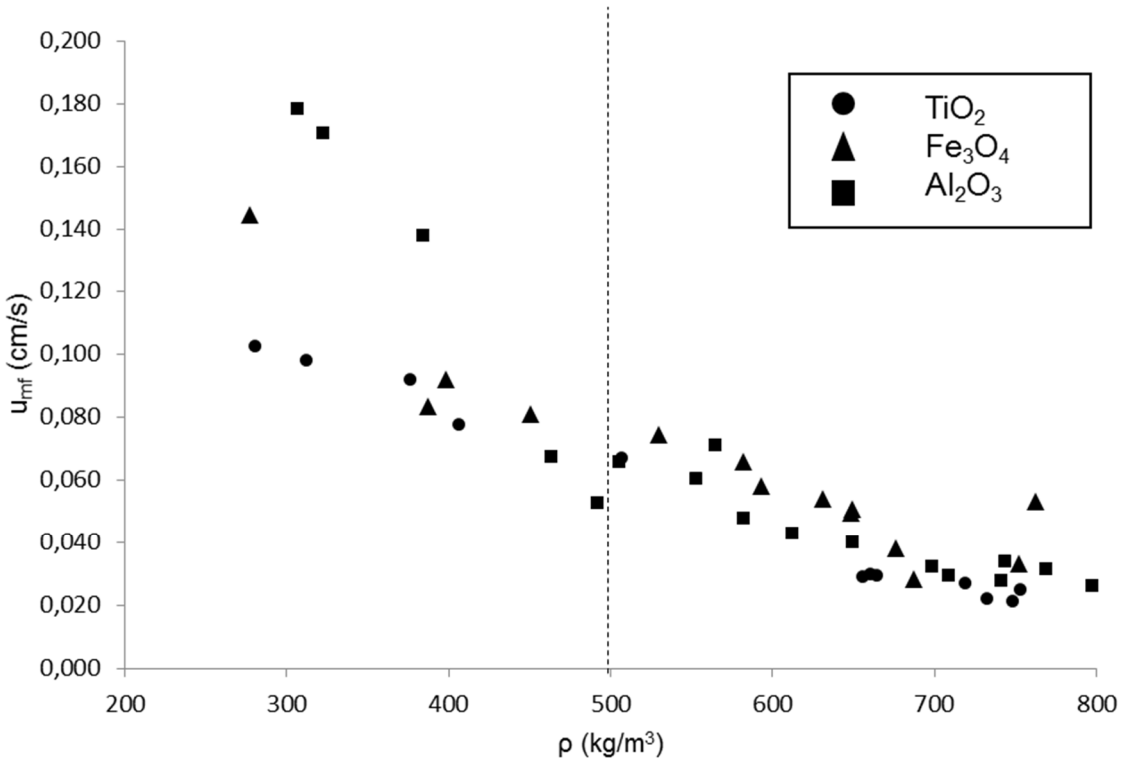

Figure 5: Variation of minimum fluidization velocity with SC-CO_2 density comparison between titanium dioxide, magnetite and aluminum oxide nanoparticles.

4. Conclusion

Fluidization of nanoparticles with supercritical fluids is a good option to enhance fluidized bed quality. The improvement achieved is higher or similar to other techniques used to avoid bed channeling and other problems associated with aggregation and cohesive forces, without the use of mechanical complex devices. Two regimens have been found in nanoparticles fluidization with dense fluids. At higher densities only hydrodynamic forces act because they are stronger than cohesive forces. While at low densities the process is affected by fluid and cohesive forces, depending minimum fluidization velocity on fluid properties and particle properties, such as primary size or specific area. Moreover, minimum fluidization velocity can be tuned by adjusting the density, varying pressure and temperature. This simple yet effect fluidization method for nanoparticles can be easily coupled with coating or reaction processes to further exploit the benefits of supercritical fluids in that technologies.

NOMENCLATURE

$d_{p,s}$: Particle diameter

g: Gravity

H: Height bed

m_p: Particle mass

S: Bed section

u: Fluid superficial velocity

u_{mf}: Minimum fluidization velocity

ΔP: Pressure drop

ε: Porosity

ϕ: Sphericity

μ: Viscosty

ρ_s: Particle density

ρ_f: Fluid density

REFERENCES

1. L. F. Hakim, J. L. Portman, M. D. Casper, A. W. Weimer. Aggregation behavior of nanoparticles in fluidized beds. Powder technology. 2005;160:149-160.

2. J. Ruud van Ommen, J. M. Valverde, R. Pfeffer. Fluidization of nanopowders: a review. J Nanopart Res. 2012;14:737.

3. J.S.M. Botterill, Y. Teoman, K.R. Yüregir. The effect of operating temperature on the velocity of minimum fluidization, ved voidage and general behaviour. Powder technology. 1982;31:101-110.

4. H. Kröber, U. Teipel. Microencapsulation of particles using supercritical carbon dioxide. Chemical Engineering and Processing. 2005;44:215-219.

5. J. Visser. Van Der Waals and Other Cohesive forces affecting Powder Fluidization. Powder technology. 1989;58:1 - 10.

6. X. Zhu, Q Zhang, Y. Wang, F. Wei. Review on the nanoparticle fluidization science and technology. Chinese Journal of Chemical Engineering. 2016;24(1):9-22.

7. V. Tanneur, C. Joussot-Dubien, B. Fournel, S. Sarrade, B. Freiss, F. Marciacq, G.M. Rios. Group A particle fluidization in supercritical carbon dioxide: Effect of operating conditions on fluidization efficiency. Powder technology. 2008;187(2):190-194.

8. T. Zhou, H. Li. Estimation of agglomerate size for cohesive particles during fluidization. Powder technology. 1999;101:57-62.

9. J.M. Valverde, A. Castellanos. Fluidization of nanoparticles: A simple equation for estimating the size of agglomerates. Chemical Engineering Journal. 2008;140:296-304.

10. X.S. Wang, F. Rahaman, M.J. Rhodes. Nanoparticle fluidization and Geldart's classification. Chemical Engineering Science. 2007;62:3455-3461.

11. P. Ammendola, R. Chirone, F. Raganati. Fluidization of binary mixtures of nanoparticles under the effect of acoustic fields. Advanced Powder Technology. 2011;22:174-183.

12. Y. Wang, G. Gu, F. Wei, J. Wu. Fluidization and agglomerate structure of SiO2 nanoparticles. Powder technology. 2002;124:152-159.

13. C. Vogt, R. Schreiber, G. Brunner, J. Werther. Fluid dynamics of the supercritical fluidized bed. Powder technology. 2005;158(1-3):102-114.

14. J. M. Valverde, M. J. Espin, M. A. S. Quintanilla, A. Castellanos. Electrofluidized bed of silica nanoparticles. Journal of Electrostatics. 2009;67:439-444.

15. E. K. Levy, B. Celeste. Combined effects of mechanical and acoustic vibrations on fluidization of cohesive powders. Powder technology. 2006;163:41-50.

16. C. Xu, J. Zhu. Experimental and theoretical study on the agglomeration arising from fluidization of cohesive particles-effects of mechanical vibration. Chemical Engineering Science. 2005(60):6529 - 6541.

17. X. Liang, H. Duan, T. Zhou, J. Kong. Fluidization behaviour of binary mixtures of nanoparticles in vibro-fluidized bed. Advanced Powder Technology. 2014;25(1):236-243.

18. X. Liang, Y. Zhou, L. Zou, J. Kong, J. Wang, T. Zhou. Fluidization behavior of binary iron-containing nanoparticle mixtures in a vibro-fluidized bed. Powder technology. 2016.

19. G. Brunner. Supercritical fluids: technology and application to food processing. Journal of Food Engineering. 2005;67:21-33.

20. A. Marzocchella, P. Salatino. Fluidization of solids with CO_2 at pressures from ambient to supercritical. AIChE Journal. 2000;46(5):901-910.

21. S. Rodríguez-Rojo, N. López-Valdezate, M.J. Cocero. Residence time distribution studies of high pressure fluidized bed of microparticles. Journal of Supercritical Fluids. 2008;44:433-440.

22. V. Martín, R. Romero-Díez, S. Rodríguez-Rojo, M.J. Cocero. Titanium dioxide nanoparticle coating in fluidized bed via supercritical anti-solvent process (SAS). Chemical Engineering Journal. 2015;279:425-432.

23. F. Zabihi, N. Xin, S. Li, J. Jia, T. Cheng, Y. Zhao. Polymeric coating of fluidizing nano-curcumin via anti-solvent supercritical method for sustained release. Journal of Supercritical Fluids. 2014;89:99–105.

24. A. Akhavan, F. Rahaman, S. Wang, M. Rhodes. Enhanced fluidization of nanoparticles with gas phase pulsation assistance. Powder technology. 2015;284:521-529.

CHAPTER 4

Titanium Dioxide Nanoparticle Coating in Fluidized Bed via Supercritical Anti-solvent process (SAS)

Published:
Víctor Martín, Rut Romero-Díez, Soraya Rodríguez-Rojo, María José Cocero.
Chemical Engineering Journal 279 (2015) 425-432

Abstract

A process to coat nanoparticle agglomerates has been developed and its critical operation parameters have been studied in this work. It consists on a fluidized bed where a supercritical anti-solvent process (SAS) takes place. Titanium dioxide (TiO_2), used as model nanoparticle, has been coated with a polymer, Pluronic F-127, from an ethanolic solution. As main factors that can affect the coating process, the following process parameters were studied: the ratio between the velocity of carbon dioxide through the bed and the minimum fluidization velocity (u_{mf}), with values from 1.5 to 2.5 times the u_{mf}; the density of carbon dioxide, varying from 640 kg/m^3 to 735 kg/m^3 approximately; the flow rate of solution, within an interval between 0.5-2 mL/min; the concentration of the solution, from 0.030 mg/mL to 0.090 mg/mL and the mass ratio polymer-particle, 0.45-1.8 g/g.

The process parameters were selected taking into account the values that increased the yield, defined as gram of coating material per gram of introduced polymer amount, and maintained a unimodal particle size distribution (PSD), with low increment in the mean particle size with respect to raw TiO_2. All the samples were analyzed by four different methods, which showed the successful results of the experiments. The yield was analyzed gravimetrically, and the PSD was determined by laser diffraction. The presence of polymer on the surface of the nanoparticle agglomerates was verified by FT-IR spectrum and fluorescence microscopy, which also showed the quality and uniformity of the coating. Furthermore, the bulk density of the samples was measured showing a lineal variation with the mass ratio polymer-particle.

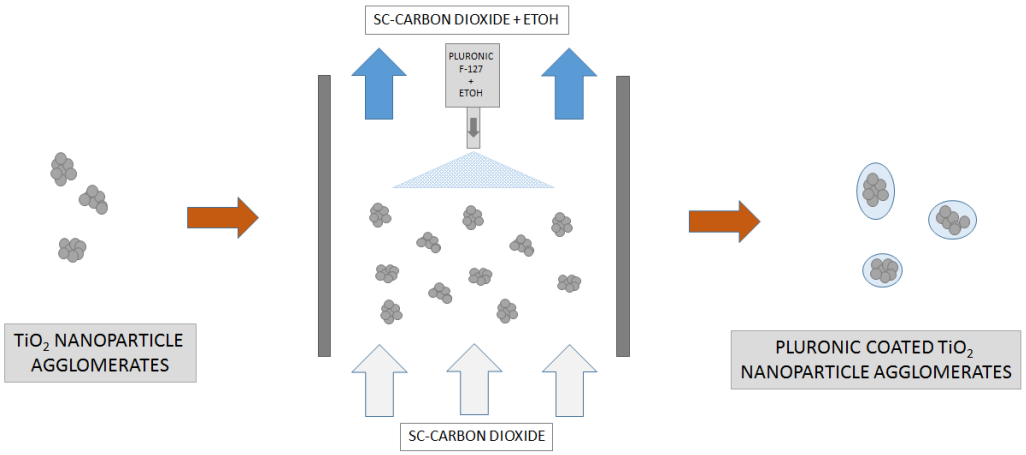

1. Introduction

Nowadays, nanoparticle technology has found important applications in fields such as electronics, catalysis, biomedicine, biotechnology or food industry. This interest in nanoparticles resides in their small size (<100 nm), morphology, particle size distribution and composition, which represents a bridge between bulk materials and atomic or molecular structures. However, working with fine particles, agglomeration presents a serious problem because of their strong cohesive forces. Nanoparticles are in 'Geldart group C' [1], which is characterized by the rise of cohesive forces like Van der Waals, electrostatics and liquid bridge forces [2]. Van der Waals force intensity, which is inversely proportional to the diameter to the sixth power, is assumed as the most important cohesive force in nanoparticles that lead to the formation of agglomerates.

A large number of nanoparticles require special treatments in order to improve their properties to be used in some fields such as pharmaceutical, alimentary or fertilizing industries. With the addition of a coating layer, some of their properties can be modified, like hygroscopicity, morphology or bulk density [3]. In addition, this coating is used to protect high value added products, encapsulate hydrophobic and/or toxic substances.

Fluidized bed has been commonly used in many chemical processes in order to encapsulate particles, but nanoparticles cannot be fluidized, only their agglomerates [4]. Several authors have define two different kinds of nanoparticle fluidization, agglomerate particle fluidization (APF) which is characterized by homogeneous bed expansion, absence of bubbles, uniform agglomerates distribution and high expansion relation. This type of fluidization appears in particles with a bulk density lower than 100 kg/m3 that form porous light agglomerates. The second type is the agglomerate bubbling fluidization (ABF) which takes place when bulk density is higher than 100 kg/m3, and it is characterized by low expansion relation and sedimentation of agglomerates, which are weighty and compact [4, 5]. These characteristics make APF particles profitable for coating since ABF, due to low bed expansion, have a major aggregation tendency [6].

Some technics have been developed to improve cohesive particle fluidization reducing the agglomerates size: ultrasounds, mechanical vibration, mechanical stirring, electrical fields, pulse gas flow, centrifugal field, and secondary flows [4, 7, 8]. In this work supercritical fluids (SCF), whose density and viscosity are easily tunable with small changes in pressure and temperature, are tested; since it has been proved that these

properties change the dynamic equilibrium inside the bed enhancing fluidization quality [6].

Furthermore, in the last decades, the use of SCF has grown noticeably in precipitation processes versus conventional techniques [9]. The reason is that the final particle size obtained in the processes, the size distribution and the morphology of the particles can be easily controlled [10]. Depending on the role that SCF performs, there are three different process groups: solvent, anti-solvent or co-solvent. Many authors have used the combination of fluidized beds and supercritical fluids for coating of microparticles, especially RESS process where the SCF acts as solvent. The rapid expansion of the supercritical solution (RESS) causes very high supersaturating ratio of solute in the spraying flow, forming a large number of superfine nuclei. T.J. Wang et al (2001) [3] covered core particles simulating drug compounds with paraffin and obtained a uniform covering with a thickness near 10 nm. In 2002, R.Schreiber et al [11], covered microparticles with a wax. The results were good for most of the experiments with thickness varying from 0.6-0.42 μm, except for those particles with bigger cores (100-200 μm) where thin but incomplete covers were obtained. This effect can be explained because of the insufficient mixing inside the fluidized bed. C. Vogt et al (2004) [12] achieved smooth and complete covers over different types of solids, but only with yields near 50%. In 2008, S. Rodríguez-Rojo et al [13], tested two different ways of injecting a paraffin coating solution in the SC-CO2, bottom and top spray. The results showed the microparticles glass beads were totally covered and no aggregation was achieved when the solution is feed through the top spray. The RESS process limit the range of coating agents that can be used since it must be soluble in the SCF. A better option is performing a process in which the SCF acts like an anti-solvent, like supercritical anti-solvent process (SAS), that has been widely used in preparing micro/nanoparticles because of lower residual solvent in products, simple step and mild operating conditions [14]. To carry on this process the solute of interest has to be dissolved in an organic solvent. The solute must be insoluble in the supercritical phase; however, the organic solvent must be soluble in the SCF. When the solution enters in the super critical phase through a nozzle, the solvent is dissolved in the SCF, which acts as anti-solvent, reaching the super-saturation and causing the precipitation of the solute as fine particles. The only example so far exists consist on a curcumin nanoparticles coated by PLGA using a novel fluidization assisted supercritical anti-solvent procedure [15]. Furthermore, in this work, supercritical anti-solvent is assisted

with ultrasonic vibration to improve mixing effects. At best operating conditions the minimum diameter obtain after the coating process is three times the initial diameter but precipitation yields were only of 51%.

This work presents a combination between a supercritical fluidized bed of nanoparticle agglomerates in SCF-CO2, with a SAS process. The objective is to study the coating process of nanoparticle agglomerates with a polymer taking the advantages of the heat and mass transference in fluidized bed and the solvent power of SCFs. In addition, the parameters that define the process are discussed in order to optimize the process. Titanium dioxide (TiO2) was chosen as nanoparticle model material, meanwhile the selected organic solvent was ethanol (EtOH) due to its high solubility in SCF-CO2 and it is one of the most used in anti-solvent processes [16, 17]. The coating agent used in all the experiments was Pluronic-127 (F-127), a hydrophylic block copolymer with applications in drug delivery systems [18-20]. Besides, it good properties as coating agent, it has excellent wetting properties in solution and readily forms films after solvent evaporation.

2. Experimental

2.1 Materials

Titanium dioxide, AEROXIDE® TiO_2 P 25, was a gift from Evonik Industries. The powder properties are displayed in Table 1. As it can be observed in Figure 1, TiO_2 agglomerates have a porous structure due to cohesive forces. The fluidization agent chosen was carbon dioxide provided by Carburos Metalicos S. A with a purity of 99.95%. Ethanol, supplied by Panreac with a purity of 99.5%, was selected as organic solvent. The coating agent, Pluronic F-127, with an approximate density of 500kg/m^3, was supplied by Panreac. Fluorescein sodium salt, purchased from Sigma, has been used as fluorophore to dye the polymer solution.

Table 1: *Powder physical properties.*

Powder	Size (nm)	Skeletal density (kg/m^3)	Bulk density (kg/m^3)	Tapped density (kg/m^3)
TiO_2	21	3800	90	130

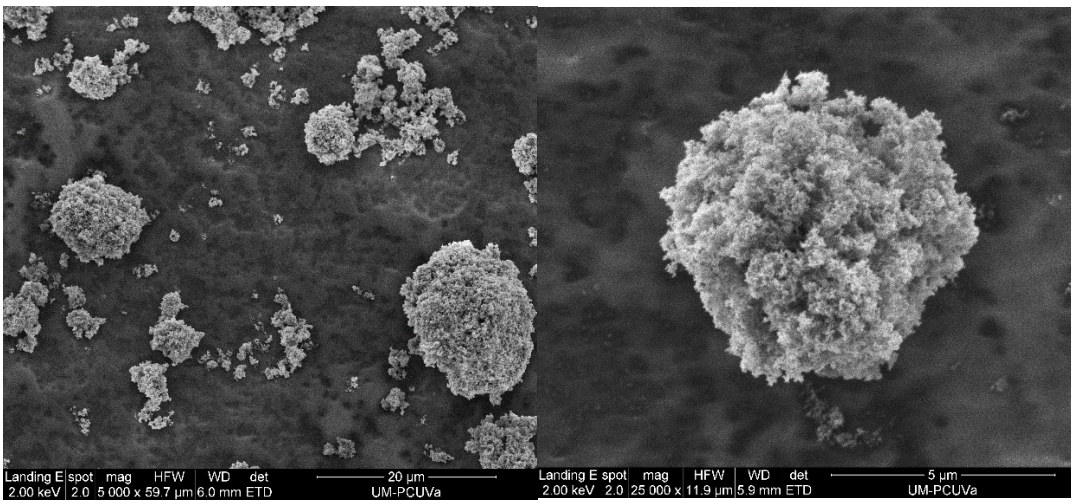

Figure 1: *SEM photography of titanium dioxide.*

2.2 Experimental device

In Figure 2, a schematic flow diagram of the equipment is displayed. Carbon dioxide, stored in a gas cylinder, T-3, at a pressure around 5.0 – 5.5 MPa, is pumped in liquid state by the membrane pump, P-1 (EH-M-510V1, Lewa) into the first vessel, T-1, until the operating pressure is achieved. The vessel T-2 has been previously charged with 4 g of titanium dioxide, with a volume of 44.5 cm^3 according to its bulk density. The operating pressure is controlled at the end of the line by the backpressure valve, V-1 (BP-66, Go Inc.). The vessel T-1 acts like an equalizing reservoir in order to avoid pressure and flow oscillations due to the pulsating flow of the pump. As a good operation of the plant requires high flow of CO_2, a recirculation line and a bypass line were implemented in order to reduce the CO_2 consumption. Both are simultaneously used and manually controlled by backpressure valve V-2 (BP 301, Pressure Tech) and the valve V-3, respectively. A Coriolis flow controller, FC-1, (Mini Cori-Flow M14- RGD-220S, Bronkhorst) is used to maintain a constant flow. After passing through T-1, carbon dioxide goes directly to the second vessel, T-2, which is used for the fluidization. Both vessels have a volume of 1.2 L and they are heated by a hot-water jacket from two external thermostatic baths in order to reach the operating temperature. Inside T-2, there is a stainless steel basket (h = 323 mm; d= 41 mm), with stainless steel sintered plates at bottom and top, which is used to introduce the nanoparticles inside the vessel and to make their handling easier. The bottom plate acts as fluid distributor. At the outlet of the fluidized bed vessel, T-2, there is a filter, F-1, to avoid that any dragged particle could be recirculated with the fluid.

Once the operational conditions of pressure and temperature are reached, the solution of the polymer in ethanol is pumped at 318 K, P-2 (membrane pump EH-M-510V1, Lewa), inside the fluidized bed through a nozzle with an internal diameter of 0.572 mm situated inside the basket. When the solution get in contact with the supercritical carbon dioxide, the SAS process takes place. The ethanol is solved by the CO_2 and this mixture is expanded until ambient conditions in the last vessel, T-3, which acts as a liquid-vapor separator in order to get a gaseous phase rich in CO_2 and a liquid phase, ethanol, gathered by opening valve V-5. After a defined operating time, there is a drying period of 30 minutes in order to eliminate any residual ethanol from T-2.

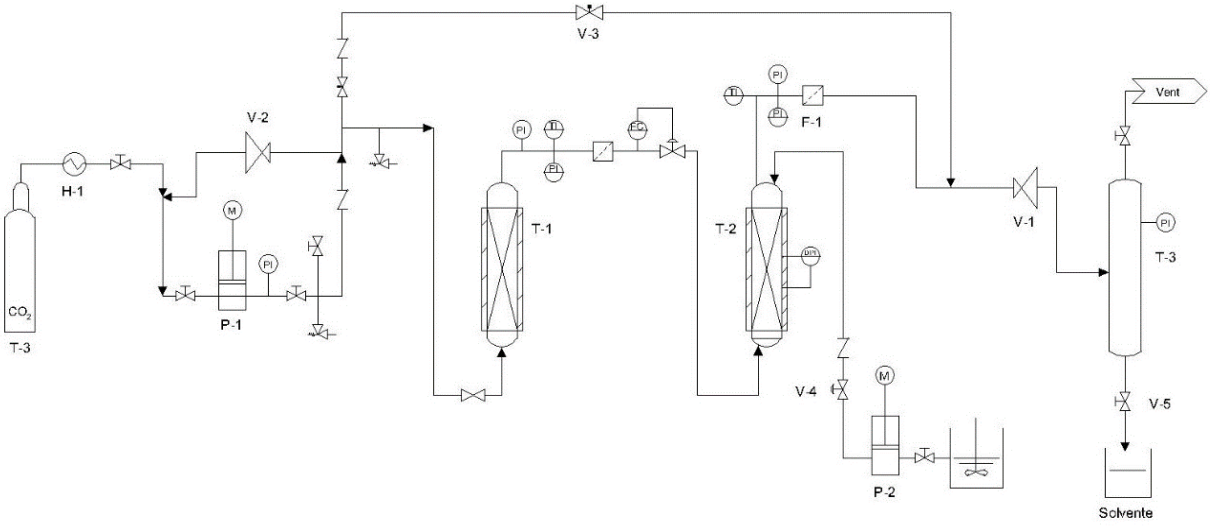

Figure 2: *Schematic flow diagram of the equipment.*

2.3 Product characterization

In order to determine the coating quality and the process efficiency, several qualitative and quantitative techniques have been used.

2.3.1. Coating yield

Coating yield (%η) is defined as the percentage of the ratio of the mass of Pluronic F-127 deposited on the particles ($m_{deposited}$) to the total amount of polymer pumped into the vessel ($m_{introduced}$) (1). It has been calculated by means of a gravimetric analysis. The samples were divided in three crucible and introduced in a furnace at a temperature of 550 ºC for the period of 72 hours to determine the mass of polymer deposited during the process by weight difference of particles before and after the calcination of the polymer.

$$\%\eta = \frac{m_{deposited}}{m_{introduced}} \quad \textbf{(1)}$$

2.3.2. Mean particle size and particle size distribution

In order to determine the particle size distribution, the laser light scattering equipment Malvern Mastersize 2000 in dry via (Scirocco 2000 accessory) with red light (Max. 4mW helium-neon, 632.8nm) was used. The equipment has an accuracy and a

reproducibility better than 1%. The particle size distribution has been expressed in % number and % mass (volume). Besides, the mean particle size of the distribution was characterized by the $d_{3.2}$, or Sauter Diameter, which is the diameter of a sphere that has the same volume/surface area ratio as the entire particle size distribution. Pluronic F-127 refractive index chosen was 1.467 while titanium dioxide was 2.741.

2.3.3. Morphology: Fluorescence Microscopy

Additionally, in some experiments fluorescein sodium salt was added to F-127 at a concentration of ca. 0.01 µg/mL. In this case the fluorescein sodium salt acts like a fluorophore, a chemical compounds that can re-emit light upon light excitation. The samples are illuminated with a green light of a specific wavelength (495 - 570 nm) which is absorbed by the fluorophores causing them to emit light of longer wavelengths. By this re-emission, it is possible to observe if the polymer with the fluorescein sodium salt is deposited over the particle surface. The microscopy used to obtain the images of the samples was a Leica DM4000 B (Wetzlar, Germany).

2.3.4. Bulk density determination

The bulk density of coated particles was determined as follows, a constant volume of 1 mL of each sample was measured and then weight in order to calculate the density of the powder. This procedure was repeated five time for each sample to minimize the error.

2.3.5. Structural characterization: FTIR analysis

The fingerprint of the pure components and the samples has been determined by Fourier Transform Infrared Spectroscopy (FT-IR) to check the presence of the coating agent on the particle surface and if it covers the core particles completely. IR spectra of the samples were recorded on a Bruker ALPHA FT-IR apparatus equipped with a Platinum ATR module including a diamond crystal. The spectra in the range from 4000 cm^{-1} to 400 cm^{-1}, were the average of 60 scans at a resolution of 4 cm^{-1}. The ATR signal was transformed to transmittance and the obtained spectra were normalized after the correction of the baseline.

3 .Results and discussion

The effect of several operational parameters on yield, final particle size and particle size distribution has been studied. The value of each parameter was chosen to reach the maximum yield and to obtain the narrowest PSD and the smallest mean particle size. These parameters were the flow ratio between the flow rate of carbon dioxide and the minimum fluidization flow rate, the density of the carbon dioxide, the flow of solution, the concentration of the solution and mass ratio polymer-particle. The conditions and the results of all the experiments are gathered in Table 2.

Table 2: *Conditions and results of F-127-coated titanium dioxide in a fluidized via supercritical antis-solvent process (SAS). Titanium dioxide with average* $d_{3,2}$ *= 2.2µm*

No.	P (MPa)	T (K)	Density (kg/m^3)	CO_2 flow rate (mL/min)	u/u_{mf}	Solution flow rate (mL/min)	Solution concentration (g/mL)	Ratio polymer-particle (g/g)	Yield (%)	Time (min)	$d_{3,2}$ (µm)
1	10.5	308.1	731.0	31.9	1.5	1.0	0.06	0.90	79.9	60	3.7
2	10.2	309.7	699.0	43.9	2.0	1.0	0.06	0.90	94.1	60	2.7
3	10.1	309.4	700.5	55.7	2.5	1.0	0.06	0.90	95.1	60	2.6
4	8.8	308.4	642.3	47.3	2.5	1.0	0.06	0.90	81.2	60	3.3
5	10.8	308.7	733.2	53.2	2.5	1.0	0.06	0.90	99.5	60	4.6
6	10.4	309.5	722.0	54.0	2.5	1.0	0.06	0.45	71.4	30	3.0
7	10.2	307.6	707.0	55.2	2.5	1.0	0.03	0.45	93.2	60	3.3
8	10.5	309.0	727.7	53.6	2.5	1.0	0.09	0.45	23.5	20	4.3
9	10.0	308.4	723.0	54.0	2.5	1.0	0.06	1.80	83.8	120	12.6
10	10.1	307.3	728.0	53.6	2.5	1.0	0.06	1.35	94.7	90	3.6
11	10.6	309.6	719.0	54.2	2.5	2.0	0.06	0.45	29.3	15	5.5
12	10.3	307.2	735.0	53.1	2.5	0.5	0.06	0.45	91.7	60	3.3

3.1 Carbon dioxide flow rate

The effect of the CO_2 flow rate has been analyzed in experiments 1-3, where the ratio u/umf was varied between 1.5 and 2.5 times the u_{mf}. To ensure the fluidization state, the minimum flow selected was 1.5 times the u_{mf} . The maximum flow was 2.5 times the u_{mf} in order to avoid dragging of the particles. Minimum fluidization velocity (u_{mf}) for titanium dioxide nanoaglomerates was determined in a previous study (P = 10.5 MPa, T = 309.15 K, u_{mf} = 0.027 cm/s) by the determination of pressure drop across the bed [21] using the system described in Rodriguez-Rojo et al. [22]. As shown in Table 2, the higher the

relation u/u_{mf} is, the higher the yield achieved. Besides, the smallest particles were obtained in run 3, which corresponds to a relation u/u_{mf} of 2.5 as Figure 3 shows. When the flow of carbon dioxide is higher, the fluidized bed is more expanded, the mixing is better [22] and the solution can wet better the particles. In addition, at higher flows, ethanol is faster solubilized and any possible residue on the polymer film can be easily dried resulting in smaller and less agglomerated product.

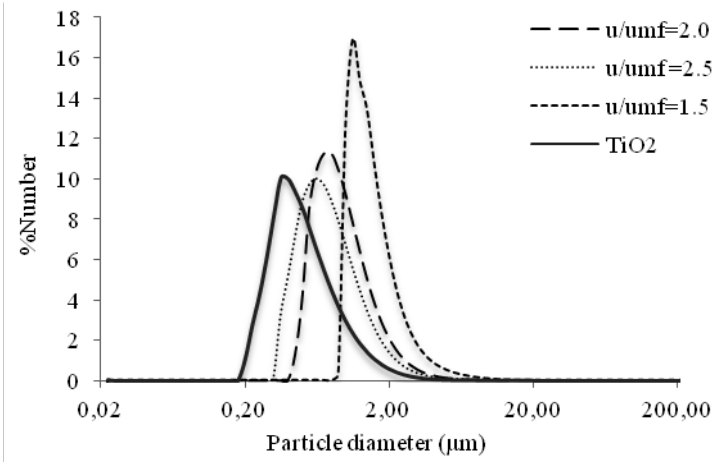

Figure 3: *Variation of the final particle diameter and the particle size distribution with the flow of carbon dioxide.*

3.2 Carbon dioxide density

Fluid density is an important parameter regarding fluidization, since high values enhance fluidization, as fluid molecules are closer. Supercritical carbon dioxide density can be easily tuned by moderate changes in pressure and temperature. Besides, its solvent power is also modified [22].

In this work the variation of pressure and temperature was limited due to the reduction of the melting point of the polymer in the presence of pressurized CO_2 to 310.1K at pressure above 8.8MPa. Therefore, operating temperature was fixed at 309K (±1) and the minimum operating pressure was set at 8.8 MPa [23]. So, the operating temperature was always below this value. Runs *3*, *4* and *5* are compared, with densities near 700 kg/m^3, 642 kg/m^3 and 733 kg/m^3 respectively. On one hand, the yield increases with the density because the solvent power of the carbon dioxide increases and ethanol is better solubilized. On the other hand, there is not a clear tendency in the product size variations with the

density. Density is a difficult variable to control since it depends on pressure and temperature and it can affect the growing kinetics and the deposition effect. Furthermore, the variations in temperature and pressure would affect to the transport properties of the fluid. Nevertheless, the value, which produces the thinner coating (i.e. product particle size distribution most similar to the initial one), is 700 kg/m^3 (P: 10.1 MPa, T: 309 K). However, at this value the yield (95.1%) is slightly lower than the obtained at higher densities (733 kg/m^3, P: 10.8 MPa, T: 308K, 99.5%).

3.3 Solution flow rate

The volumetric flow rate of the solution was also tested with three different values, 0.5 mL/min, 1 mL/min and 2 mL/min, in runs *12*, *11* and *6*, respectively. These values were selected taking into account SAS process studies of other authors [24-26], where the mass flow of CO_2 varies from 0.5-2 kg/h. The results showed in Table 2 prove that the yield decreases with solution flow because when more, and also faster, ethanol is introduced in the fluidized bed, more difficult will be to remove it. Theoretically, CO_2 and ethanol find itself, according to the phase diagram, in a unique phase at experimental conditions. However, in the presence of F-127 this equilibrium varies and it might be possible not to be a unique phase which complicate the drying. In the case of the final diameter of the particles, no significate changes can be seen. All $d_{3,2}$ values are between 3-5.5 µm. This behavior could be caused by the fact that the deposited amount of polymer does not increase with the solution flow because the polymer-particle mass ratio is kept constant [25]. A different behavior for the yield is observed in the work of F. Zabihi et al.[15], where the yield increases with the solution flow. Besides, the highest yield value achieved is smaller (50%) than the presented in this work (92%). Another difference between both works resides in the tendency of the final particle size. F. Zabihi et al. obtained diameters varying from 700-63 nm, meanwhile the diameters achieved in this work are between 3-5.5 µm

3.4 Solution concentration

Three different concentrations of the solution were tested: 0.03 g/mL, 0.06 g/mL and 0.09 g/mL, being the last concentration the solubility value that has been found experimentally for F-127 in ethanol at 318 K. The operating time for each concentration was: 60 min, 30 min and 20 min, respectively for runs *6*, *7*, *8*, in order to obtain the same polymer-particle ratio. Overall, the results presented in Table 2 show that the yield decrease with the concentration. The main reason for this behavior is that, the more concentrate the

solution is, the faster the process is, and hence, there is not enough time to distribute the polymer uniformly over the agglomerate surface.

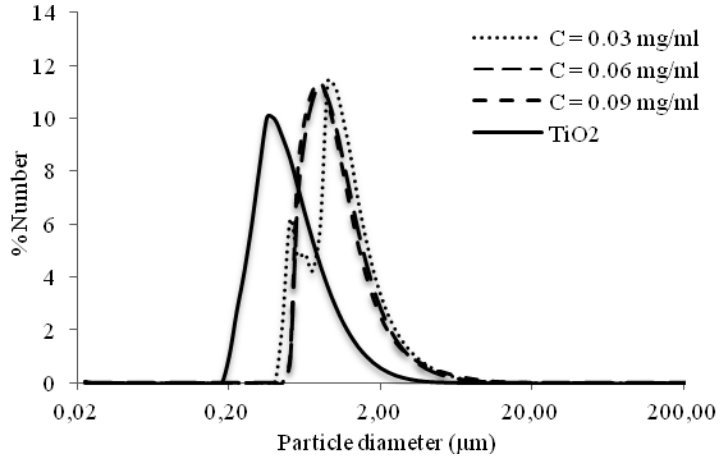

Figure 4: *Variation of the final particle diameter and the particle size distribution with the concentration of the solution.*

Furthermore, the diameter of the coated particles did not show significant differences between the three experiments, with values for $d_{3,2}$ between 0.8-1.0 µm, being the smallest for a concentration of 0.03 g/mL. Similarly, particle size distribution in number did not show important differences between the three experiments, apart from the fact that PSD at 0.03 mg/mL show a multimodal distribution in the same range of particle size (Figure 4). Therefore, the PSD in volume was analyzed since it allows detecting the presence of big agglomerates. These data are collected in Figure 5 and show that the biggest particles are obtained with a concentration of 0.03 mg/mL, which, in principle, is not coherent since the deposition velocity is smaller. This result can be explained taking into account that the experiment time is longer in this case (60 min) to achieve the same theoretical polymer-particle ratio. Therefore, more ethanol was used that may have make more difficult the drying process producing a bigger number of agglomerates. Meanwhile, the smallest particles are obtained with a concentration of 0.06 mg/mL.

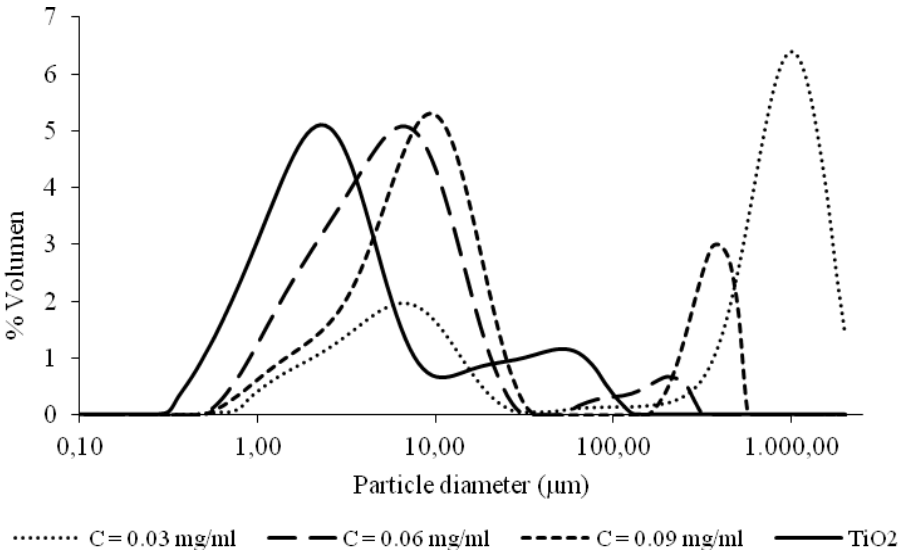

Figure 3: *Variation of the final particle diameter and the particle size distribution with the concentration of the solution in % volume.*

3.5 Mass ratio polymer-particle

Four different values of $m_{polymer}/m_{particle}$ (g/g) were tested: 0.45, 0.9, 1.35 and 1.8 g/g in runs *6*, *3*, *9* and *10* respectively. These values have been selected according to the literature [27]. The variation of the yield with the mass ratio showed a convex form with a maximum value near 0.9 g/g. Besides, with this mass ratio the obtained particle size distribution is closer to the initial size distribution of TiO_2. This behavior is explained for the same reason as in the previous section: on one hand, if the ratio $m_{polymer}/m_{particle}$ (g/g) increases, the number of agglomerates also increase and there is no uniformity on the product size.

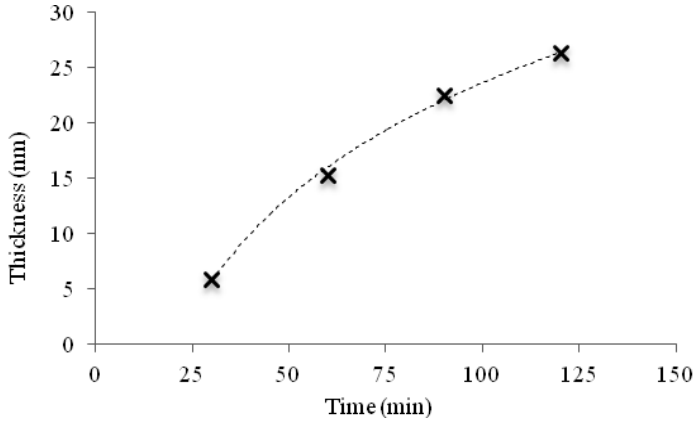

Figure 6: *Variation of the thickness of the coating with the operating time.*

Due to the fact that the yield is calculated by the weight difference between the calcined and the total amount of polymer introduced there must be a minimum quantity of polymer, as Wang et al. indicated [28], to encapsulate the particle. This parameter cannot be optimize because it depends on the requirement of the product. Also, the thickness of the coating depends on a technical limitation as the tendency on Figure 6 shows. This behavior is also explained by other authors [29]. There is a maximum quantity of polymer that can be deposited because the deposition is formed by a layer succession. The theoretical coating thickness varies from 5 to 25 nm, depending on the time and, at long time the thickness approaches a constant value. Thickness was calculated assuming that the particles are spheres and the polymer is distributed uniformly (vide equation (**2)**)).

$$V_T = \frac{4}{3}\pi\left(r_p + t\right)^3 = V_p + V_D \qquad \textbf{(2)}$$

Where $\mathbf{r_p}$ is the averaged radius of the particle, **t** the thickness of the coating, $\mathbf{v_T}$ is the total volume of the particle with the polymer, $\mathbf{v_p}$ the volume of the particle without the polymer and $\mathbf{v_D}$ the volume of the deposited polymer. The latter is calculated by the relation between the mass of the particle and the amount of polymer (equation 3). Where $\boldsymbol{\rho_{polymer}}$ is the density of the polymer, **R** the mass ratio between polymer and particle and **η** coating yield.

$$V_D = \frac{R\, m_{particle}}{\rho_{polymer}}\eta \qquad \textbf{(3)}$$

However, it is possible to define an optimum operational range taking into account values of yield and particle size, from value 1 g/g and 1.4 g/g. Working at mass ratio near 2 g/g, the number of agglomerates and the product size increase dramatically. If more time is required, more ethanol will be introduced and the drying will be more difficult.

3.6 Bulk density

An interesting property modified with the coating is bulk density. When particles are coated, their bulk density changes as more matter is added to the substance. Titanium dioxide presents a very low bulk density, 90 kg/m^3, which makes difficult to handle it. The coating process increases linearly the bulk density of the powder with the mass ratio

polymer-particle, as shown in Figure 7 and improves their handling. This evidence the presence of a polymer coating and it is an easy way to analyze if the process is working properly.

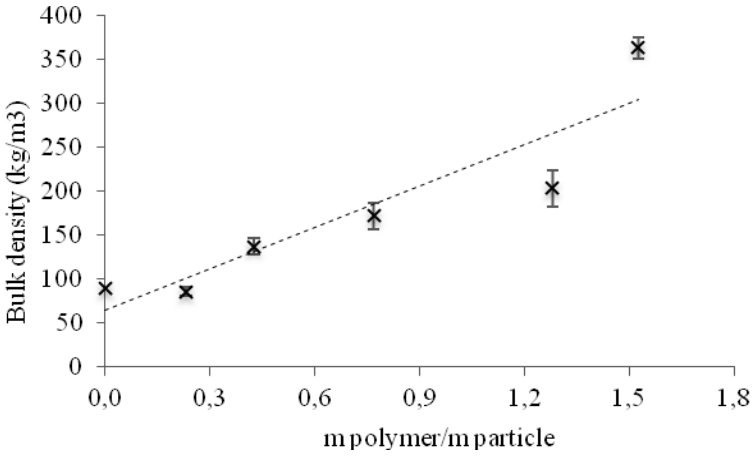

***Figure 7**: Variation of the bulk density with the mass ratio polymer-particle*

3.7 Morphology: Fluorescence Microscopy

Fluorescence microscopy was used in order to prove the polymer was deposited over the surface of the nanoparticles agglomerates. As shown in Figure 8, the polymer dyed with fluorescein sodium salt is uniformly distributed over the agglomerates. Therefore, it is showed that this new method is suitable for a good coating of nanoparticle agglomerates.

3.8 FT-IR spectrums

The deposition of Pluronic over titanium dioxide particles surface has been demonstrated also by FT-IR analysis**.** To perform these analysis, a representative and homogeneus quantity of the coated particles from each experiment were used. Coated particles from all experiments have a similar fingerprint. These spectrums, as shown in Figure 9, are similar to that of titanium dioxide and present the most representative Pluronic peaks at 1,100 and 2,900 cm^{-1}. Since the penetration beam of the equipment is 2 μm, the thickness of the coating agent is totally pierced being the major sample compound analyzed titanium dioxide in all the cases. Nevertheless, these spectrums are a hint that particles are covered with the polymer.

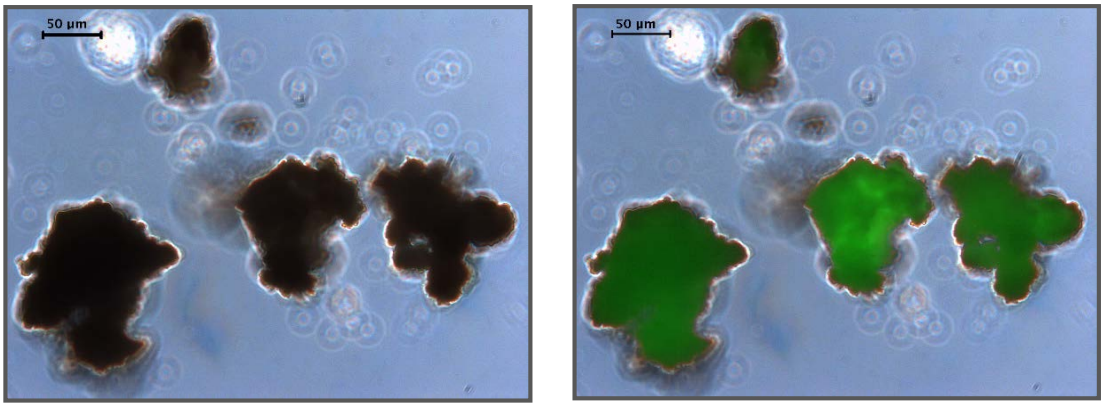

Figure 8: *photograph of run No.5 without/with green light illumination.*

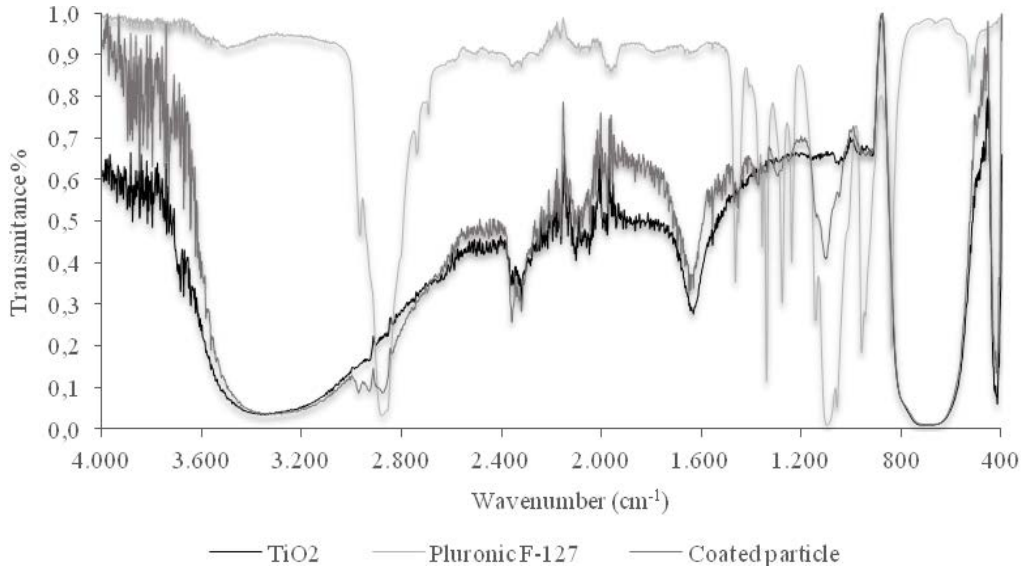

Figure 9: *FT-IR spectrum of the experiment at conditions of; CO_2 flow: 2.5·umf; solution flow: 0.5 mL/min; solution concentration: 0.04 mg/mL; CO_2 density: 700 kg/m^3; ratio polymer-particle: 0.3 g/g*

4. Conclusions

A nanoparticle agglomerate coating technique in a fluidized bed via SAS process has been studied and its operational parameters have been analyzed. This process, combining the advantageous characteristics of fluidized beds **(**good mass and heat transfer and easy temperature control) and anti-solvent process, has been found to be a good alternative to cover nanoparticle agglomerates obtaining thin and uniform coatings maintaining a narrow and unimodal distributions**.** Further, the operational parameters were selected based on the yield and the PSD.

Although a statistical studio was not done, the variables that have produce more variations on the yield are the solution flow and the solution concentration. In the range studied, this parameter change from 30% to 100%, being the best option to work at low flows and dilute concentrations. Meanwhile, the mass ratio polymer-particle affects significantly the final particle size varying from 0.60 – 3.00 μm. In addition, it is not a parameter that can be optimize because it depends on the specifications of the product and also on the operational maximum due to the formation of the coating by a layer succession.

Furthermore, it was observed by fluorescence microscopy that the polymer was present over the whole agglomerate surface. Other evidence that shows this process works is the variation on the bulk density, which increases linearly with the ratio polymer-particle. Besides, the FT-IR spectrum point out there are variations between the result for the particle with polymer and without it. Thanks to the coating, the bulk density changed and the manipulation of the particles is enhanced.

NOMENCLATURE

ACRONYMS

SAS: Supercritical Anti-solvent Process.

RESS: Rapid Expansion of Supercritical Solutions.

GAS: Gas Anti-solvent

PCA: Precipitation with a compressed fluid Anti-solvent)

PGSS: Precipitation from a Gas Saturated Solution

SCF: Supercritical Fluid.

PSD: Particle Size Distribution.

FT-IR: Fourier Transform Infrared Spectroscopy.

APF: Agglomerate Particle Fluidization.

ABF: Agglomerate Bubbling Fluidization.

EtOH: Ethanol

SYMBOLS

u_{mf}: Minimum fluidization velocity, cm/s

P: Operating pressure, MPa

T: Operating temperature, K.

C: Operating solution concentration, mg/mL.

$\frac{m_{polymer}}{m_{particle}}$: Mass ratio between the polymer and the particle, g/g.

m_{coated}: Amount of polymer over the particle

$m_{introduced}$: Amount of polymer pumped in fluidization chamber

V_T: Total volume of the coated particle, m^3.

r_p: Radius of the particle, m.

t: Thickness of the deposited layer of polymer, m.

V_D: Deposited volume of the polymer, m^3.

ρ_p: Density of the particle, kg/m^3.

η: Coating yield

REFERENCES

1. D. Geraldt, *Types of gas fluidization.* Powder Technology, 1973. **7**(5): p. 285-292.

2. J. Visser, *Van Der Waals and Other Cohesive forces affecting Powder Fluidization.* Powder Technology, 1989. **58**: p. 1 - 10.

3. A. Tsutsumi T. J. Wang, H. Hasegawa, T. Mineo, *Mechanism of particle coating granulation with RESS process in a fluidized bed.* Powder Technology, 2001. **118**: p. 229-235.

4. J. Ruud van Ommen, J. M. Valverde, and R. Pfeffer, *Fluidization of nanopowders: a review*. J Nanopart Res 2012. **14**: p. 737.

5. W. Yao, G. Guangsheng, W. Fei, W. Jun, *Fluidization and agglomerate structure of SiO2 nanoparticles.* Powder Technology 2002. **124**: p. 152-159.

6. C. Vogt, R. Schreiber, G. Brunner, J. Werther, *Fluid dynamics of the supercritical fluidized bed.* Powder Technology, 2005. **158**(1-3): p. 102-114.

7. E. K. Levy and B. Celeste, *Combined effects of mechanical and acoustic vibrations on fluidization of cohesive powders.* Powder Technology, 2006. **163**: p. 41-50.

8. J. M. Valverde, M. J. Espin, M. A. S. Quintanilla,. A. Castellanos, *Electrofluidized bed of silica nanoparticles.* Journal of Electrostatics 2009. **67**: p. 439-444.

9. R. Schreiber, B. Reinke, C. Vogt, J. Werther, G. Brunner, *High-pressure fluidized bed coating utilizing supercritical carbon dioxide.* Powder Technology, 2003. **138**: p. 31-38.

10. I. Kikic, N. Zordi, M. R. Moneghini, .D. Solinas, *Solubility estimation of drugs in ternary systems of interest for the antisolvent precipitation processes.* The Journal of Supercritical Fluids, 2010. **55**(2): p. 616-622.

11. R. Schreiber, C. Vogt, J. Werther, G. Brunner, *Fluidized bed coating at supercritical fluid conditions.* Journal of Supercritical Fluids, 2002. **24**: p. 137-151.

12. C. Vogt, R. Schreiber, J. Werther, G. Brunner, *Coating of particles in a fluidized bed operated at supercritical fluid conditions.* Chem. Eng. Technol., 2004. **27**: p. 943-945.

13. S. Rodríguez-Rojo, J. Marienfeld, and M. J. Cocero, *RESS process in coating applications in a high pressure fluidized bed enviroment: Bottom and top spray experiments.* Chemical Engineering Journal, 2008. **144**: p. 531-539.

14. A. Martín, S. Varona, A. Navarrete, M. J. Cocero, *Encapsulation and co-precipitation precesses with supercritical fluids: applications with essential oils.* Open Chemical Engineering, 2010. **4**: p. 31-41.

15. F. Zabihi, S. L. N. Xin, J. Jia, T. Cheng, Y. Zhao, *Polymeric coating of fluidizing nano-curcumin via anti-solvent supercritical method for sustained release.* The Journal of Supercritical Fluids, 2014. **89**: p. 99-105.

16. M. Rossmann, A. Braeuer, A. Leipertz, E. Schluecker, *Manipulating the size, the morphology and the polymorphism of acetaminophen using supercritical antisolvent (SAS) precipitation.* The Journal of Supercritical Fluids, 2013. **82**: p. 230-237.

17. M. Rossmann, A. Braeuer, S. Dowy, T. G. Gallinger, A. Leipertz, E. Schluecker, *Solute solubility as criterion for the appearance of amorphous particle precipitation or crystallization in the supercritical antisolvent (SAS) process.* The Journal of Supercritical Fluids, 2012. **66**: p. 350-358.

18. D. L. Sellers, T. H. Kim, C. W. Mount, S. H. Pun, P. J.Horner, *Poly(lactic-co-glycolic) acid microspheres encapsulated in Pluronic F-127 prolong hirudin delivery and improve functional recovery from a demyelination lesion.* Biomaterials, 2014. **35**(31): p. 8895–8902.

19. J. C. Gilbert, J. Hadgraft, A. Bye, L. G. Brookes, *Drug release from Pluronic F-127 gel.* International Journal of Pharmaceutics, 1986. **32**(2-3): p. 223-228.

20. M. Farrugia, S. P. Morgan, C. Alexander, M. L. Mather, *Ultrasonic monitoring of drug loaded Pluronic F127 micellular hydrogel phase behaviour.* Materials Science and Engineering:, 2014. **34**: p. 280-286.

21. V. Martín, S. Rodriguez-Rojo, M. J. Cocero, *Determination of Minimum Fluidization Velocity of Nanoparticle Agglomerates Using High Pressure Carbon Dioxide.* 6th International symposium on high pressure processes technology, Belgrade, Serbia, 2013.

22. S. Rodríguez-Rojo, N. López-Valverde, M. J. Cocero, *Residence time distribution studies of high pressure fluidized bed of microparticles.* The Journal of Supercritical Fluids, 2007. **44**: p. 433-440.

23. M. Fraile , Á. Martína, D. Deodatob, S. Rodriguez-Rojoa, I.D. Nogueirad, A.L. Simplíciob, M.J. Cocero, C.M.M. Duarte, *Production of new hybrid systems for drug delivery by PGSS (Particles from Gas Saturated Solutions) process.* Journal of Supercritical Fluids, 2013. **81**: p. 226-235.

24. F. Niu, J. Haslam, R. Rajewski, B. Subramaniam, *A fluidized-bed coating technology using near-critical carbon dioxide as fluidizing and drying medium.* The Journal of Supercritical Fluids, 2012. **66**: p. 315-320.

25. H. Jin, F. Xia, C. Jiang, Y. Zhao, L. He, *Nanoencapsulation of Lutein with Hydroxypropylmethyl Cellulose Phthalate by Supercritical Antisolvent.* Chiese Journal of Chemical Engineering, 2009. **17**(4): p. 672-677.

26. R. N. Dave, Y. Wang, R. Pfeffer, *Polymer coating/encapsulation of nanoparticles using a supercritical anti-solvent process.* The Journal of Supercritical Fluids, 2004. **28**(1): p. 85-99.

27. Y. Wang, Y. Wang, J. Yana, R. Pfeffer, R. Dave, B. Michniak, *The application of a supercritical antisolvent process for sustained drug delivery*. Powder Technology, 2006. **164**(2): p. 94-102.

28. I. N. Uzun, O. Sipahigil, S. Dinçer, *Coprecipitation of Cefuroxime Axetil–PVP composite microparticles by batch supercritical antisolvent process.* The Journal of Supercritical Fluids, 2011. **55**(3): p. 1059-1069.

29. H. Kröber and U. Teipel, *Microencapsulation of particles using supercritical carbon dioxide.* Chemical Engineering and Processing, 2005. **44**: p. 215-219.

CONCLUSIONS

Conclusions

This thesis is a contribution for the industrial development of alternative processes involving inorganic nanoparticles, which follow green chemistry and engineering principles. The main conclusions of this work according to the obtained results, taking into account the objectives proposed at the beginning, are the following:

Green synthesis of copper nanoparticles

Green synthesis is a good alternative for nanoparticle formation due to it is possible to obtain particles with the desired sizer changing process conditions, using natural cheap reagents:

- ✓ Copper nanoparticles, as confirmed by EDS and XRD, can be synthetized using grape pomace extract, as only reagent, owing to the extract content in phenolic acids, which work as reducing agents, and flavonols that control the particle size because of their capping properties.

- ✓ Temperature and time are the most critical operation variables, while extract-copper ion ratio only it is important in particle size. The effect of these variables on particle size, which must be the smallest possible, and reaction yield, which must be the highest, is reverse. For this reason, is possible to obtain low particle size (< 100 nm) by mean of adjust the reaction conditions, but only with yields lower than 35%, in the studied range.

Copper nanoparticles formulation in a lipid matrix

Nanoparticles in biomedicine must be encapsulated to improve their efficiency and avoid collateral problems associated with them. PGSS® process offers a good alternative since is a versatile technic that allows high encapsulation yields.

- ✓ Copper nanoparticles can be formulated by their inclusion in a lipid matrix, using PGSS® process which involves the use of supercritical carbon dioxide, a clean solvent, to micronize the particles, avoiding separation steps.

- ✓ Low copper loaded lipid particles present a good process yield and a good distribution of copper in the lipid matrix. When copper load is increased due to sedimentation process yield is drastically reduce, but this reduction is compensated adding more copper, presenting a minimum in the tendency. Furthermore, at high loads copper particles form aggregates and the dispersion is worse.

- ✓ This formulation process can be carry out with an aqueous suspension of copper nanoparticles instead of dried solid. The effect of water varies depending on copper load. Water enhances dispersion in spite of agglomeration is still produced.

Nanoparticle coating by SAS in a SC-CO_2 fluidized bed

Coating by means of a fluidized bed is a well know technic at industrial level, but nanoparticles present problems that make difficult to apply it. Supercritical carbon dioxide fluidized bed connected to supercritical antisolvent process has been demonstrated to be a good option to achieve it.

- ✓ Fluidization of nanoparticles with supercritical carbon dioxide reduces minimum fluidization velocity, enhancing the process better or at the same level of other technics, such as vibrations. Meaning, this process avoid channeling and other problems derived because of working with group C Geldart particles.

- ✓ Depending on fluid density, there is a predominance of hydrodynamic forces when fluid density is high (>800 kg/m^3), but at lower densities (<500 kg/m^3) interparticle forces (Van der Waals, electrostatic and liquid bridges) have influence as well as hydrodynamic forces. The behavior of interparticle forces in each kind of particle is consequence of material nature (primary size, bulk density…).

- ✓ A green coating method for nanoparticles has been developed. Inorganic nanoparticle agglomerates (TiO_2) have been coated with the combined process of SC-CO_2 fluidized bed and supercritical antisolvent (SAS) method using ethanol as solvent. This equipment can work at pressures from 80 to 120 bar and temperatures from 35 to 60ºC and coating solution flows from 0.5 to 2 ml/min.

- ✓ Nanoparticles agglomerates (3µm approx.) were successfully fluidized and coating with films ranging from 5 – 30 nm thickness depending on operating time. The variables that have produce more variations on the yield (up to 95%) were the solution flow and the solution concentration.

- ✓ The effectivity of this technic have been measure directly by fluorescence microscopy, and indirectly by means of studying the variation of nanoparticles bulk density (from 50 to 350 kg/m^3) facilitating its incorporation to different products.

FUTURE WORK

Future work

As a future work, some thesis aspects can be explored:

Bioreduction

- Other plant extract can be proved in order to compare the effect in nanoparticles, even extract can be enrich in some compound families to control nanoparticle properties (color, size, shape…).

- Study of reaction kinetics and stablish a growth model to predict the green synthesis process.

- Apply green synthesis to deposit metallic nanoparticles over a catalytic support surface.

Copper loaded lipid microparticles

- Copper loaded lipid nanoparticles effect in cancer cells can be studied as well as a release study can be performed owing to simulate the behavior of particles in the human organism.

Fluidization of nanoparticles

- A visual column can be used to observe all the column and check if fluidization regime, with the different particles, is the expected.

- Establish a physical model to explain the effect of supercritical carbon dioxide effect on nanoparticles.

RESUMEN

Introducción

Esta tesis está enmarcada en el ámbito del Proyecto SHYMAN (Sustainable Hydrothermal Manufacturing of Nanomaterials), financiado por el FP7 europeo para la investigación y el desarrollo tecnológico. El consorcio está coordinado por la Universidad de Nottingham (Reino Unido), el grupo de investigación Ingeniería de procesos a presión participa en los paquetes de trabajo de formulación de nanopartículas, modelado y diseño del reactor, nuevos productos y aplicaciones basados en la síntesis hidrotermal de nuevos compuestos, y en el diseño de la planta demostración que con una capacidad de producir 100 Tm/año de nanopartículas. Actualmente está operativa en la Universidad de Nottingham.

El proyecto tiene por objetivo general establecer el uso de la síntesis hidrotermal como uno de los métodos más flexibles y sostenibles para la producción de nanomateriales, que sirva a la industria europea para posicionarse en el sector industrial de uso de nanomateriales y nanocompuestos. Este sector, que en 2009generaba 9,000 millones de dólares en ventas, se prevé que alcance los 75,800 millones en 2020.

La síntesis hidrotermal en continuo es una tecnología estudiada a nivel de laboratorio y lista para ser probada a escala industrial gracias a las mejoras en el diseño de reactores de los últimos años, que permite llegar a producir miles de toneladas de nanopartículas al año. En este sentido, el proyecto SHYMAN ha desarrollado el escalado del reactor y de toda la instalación, basado en modelado de reactores, la cinética química y la metrología del proceso. Los estudios realizados se aplicarán en cuatro áreas diferentes: impresión de circuitos, recubrimientos superficiales, biomedicina y materiales híbridos.

Esta tesis se desarrolla en el paquete de trabajo número tres del proyecto, que trata sobre la formulación de nanomateriales. Ya que los usuarios finales requieren que la tecnología mejore la funcionalidad del producto y la dispersión de las nanopartículas, resulta indispensable la formulación de las mismas. Existen dos vías potenciales para lograr la obtención de materiales formulados: la vía seca y la vía húmeda. Mediante la primera las partículas se producen y se formulan en dos pasos diferentes, mientras que a través de la segunda en un solo paso se podría realizar la síntesis y la formulación. El proceso hidrotermal es un ejemplo de esta vía.

El principal inconveniente de la síntesis hidrotermal, y por tanto de la formulación por vía húmeda, es que las partículas se obtienen en una concentración inferior al 5% en masa. El proyecto tratará de resolver justamente este problema, ya que para su uso industrial se necesitan concentraciones mínimas de partículas entre el 5 y el 30% en masa, y la eliminación de agua conlleva un alto coste. Además, el contenido de agua causa problemas en ciertas aplicaciones, como en la catálisis o en la polimerización, en los que se requieren partículas completamente secas.

En esta tesis se tratarán algunos aspectos relacionados con el proyecto SHYMAN, haciendo hincapié en el paquete de trabajo de formulación, tanto en vía húmeda como seca, y presentando alternativas, que mantengan la premisa de procesos amigables con el medio ambiente respetando los principios de la química y la ingeniería verde.

En el primer capítulo, se estudiará una síntesis alternativa para la obtención de nanopartículas en vía acuosa llamada biorreducción, que también respeta los principios de la química verde. Este proceso está basado en la capacidad reductora de ciertos compuestos presentes en el metabolismo de las plantas, que se extraen fácilmente por procesos convencionales. En este trabajo, la biorreducción se lleva a cabo con extracto de hollejos y semillas de uva, residuos importantes de la industria vinícola, que, de esta manera, se revalorizan.

A continuación, se analizarán dos procesos de formulación de nanopartículas basados en la tecnología de fluidos supercríticos, una de las tecnologías verdes desarrolladas en las últimas décadas. La formulación tiene como objetivos principales la protección y la alteración de propiedades físico químicas del producto original. Lo que optimiza las nanopartículas para su uso en aplicaciones biomédicas, para la producción de nuevos materiales, catálisis u otras aplicaciones.

En el segundo capítulo, se estudiará la obtención de partículas de lípido cargadas con cobre, el cual tiene aplicaciones biomédicas, mediante la técnica PGSS® (Particles form Gas Saturated Solutions) (figura 1), proceso que consiste en la disolución de dióxido de carbono en un material fundido en el que es soluble, seguida por su descompresión a través de una boquilla, la cual provoca la micronización del material.

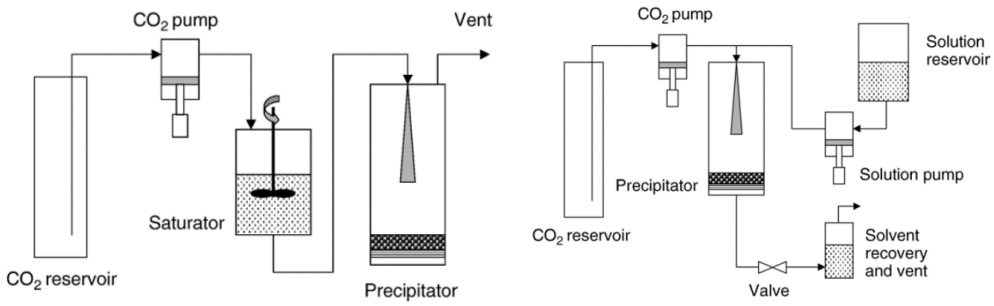

Figura 1: Procesos de formulación con fluidos supercríticos: PGSS® (izquierda) y SAS (derecha).

En los capítulos tercero y cuarto, El segundo proceso de formulación consiste en aplicar la técnica SAS (Supercritical Antisolvent process) (figura 1) en combinación con un lecho fluidizado con el fin recubrir nanopartículas de dióxido de titanio con polímero. En el tercer capítulo, Como paso previo, es necesario el estudio de la fluidización de nanopartículas con dióxido de carbono en estado supercrítico, que se incluye en el capítulo tercero. En el cuarto, se desarrollará el proceso conjunto de recubrimiento, en el cual se bombea una disolución alcohólica de polímero sobre las partículas del lecho fluidizado: a medida que el alcohol se disuelve en el fluido supercrítico, el polímero precipita sobre el material.

Objetivos

1. Síntesis de nanopartículas de cobre metálico con extracto polifenólico de residuos de la industria vinícola como agente reductor y controlador de tamaño:
    - Estudio de las principales variables del proceso (temperatura, tiempo de operación y la relación entre masa de polifenoles e ion cobre, en el tamaño y en la eficiencia de la síntesis.
    - Estudio del crecimiento de las partículas durante la síntesis y de la influencia de la concentración de los principales compuestos fenólicos a lo largo de la reacción.
    - Caracterización físico química del producto.

2. Formulación de nanopartículas de cobre con un compuesto lipídico mediante PGSS®: para potenciales aplicaciones biomédicas:
    - Establecimiento de las condiciones óptimas de operación: temperatura, presión, contenido en cobre y cantidad de agua.
    - Estudio de la dispersión de las nanopartículas de cobre en la matriz lipídica.

3. Recubrimiento de nanopartículas de dióxido de titanio con polímero por medio de un proceso que combina un lecho fluidizado con CO_2 supercrítico y una precipitación SAS:
    - Estudio de la fluidización de nanopartículas en condiciones supercríticas del fluido: variación de la velocidad mínima de fluidización con la densidad del fluido y con las propiedades del material (tamaño de la partícula primaria, tamaño de aglomerado y densidad del lecho).
    - Estudio del efecto de las principales variables del proceso de recubrimiento combinado (velocidad y densidad del fluido, flujo y concentración de la disolución de polímero y relación entre la masa de polímero y partículas) en la calidad del proceso de recubrimiento (rendimiento, uniformidad de la capa de polímero sobre el aglomerado de nanopartículas y el tamaño final).

Capítulo 1: Síntesis verde de nanopartículas de cobre con extracto de hollejo de uva

La síntesis de nanopartículas metálicas es un campo prometedor para la química verde, la cual está enfocada en el diseño de nuevos procesos que reduzcan o eliminen los reactivos orgánicos peligrosos, que se utilizan en los métodos convencionales (por ejemplo el sol-gel), así como el ahorro energético y de pasos de purificación.

En este trabajo, la biorreducción ha sido estudiada como alternativa a los procesos convencionales para la obtención de nanopartículas de cobre. El proceso consiste en la reducción de iones mediante el uso de células de plantas, hongos o algas, ya que éstos en su metabolismo realizan el mismo proceso y para ello generan compuestos reductores. Por lo tanto, no es imprescindible realizar un cultivo biológico para obtener tales nanopartículas, pues el extracto de estos organismos permite llevar a cabo el proceso de manera más rápida.

El proceso es sencillo de llevar a cabo: basta con poner en contacto el extracto previamente mencionado con una disolución de una sal del compuesto metálico que queremos obtener; de esta manera, los compuestos reductores se oxidarán, reduciendo el catión a la forma metálica. Estos extractos también poseen agentes que controlan el tamaño, lo cual permite la producción de nanopartículas con un tamaño uniforme.

Para la realización de este estudio, se ha utilizado extracto de residuos de la industria vinícola (hollejo, tallos y semillas) procedentes de la primera fermentación, que suponen 240 millones de toneladas a nivel mundial cada año. Dicho extracto es rico en compuestos polifenólicos como ácidos (ácido gálico, ácido elágico), flavonoles (catequina) y antocianinas (10-cianidin-3-glucóxido). Durante el proceso, los ácidos actúan como agentes reductores, mientras que los flavonoides estabilizan el tamaño de las partículas.

En primer lugar, se ha estudiado mediante un análisis estadístico sistemático el efecto de las variables tiempo de operación (1-3 horas), temperatura de reacción (30-55-80ºC) y proporción de antioxidante por masa de catión cobre (0.01-0.05-0.1 gAGE/g Cu^{+2}) sobre el tamaño de partícula y el rendimiento del proceso. Los resultados mostraron que los parámetros críticos para el rango de trabajo son, en ambos casos, tiempo y temperatura, influyendo más la proporción entre reactivos en el rendimiento de la reacción que en el tamaño de partícula. Las variables tienen efectos opuestos: el mayor rendimiento se obtiene a altas temperaturas y grandes tiempos, mientras que el menor

tamaño se obtiene a bajas temperaturas y reducidos tiempos, teniéndose que alcanzar un compromiso entre tiempo y temperatura para realizar un proceso eficiente con las características de producto deseadas.

El proceso de crecimiento se ha estudiado mediante el seguimiento del tamaño con el tiempo para diferentes temperaturas y ratios de antioxidante, como se puede observar en la figura 2a.

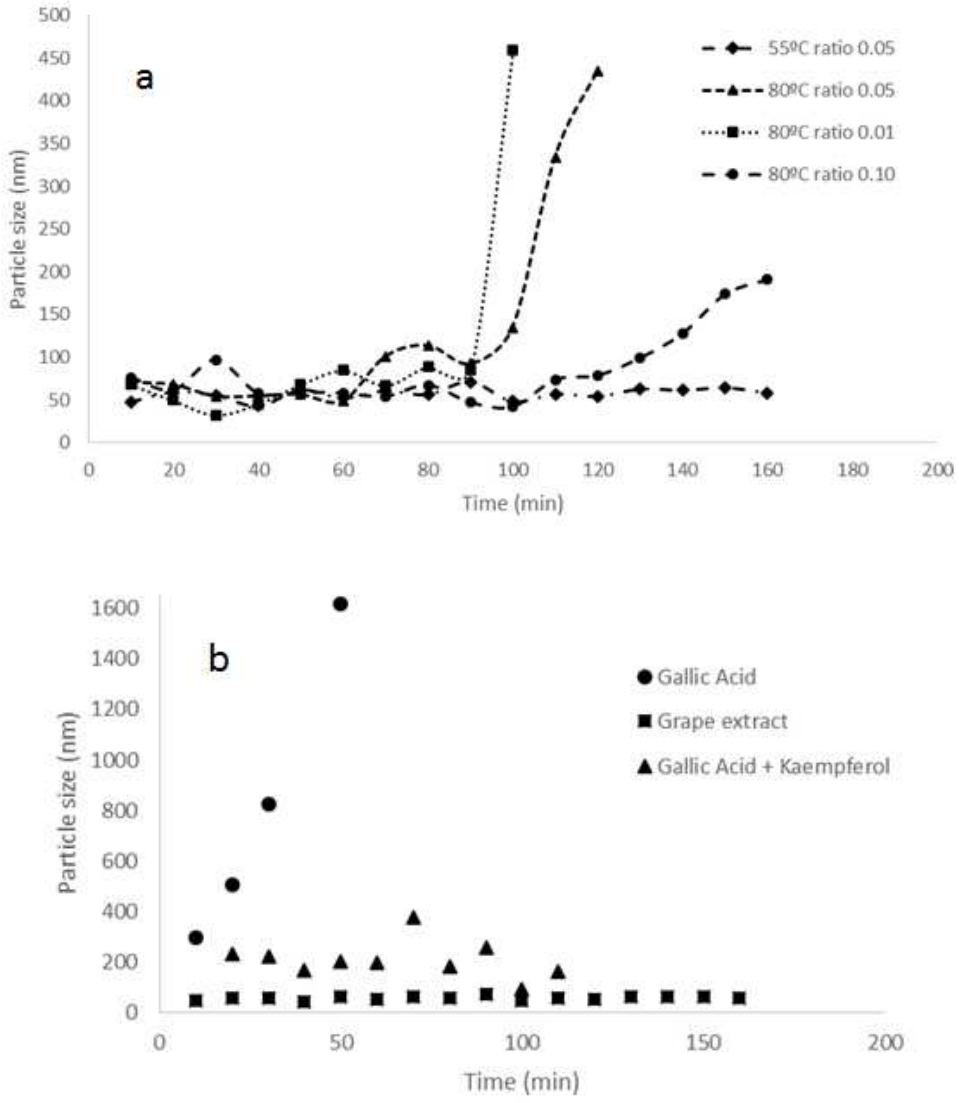

Figura 2: Evolución del tamaño de partícula con el tiempo: a) a diferentes condiciones de operación. b) a 55ºC con una proporción de 0.05 g GAE/gCu^{+2} utilizando diferentes agentes reductores.

Como se puede observar, hay dos zonas en el crecimiento: a bajos tiempos el tamaño permanece constante hasta que se consumen los agentes que mantienen el tamaño constante, provocando un súbito aumento de tamaño. Por lo tanto, el aumento depende de

la cantidad de antioxidante y la temperatura. Como se puede ver, el crecimiento descontrolado está potenciado por la temperatura y bajas proporciones de antioxidante-catión cobre (II).

Por otro lado, se ha estudiado la influencia de los compuestos del extracto en este crecimiento. Se ha realizado el mismo estudio sólo con ácido gálico (figura 2b), pudiéndose observar que no tiene ningún efecto estabilizador de tamaño de partícula, ya que éste aumenta rápidamente, confirmándose su actividad únicamente como agente reductor. Añadiendo una pequeña cantidad de kaempferol, un flavonoide, en cambio, se puede observar que el crecimiento se estabiliza en un tamaño de partícula determinado, obteniéndose una cinética de crecimiento de las nanopartículas de cobre similar al obtenido con el extracto.

Finalmente, las nanopartículas de cobre se han caracterizado por TEM (figura 3), XRD y EDS, y se ha podido certificar que las partículas están compuestas por cobre metálico.

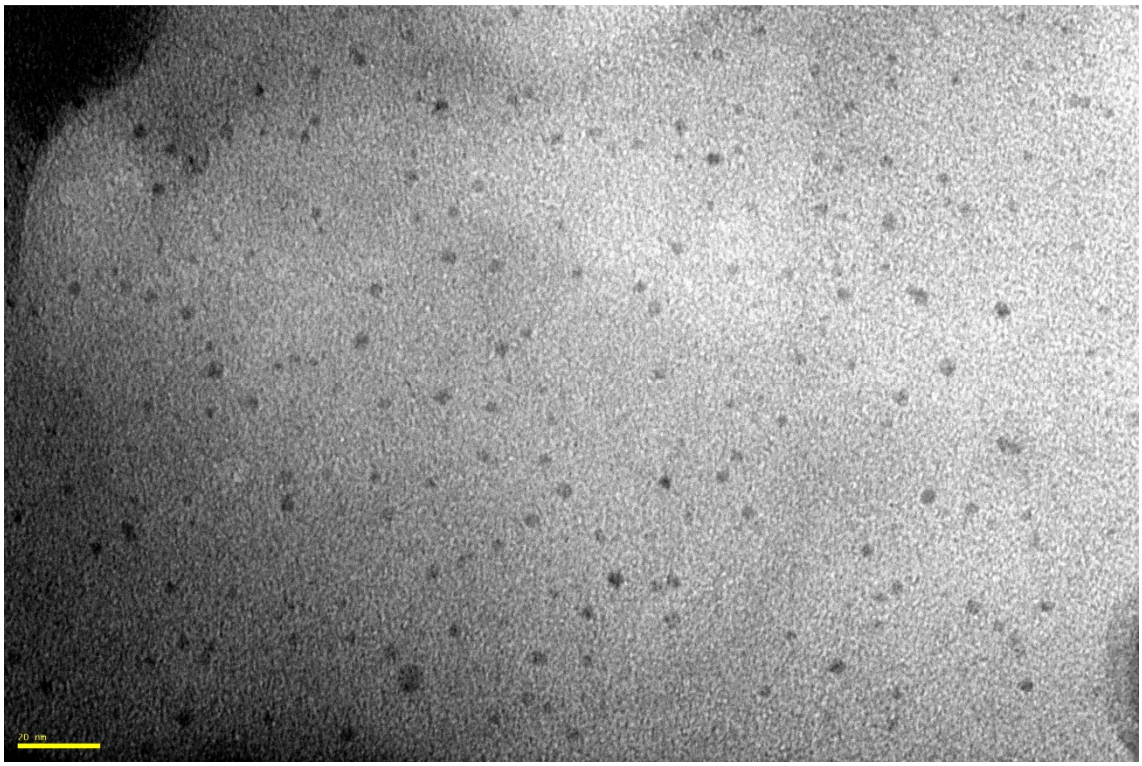

Figura 3: Imagen TEM de nanopartículas de cobre obtenidas a 80°C, 100 minutos y un ratio de antioxidante de 0.05 (barra de escala de 20 nm).

Capítulo 2: Producción de micropartículas de lípido cargadas con cobre

Las nanopartículas –especialmente las de los metales nobles– tienen una importancia emergente en el campo de la biomedicina. En efecto, sus usos son diversos: imagen molecular, sistemas de liberación de compuestos activos sobre objetivos definidos, terapias dirigidas como la hipertermia, silenciamiento de genes, radioterapia y biosensores. La importancia de estos materiales reside en algunas de sus propiedades, como por ejemplo el área superficial, los puntos cuánticos o la posibilidad de ser funcionalizados.

El cobre es un excelente compuesto con aplicaciones en biomedicina, ya que tiene propiedades antiinflamatorias, antiproliferativas y biocidas. Para poder aplicarlas sobre las células objetivo y no sobre células sanas, que podrían resultar dañadas, es necesaria su formulación. En este trabajo, las nanopartículas de cobre han sido encapsuladas en gliceril palmitoesterato, un compuesto lipídico con baja toxicidad que es tolerado por el cuerpo humano. Para ello, se ha utilizado el proceso PGSS® que se encuentra descrito en la introducción. Para la obtención de las micropartículas, el lípido se ha fundido y mezclado con nanopartículas de cobre. La mezcla se ha mantenido agitada para favorecer la suspensión del cobre en el seno del fluido. Después, se la ha puesto en contacto con dióxido de carbono en condiciones supercríticas, el cual se ha disuelto en el lípido hasta saturación. Finalmente, la mezcla se ha expandido a través de una boquilla, de tal manera que las partículas se forman con un tamaño del orden de micras.

Para la realización de este estudio, en primer lugar, se han fijado las condiciones de trabajo. Para ello, se ha elegido una presión entre 100-150 bar, de modo que la cantidad de dióxido de carbono disuelto en el lípido fuera alta. Mediante búsqueda bibliográfica, se ha obtenido como varía la temperatura de fusión del polímero con la presión del CO_2 y se ha hecho un estudio del efecto de la temperatura en la morfología y el tamaño final de partícula. De esta manera, se ha podido ver que en el rango de temperaturas estudiado (60-80ºC) no hay una variación significativa, por esta razón se ha elegido la temperatura más baja. En cuanto a presión, sin embargo, no se han observado grandes variaciones de tamaño de partícula, por lo que se ha elegido el valor inferior que permite obtener partículas más pequeñas.

Una vez fijadas las condiciones de presión y temperatura, se ha visto cómo afecta la cantidad de cobre introducida en las características del producto final y en la eficiencia

de la encapsulación. El tamaño de las partículas de lípido no varía, sino que permanece constante en torno a 45 µm, mientras que la eficiencia de encapsulación presenta un mínimo, alcanzando valores mayores del 60% a muy bajas (0.2%) y altas cantidades (5.0%), como se puede apreciar en la figura 4.

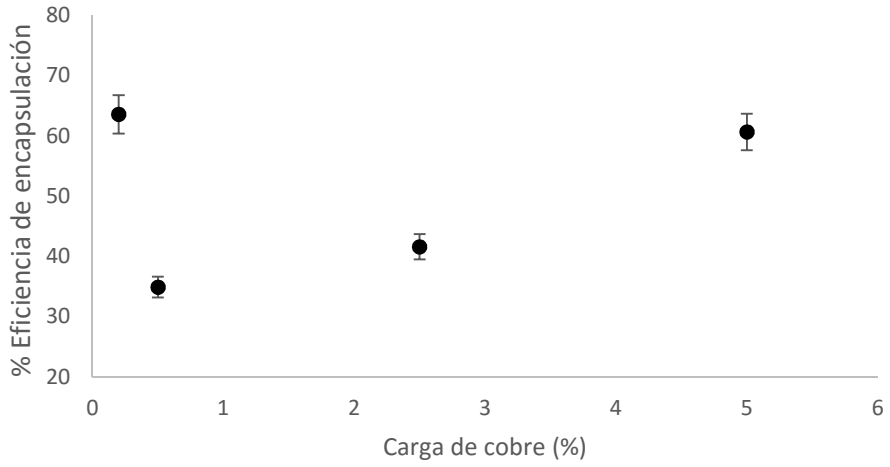

Figura 4: Influencia de la masa de cobre en la eficiencia de encapsulación.

En la gran mayoría de los métodos de síntesis, las nanopartículas se obtienen dispersas en un medio acuoso; por esa razón se ha simulado la utilización de la corriente de salida de uno de estos procesos húmedos de síntesis (por ejemplo, hidrotermal o la biorreducción) mediante la adición de agua a la mezcla de lípido y cobre antes de la expansión. Los resultados muestran que a altas cargas de cobre (5.0%) el tamaño disminuye con cantidades de agua superiores al 20%, mientras que a cargas de 0.2% el tamaño aumenta bruscamente con cantidades de agua superiores al 20%. En cuanto a la eficiencia de encapsulación, a cargas del 5% ésta permanece constante, mientras que con cargas del 0.2% a altas cantidades de agua desciende. También cabe mencionar que la presencia de agua aumenta la plastificación del polímero y se difumina la morfología tipo "flake" inicial.

Además, un análisis SEM-FIB de mapeo con EDS revela que la dispersión es mejor a bajas cargas de cobre, ya que para valores elevados las nanopartículas se aglomeran. La temperatura no tiene un efecto apreciable en la dispersión, mientras que el agua mejora el proceso de dispersión notablemente, tal y como se puede apreciar en la figura 5.

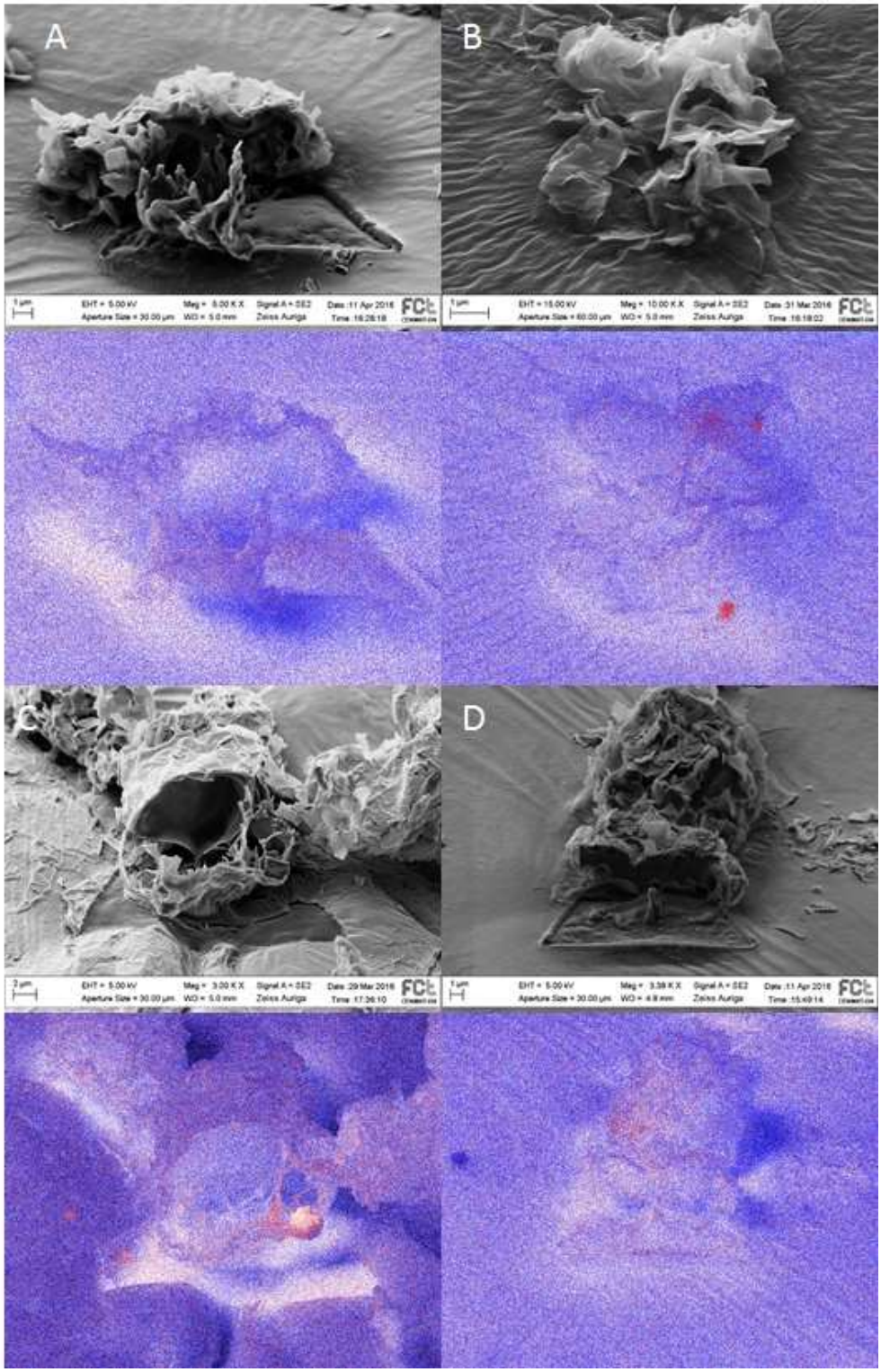

Figura 5: Análisis SEM-FIB con mapeo EDS (Azul-Carbono y rojo-Cobre): A-0.2% Cu, T = 60°C , P = 100 bar, agua inicial = 0%, B- 5% Cu, T=60°C, P= 100 bar, agua inicial = 0%, C- 5% Cu, T=60ºC, P= 100 bar, agua inicial = 40% and D- 5% Cu, T=80ºC, P= 100 bar, agua inicial = 0%.

Capítulo 3: Mejora de la fluidización de aglomerados de nanopartículas mediante dióxido de carbono en estado supercrítico.

La fluidización de nanopartículas presenta diversos problemas; uno de ellos es la formación de caminos preferenciales en el lecho, por la naturaleza de estas partículas, ya que debido a su pequeño tamaño, las fuerzas entre partículas alcanzan grandes magnitudes. De hecho, no se pueden fluidizar como partículas individuales, sino como aglomerados. Las fuerzas cohesivas que controlan la aglomeración son de tres tipos: London-Van der Waals, electrostáticas y puentes de líquido. Las más importantes en partículas secas no cargadas son las de London-Van der Waals, que tienen carácter atractivo y se producen como resultado de fluctuaciones temporales en el carácter dipolar. La intensidad de estas fuerzas es inversamente proporcional al radio de la partícula elevado a la sexta potencia. La segunda fuerza en importancia es la electrostática, que tiene lugar cuando las partículas se cargan superficialmente, y puede ser atractiva o repulsiva. Por último, los puentes de líquido, que tienen lugar cuando un líquido se adsorbe en la superficie de la partícula y forma uniones entre partículas.

Debido a estas peculiaridades, la fluidización de nanopartículas puede ser de dos tipos: particulada o burbujeante. La primera tiene lugar cuando la densidad del lecho es inferior a 100 kg/m^3 y se caracteriza por la formación de aglomerados ligeros en varias etapas. Se realiza a velocidades de fluidización bajas, sin formación de burbujas. En cambio, la fluidización burbujeante es característica de materiales con densidades de lecho superiores a 100 kg/m^3 y forma aglomerados compactos en una única etapa. Por lo tanto, la fluidización de aglomerados particulada es ideal para procesos de recubrimiento o para reacciones catalíticas, mientras que la burbujeante es mejor a la hora de mantener la temperatura del lecho constante y homogénea en reacciones exotérmicas, mediante la mejora de la mezcla de los sólidos.

Para mejorar la fluidización de aglomerados de nanopartículas, se utilizan diversos métodos, como el uso de surfactantes, vibraciones mecánicas, agitación, campos acústicos, flujos de gas pulsado, campos centrífugos o campos electromagnéticos. Estos sistemas reducen el tamaño de los aglomerados mejorando la calidad de la fluidización. Otro método que ha sido probado con éxito es el uso de fluidos supercríticos, aunque no hay muchos estudios científicos al respecto para nanopartículas, en micropartículas está comprobado.

El objetivo de este trabajo es el estudio de la variación en la calidad de la fluidización de nanopartículas seguida a través de la velocidad mínima de fluidización con la densidad del fluido. También ha sido estudiada la influencia de la naturaleza de las diferentes partículas (tamaño inicial, densidad del lecho, morfología). Finalmente, se han comparado los resultados con otras técnicas encontradas en bibliografía.

La velocidad mínima de fluidización de nanopartículas de óxido de aluminio, dióxido de titanio y magnetita, a diferentes densidades de dióxido de carbono, se ha determinado mediante el método de la medida de la presión diferencial, el cual se basa en la variación sufrida por esta variable, que en el lecho está fijo aumenta al aumentar la velocidad del fluido a su través mientras que es constante cuando se alcanza el régimen fluidizado, Los resultados pueden verse en el gráfico presentado a continuación (figura 6).

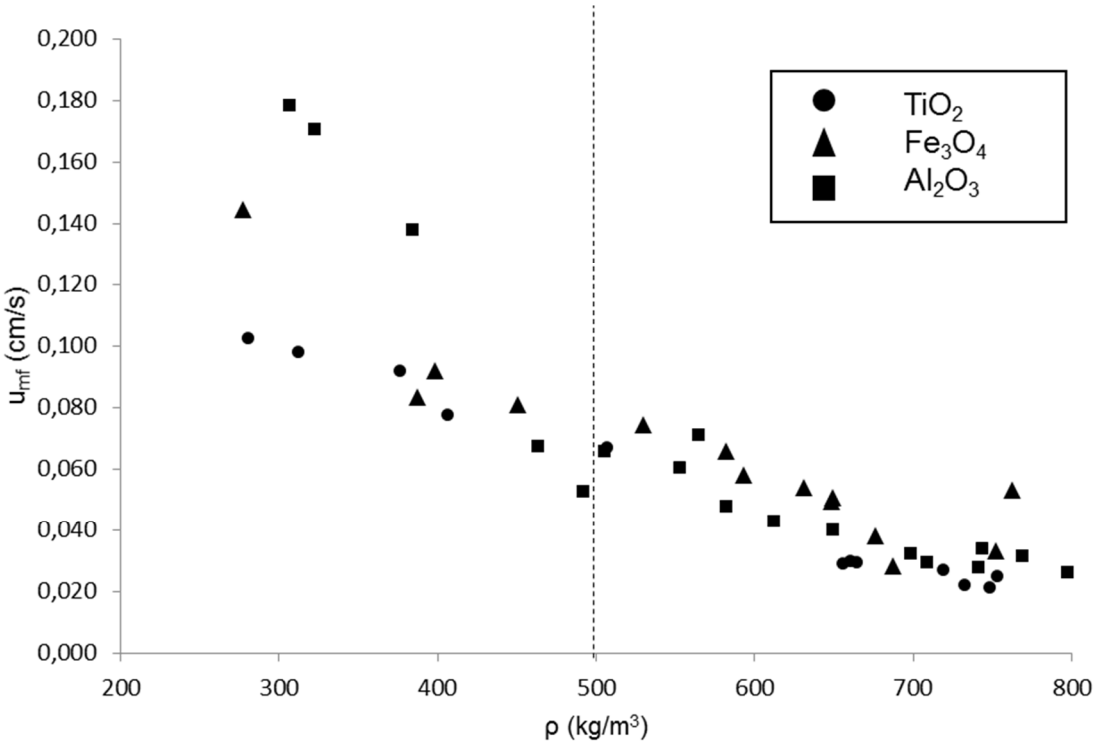

Figura 6: Variación de la velocidad mínima de fluidización con la densidad del fluido.

Como se puede observar, hay dos zonas claramente diferenciadas. A densidades superiores a 500 kg/m^3, los tres materiales se comportan de la misma manera. Esto puede ser debido a que las fuerzas hidrodinámicas del fluido son muy superiores a las fuerzas cohesivas, por lo que solo depende de la densidad del fluido por lo que todas tienen valores similares de velocidad. Por otra parte, a densidades inferiores, cada partícula se comporta de una forma diferente, pero este comportamiento no es al azar: la velocidad

mínima de fluidización toma valores superiores cuando el tamaño inicial de la partícula es menor. Por esto, se puede afirmar que hay una influencia de las fuerzas entre partículas que rigen la aglomeración, así como de las fuerzas hidrodinámicas.

Por último, se han comparado los resultados obtenidos con otras técnicas utilizadas en bibliografía. El dióxido de titanio en condiciones ambientes con nitrógeno tiene una velocidad mínima de fluidización de 5.76 cm/s. Este valor se ve reducido a 1.62 cm/s con pulsaciones de gas. Con el uso de dióxido de carbono supercrítico se reduce el valor a 0.1-0.02 cm/s (dependiendo de la densidad). Por otra parte, el óxido de aluminio fluidiza en condiciones ambiente con nitrógeno a 3 cm/s, un campo acústico a 140 dB y 120 Hz, reduce este valor hasta 0.05 cm/s. Con el CO_2 supercrítico se alcanzan valores similares (0.03 cm/s).

Capítulo 4: Recubrimiento de nanopartículas de dióxido de titanio en lecho fluidizado vía SAS

Una vez estudiado el proceso de fluidización de nanopartículas y sus aglomerados, se ha elegido como partícula modelo el dióxido de titanio (tamaño 21 nm y densidad del lecho 90 kg/m^3). Los aglomerados se han recubierto de Pluronic F-127, polímero anfifílico que no es soluble en dióxido de carbono supercrítico, pero sí en etanol. Este recubrimiento ofrece a los aglomerados una mejora de sus propiedades, como el aumento de la densidad de lecho, que sirve para mejorar el manejo de las partículas muy pulverulentas, y la protección del material en ciertas aplicaciones.

El recubrimiento se ha realizado mediante el proceso SAS (Supercritical Anti-solvent), que consiste en el bombeo de una disolución de etanol con Pluronic a una boquilla situada en la parte superior de la cámara de fluidización. Gracias a este proceso, esta disolución se deposita sobre los aglomerados, donde el disolvente se evapora gracias a su gran afinidad con el CO_2, dejando una capa de Pluronic depositada sobre la superficie de los aglomerados.

En este trabajo se ha llevado a cabo un amplio estudio sobre el proceso previamente mencionado a través del efecto de las variables principales del lecho (densidad y velocidad del dióxido de carbono, de la disolución, flujo y concentración del polímero) y de la proporción partícula- polímero en el rendimiento del proceso y en el tamaño de partícula obtenido.

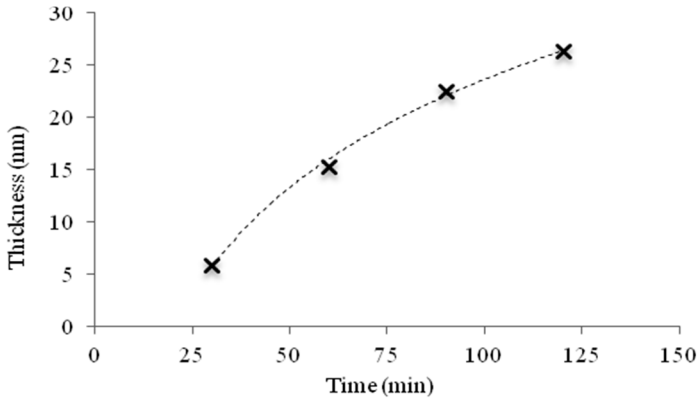

Figura 7: Variación del espesor de recubrimiento con el tiempo de operación (densidad del CO_2 700 kg/m^3, 2.5 veces la velocidad de fluidización, 1ml/min de disolución de 0.06 g/ml).

Los resultados obtenidos muestran que las variables que producen una mayor variación en el rendimiento son las que implican la disolución: el flujo y la concentración.

Éstos producen una variación desde el 30 al 100%; siendo disoluciones diluidas alimentadas a flujos bajos las que mayor rendimiento producen. En cambio, la relación entre las masa de polímero y del TiO_2 afecta mucho al tamaño del producto final, ya que varía de 0.6 a 3.00 μm. Además, se trata de un parámetro que no puede ser optimizado porque depende de las especificaciones requeridas por la aplicación que se va a dar al producto final. No obstante, presenta un máximo operacional debido a la formación de un recubrimiento por sucesión de capas. En la figura 7 se puede ver la variación del espesor del recubrimiento con el tiempo de operación, el cual está relacionado con la cantidad de polímero introducido.

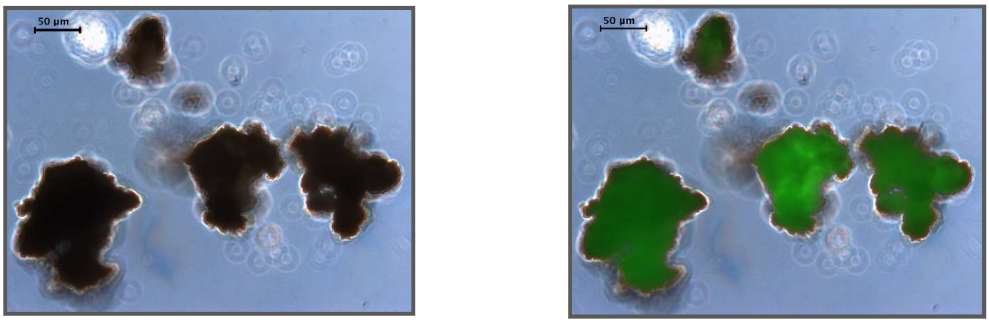

Figura 8: Imagen de microscopía óptica en campo claro y con fluorescencia.

Finalmente, para comprobar la calidad del recubrimiento, se ha añadido fluoresceína al polímero y se ha observado el producto final con microscopia de fluorescencia (figura 8). De esta manera, se ha podido apreciar un recubrimiento homogéneo en las partículas. También se ha medido la variación de la densidad del lecho al variar la cantidad de recubrimiento, y así se ha podido comprobar el aumento de la misma (figura 9).

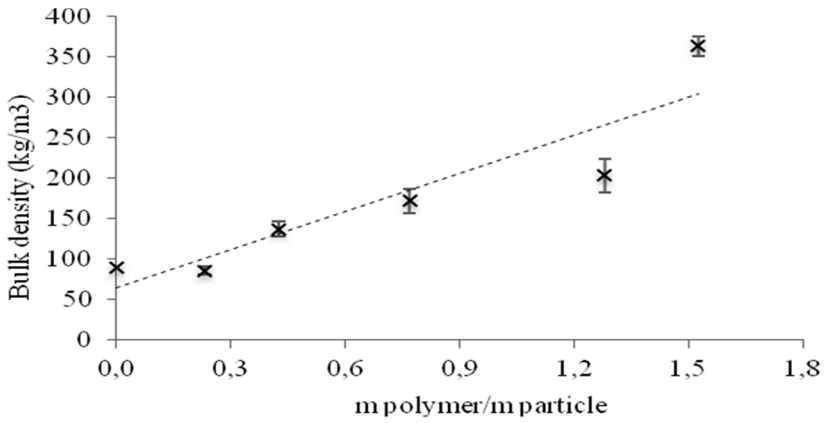

Figura 9: Variación de la densidad del lecho con el ratio de masa polímero-partícula.

Conclusiones

Esta tesis representa una contribución al desarrollo industrial de procesos de síntesis y formulación alternativos que involucran partículas inorgánicas y que siguen los principios de la química y de la ingeniería verde. En base a los objetivos de la tesis, las conclusiones obtenidas son las siguientes:

1. Síntesis verde (biorreducción) de nanopartículas de cobre

    - Es posible obtener nanopartículas de cobre a partir de extracto de residuos de la industria vinícola, ya que contiene ácidos fenólicos que actúan de agentes reductores y flavonoles que estabilizan el tamaño de las nanopartículas.
    - Temperatura y tiempo son las variables más críticas. Ajustando estas variables es posible obtener nanopartículas de menos de 100 nanómetros. No se alcanzan rendimientos altos (35%) ya que las condiciones que favorecen el aumento del rendimiento hacen que aumente el tamaño de las nanopartículas producidas.

2. Formulación de nanopartículas de cobre en una matriz lipídica

    - El proceso PGSS permite micronizar lípido con nanopartículas metálicas en su interior con eficiencias de encapsulación superiores al 60% y sin procesos posteriores de purificación ni productos tóxicos.
    - A concentraciones de cobre bajas (0.2% en masa) se obtiene un gran rendimiento y una buena dispersión, mientras que a concentraciones más altas (5%) el rendimiento es del 60% aproximadamente, aunque la dispersión empeora debido a fenómenos de aglomeración.
    - Se pueden introducir en el proceso nanopartículas tanto secas, como en dispersión acuosa, hasta un 40%. Además, el agua mejora la dispersión a altas concentraciones de cobre, mientras que a bajas concentraciones afecta negativamente a otros parámetros, como la eficacia de encapsulación y el tamaño.

3. Recubrimiento de nanopartículas mediante SAS en un lecho fluidizado con CO_2 supercrítico

- La fluidización con CO_2 supercrítico mejora la calidad de fluidización al mismo nivel que las técnicas de fluidización asistida como los campos acústicos o las pulsaciones de gas, evitando la formación de caminos preferenciales en el lecho.
- A densidades superiores a 500 kg/m^3, las fuerzas hidrodinámicas predominan y la velocidad mínima de fluidización depende sólo de la densidad del fluido, mientras que a densidades más bajas, tanto las fuerzas del fluido como las fuerzas interpartícula tienen influencia en el proceso.
- El proceso SAS aplicado a un lecho fluidizado permite obtener partículas uniformemente recubiertas con rendimientos muy altos, cercanos al 100%.
- El espesor de la capa de recubrimiento tiene un máximo técnico de 30 nm para el sistema estudiado, como se ha demostrado.
- La uniformidad del recubrimiento generado por esta técnica se ha medido por microscopia de fluorescencia obteniéndose una capa fluorescente alrededor de las partículas.

ABOUT THE AUTHOR

About the Author

Víctor Martín Velasco (Valladolid, 9 April 1986) studied Chemical Engineering at Valladolid University from 2004 to 2010. During his studies, he started to research with the project "*Study of the discontinuous process of extraction with microwaves of lavandin essential oil*" in 2009.

In 2011, the author was graduated in a Master Degree in Engineering Thermodynamics of Fluids and began his PhD thesis in High Pressure Processes Group in the Department of Chemical Engineering and Environmental Technology from University of Valladolid, under the supervision of Doctor Soraya Rodríguez Rojo and Professor María José Cocero Alonso. In 2012, Víctor achieved a grant from University of Valladolid for his formation as a researcher. In 2013, he began a degree in Chemistry at Spanish National Distance Learning University (UNED).

In 2015, he stayed during 3 months at Instituto de tecnologia química e biológica in Oeiras (Portugal), as a guest researcher in Doctor Catarina Duarte's researching group: Nutraceuticals and Delivery, under her supervision.

PUBLICATIONS

Víctor Martín, Rut Romero-Díez, Soraya Rodríguez-Rojo, María José Cocero. *Titanium dioxide nanoparticle coating in fluidized bed via supercritical anti-solvent process (SAS).* Chemical Engineering Journal. 279, pp. 425 - 432. Elsevier, 01/11/2015.

CONFERENCES

Alexander Navarrete, Víctor Martín, Rafael B. Mato and María J. Cocero. *Application of microwave energy to the extraction of essential oil from Lavandin Super (Lavandula latifolia x angustifolia),* 18th International Congress of Chemical and Process Engineering (Prague), 2008, oral communication.

Alexander Navarrete, Víctor Martín, Rafael B. Mato and María J. Cocero. *Solvent-Free Microwave Extraction of Essential Oil from Lavandin Super*. AIChE 2008 Annual Meeting (Philadelphia). Oral communication.

Víctor Martín, Soraya Rodriguez-Rojo, Marta Salgado and María J. Cocero. *Fluidization of Nanoparticle and Nanoparticle Agglomerates with Supercritical Carbon Dioxide*. 13th European Meeting on Supercritical Fluids (The Hague). 2012. Poster.

Víctor Martín, Soraya Rodríguez-Rojo and María José Cocero. *Determination of Minimum Fluidisation Velocity of Nanoparticle Agglomerates Using High Pressure Carbon Dioxide: Pressure Drop and Visual Methods*. 6th International symposium on high pressure processes technology (Belgrade). 2013. Poster.

Víctor Martín Velasco, Rut Romero Díez, Soraya Rodríguez Rojo and María José Cocero Alonso. *Coating of nanoparticle agglomerates via SAS in fluidized bed.* 14th European Meeting on Supercritical Fluids (Marseille). 2014. Poster.

Víctor Martín Velasco, Rut Romero Díez, Soraya Rodríguez Rojo and María José Cocero Alonso. *Nanoparticle aggregates coating in supercritical fluidized bed by supercritical antisolvent Technology*. VII Reunión de expertos en fluidos comprimidos (Barcelona). 2014. Poster.

Victor Martin, Soraya Rodriguez-Rojo, Isabel Nogueira, Rosario Bronze, María José Cocero and Catarina Duarte. *Green synthesis of copper nanoparticles and their use in biomedical applications*. 10th European congress of chemical engineering (Nice). 2015. Oral communication.

Víctor Martín, Vanessa Gonçalves, Soraya Rodriguez-Rojo, María José Cocero and Catarina Duarte. *Copper loaded lipid microparticles by PGSS*. 11th International Symposium on Supercritical Fluids (Seoul). 2015. Poster.

PROJECTS

Modification of Uhmwpe and Uhmwpe- Vitamine E Grains via Supercritical CO_2 for Orthopaedic Applications. University of Valladolid. Funded by RMS Foundation Dr.H.C. Robert Mathis Stiftung. 01/06/2014 - 30/06/2015.

DIRECTED THESIS

Master thesis: Nanoparticle coating in fluidized bed via supercritical antisolvent process (SAS). Rut Romero Díez. 2014. University of Valladolid.